

**Estimation of Actual Evapotranspiration and
Water Balance using Combined Geostationary
and Polar Orbiting Satellite Products: A case
Study in Spain**

Tadesse Alemu Mamo
May, 2010

Estimation of Actual Evapotranspiration and Water Balance using Combined Geostationary and Polar Orbiting Satellite Products: A case study in Spain

by

Tadesse Alemu Mamo

Thesis submitted to the International Institute for Geo-information Science and Earth Observation in partial fulfilment of the requirements for the degree of Master of Science in Geo-information Science and Earth Observation, Specialization: Integrated watershed Modelling and management-Surface water.

Thesis Assessment Board

Prof. Dr. Ir.Z (Bob) Su	(Chairman)	WRS Dept, UTwente -ITC
Dr.Ir. Ryan Teuling	(External Examiner)	Wageningen University
Dr.Ir.Christiaan van der Tol	(First Supervisor)	WRS Dept, UTwente -ITC
Ir. Wim Timmermans	(Second Supervisor)	WRS Dept, UTwente -ITC
Ms.Dr.Mireia Romaguea	(Advisor)	WRS Dept, UTwente -ITC



**INTERNATIONAL INSTITUTE FOR GEO-INFORMATION SCIENCE AND EARTH OBSERVATION
ENSCHDEDE, THE NETHERLANDS**

Disclaimer

This document describes work undertaken as part of a programme of study at the International Institute for Geo-information Science and Earth Observation. All views and opinions expressed therein remain the sole responsibility of the author, and do not necessarily represent those of the institute.

Abstract

Actual evapotranspiration and rainfall are the key elements in water balance estimation that give scientifically sound information on water availability. Currently, satellite remote sensing is widely used for estimation of these two parameters. In the past decades, the quantification of daily actual evapotranspiration (AET) from remote sensing data was mainly based on one time observation from sun synchronous satellites by scaling instantaneous evaporative fraction (EF) under the assumption of constant daytime EF. Models and data source selections for accurate estimation of AET from remote sensing observation are also continuously improving. The sources of data for this thesis were 40 ground meteorological stations in the study area and satellite products from the European organization for the exploitation of meteorological satellites on land surface analysis, satellite application facility (EUMETSAT LSA SAF) and moderate resolution imaging spectroradiometer (MODIS). Products from EUMETSAT are mainly derived from the spinning enhanced visible and infrared imager (SEVIRI) radiometer embarked on the Meteosat second generation (MSG) platform and other European satellite systems which have an imaging-repeat cycle of 15-30 minutes. For this research, the rainfall products were taken from EUMETSAT meteorological product extraction facility-multi sensor precipitation estimate (MPEF-MPE), but AET was estimated from remote sensing and ground-based data using surface energy balance system model (SEBS).

Efforts were made in this research to estimate daily average EF, instantaneous EF at different solar times, EF from daily data, and daily AET for Castilla y Leon region in Spain using ground meteorological stations, and combined high temporal resolution geostationary satellite products and relatively high spatial resolution polar orbiting satellite products. In addition, the performance of SEBS model over different land cover classes was tested. The testing was only based on the comparison of daily averaged EF and instantaneous EF, and whether the results were reasonable or not over all land cover classes in the study area. The comparison of daily average EF with instantaneous EF and EF from daily averaged data was done over different land cover classes for 15th of March, 2009. In addition, SEBS estimated AET and Meteosat second generation evapotranspiration (MET) were compared with AET measured by an Eddy covariance system in sparse vegetation. The SEBS estimated AET was also compared with MET over different land cover classes. Finally, climatological water balance estimation "Precipitation minus evapotranspiration" was carried out over rainfed cropland during the study period (March, 15 – September, 15, 2009) using rainfall products from EUMETSAT and daily AET estimated by SEBS model.

The results indicated that the average daily EF and instantaneous EF have shown strong relation over water bodies, irrigated croplands, rainfed croplands, shrubland, mosaic forest-shrubland and mosaic crop-vegetation respectively, but it shows poor agreement over sparse vegetation, broadleaved deciduous forest and needleleaved evergreen forest. There was no agreement between daily average EF and EF from daily averaged data in all land cover classes. It was observed that SEBS estimated AET is close to the measured AET but MET overestimate. Only MET and SEBS estimated AET have close values in irrigated croplands and water body, but MET overestimated in the remaining land cover classes. In addition, it was observed during water balance estimation that there were only few days in the months of May and June which have excess rainfall during the study period.

Key words: EUMETSAT LSA SAF, MODIS, SEBS, EF, AET, MET, MPEF-MPE, Water Balance

Acknowledgements

Great thank to almighty God who is always with me and the back bone of my successes. My sincere thanks to Netherland fellowship program (NFP) for funding my study to pursue such an exceptional graduate programme, the experience has truly been one of the best I had ever.

Beyond words, I have plenty of thanks for my first supervisor Dr. Ir. Christiaan van der Tol for his guidance and scientific comments through out my work. His friendly approach, listening to my ideas and understanding are incredible for me. It is his systematic guidance which helped me on how to proceed to the research work. I do not have words to express the knowledge and experiences I shared from him. “Thank you so much!!”

My deepest gratitude goes to my second supervisor Ir. Wim Timmermans for his critical idea on my progress work and continuous evaluation of my research. His valuable comments are shaped my work. I have many thanks for him for his expert guidance and moral support. I learnt a lot from his comments.

I am grateful to my advisor Ms.Dr.Mireia Romaguea for her comments and advices during the starting of my work. Her comments were valuable and helped me to think critically during the entire work.

The processing of EUMETSAT data was challenging or almost impossible without the help of Dr. Ben Maathuis. I have very respectful thanks for him. His continuous update of GEONETCast tools helped me to execute my analysis correctly. Deep gratitude to Prof.Dr.Ir. Z (Bob) Su for his continuous replay to my questions and updating me on the formulation of SEBS model. His guidance and scientific comments helped me to critically re-think on my work. My thanks also go to all ITC staffs who contributed to the knowledge I acquired in ITC.

I have many thanks for EUMETSAT help desk for their quick replay to my enquiry and continuous supply of data for my work. I am very thankful to Francisco Javier Antolín Martínez for helping me to access the real-time meteorological data from inforiego database at critical time. The same goes to Brett (NASA Land Processes Distributed Active Archive Centre User Services) for his technical support on using HEG-tools.

I would also like to thank all WRS staff members (Particularly, my supervisors, Arno, Su, and Alain), student affairs, and all my class mates for their encouragement and support during my illness in the month of November, 2009. Really, “you are good guys!” All my class mates, “I am proud in having you as my best friends forever”.

The last but not least, my heartfelt appreciation goes to my lovely wife “Abiyot” and my honourable parents for their encouragement and continuous support during all circumstances, without them all these would have not been achievable.

Table of contents

1.	Introduction	1
1.1.	Background	1
1.2.	Problem Statement	2
1.3.	Research Objectives and Questions	3
1.4.	Research Output	4
1.5.	Software Employed	4
1.6.	Assumptions and Source of errors	4
2.	Literature Review	5
2.1.	Remote Sensing of Evapotranspiration	5
2.2.	Meteosat Second Generation Evapotranspiration	6
2.3.	Rainfall Estimation from Satellite Observation	7
2.4.	EUMETSAT Land Surface Products	7
2.5.	Aerodynamic Roughness and Displacement Heights	8
3.	Study Area	9
3.1.	Climate	9
3.2.	Geology	10
4.	Materials	11
4.1.	General	11
4.2.	Remote Sensing Data	11
4.2.1.	EUMETSAT Land Surface Products	11
4.2.2.	MODIS Land Surface product	12
4.2.3.	Digital Elevation Model	12
4.2.4.	Precipitation Products	12
4.3.	Meteorological Data	13
4.3.1.	Spain Online Climate Data (Inforiego)	13
4.3.2.	NOAA National Climate Data Center (NNDC)	13
4.4.	Field Data	14
4.4.1.	Land Cover Classification	15
4.4.2.	Crop Calendar	17
4.4.3.	Eddy Covariance Data	18
4.4.4.	Radiosonde data	19
5.	Methodology	21
5.1.	General	21
5.2.	Atmospheric Parameters	23
5.2.1.	Air and Surface Pressure	23
5.2.2.	Air Temperature	23
5.2.3.	Wind Speed	24
5.2.4.	Specific Humidity	24
5.3.	Solar Information	25
5.3.1.	Sun Zenith Angle	25
5.3.2.	Sunshine hours per day	25
5.4.	Estimation of Land Surface Emissivity	25

5.5.	Estimation of Aerodynamic Roughness and Displacement Heights	25
5.6.	Determination of Height of Atmospheric Boundary Layer	27
5.7.	Interpolation of Point Data to Grid	27
5.8.	Instantaneous to Daily Average	29
5.8.1.	Land Surface temperature.....	29
5.8.2.	Down-welling Surface Short-wave Flux	30
5.8.3.	Wind speed and Air temperature	30
5.9.	Estimation of Evaporative Fraction and Actual Evapotranspiration	30
5.9.1.	Calculation of Instantaneous and Average Daily Evaporative Fraction.....	30
5.9.2.	Estimation of Daily Actual Evapotranspiration	33
5.10.	Water Balance Estimation from Remote Sensing Observations.....	33
6.	Results and Discussion.....	35
6.1.	Land cover Classification	35
6.2.	Diurnal Evolution of Evaporative Fraction	36
6.3.	Comparison of Instantaneous and Daily Average Evaporative Fractions	38
6.4.	Comparison of Measured AET with MET and SEBS Estimated AET	46
6.5.	Comparison of SEBS Estimated AET and MET	48
6.6.	Water Balance Estimation	52
7.	Conclusions and Recommendations.....	57
7.1.	Conclusions.....	57
7.2.	Recommendations	59
	References	61
	Appendices	67
	Appendix A EUMETSAT data dissemination system for Europe and Africa.....	67
	Appendix B GEONETCast toolboxes integrated to ILWIS, and HDF-EOS to GeoTIFF (HEG) tool interfaces for remote sensing data importing and processing	68
	Appendix C The missing pattern of land surface temperature record throughout the day for randomly selected pixels	69
	Appendix D Detailed land cover classification used for the assignment of vegetation height.....	70
	Appendix E ILWIS script for assignment of vegetation height and estimation of roughness height ..	71
	Appendix F Statistical formulas used in this research	72
	Appendix G Surface Energy Balance System model SEBS interface	73
	Appendix H Diurnal variation of latent heat flux over different land cover classes on March, 15, 2009	74
	Appendix I Flow chart of MET Algorithm	75

List of figures

Figure 3-1. The RGB (channel 1, 2 and 3) color composite of MSG images covering the study area (July, 15, 2009 at 11:15 UTC)	9
Figure 3-2. Spain climate zones (source: http://www.worldweather.org/083/m083.htm).....	10
Figure 3-3. Soil Map of Spain, Source: Spanish system of water information (http://hispagua.cedex.es)	10
Figure 4-1. SRTM digital elevation model of Spain.....	12
Figure 4-2. Spatial distribution of near real time data from Inforiego.....	13
Figure 4-3. Spatial distribution of stations with daily averaged data.....	14
Figure 4-4. ESA land cover classification map overlaid with point map of observed locations	17
Figure 4-5. Schematic representation of growing stages and seasons for the two main crops in Spain	18
Figure 4-6. Location of an eddy covariance tower in the study area	19
Figure 4-7. The spatial distribution of radiosonde stations in Spain	19
Figure 5-1. A simplified flow chart of the research methodology – the main operational steps	23
Figure 5-2. Profile of potential temperature for Madrid station on August, 15, 2009, at 00:00 (left) and 12:00 (right) UTC. Note: The arrows indicate the location of inversion height.....	27
Figure 5-3. Profile of potential temperature for Madrid station on March, 15, 2009, at 00:00 (left) and 12:00 (right) UTC. Note: The arrows indicate the location of inversion height	27
Figure 5-4. Comparison of nearest point and Moving average interpolation methods. Note: The arrows indicate the test stations that were not involved in the interpolation.....	28
Figure 5-5. Meteorological stations, land cover classes and drainage network of Castilla y Leon region, Spain	32
Figure 6-1. Globcover ESA land cover classification map overlaid with point map of observed locations in the study area.....	35
Figure 6-2. Diurnal variation of evaporative fraction for different land cover classes (March, 15, 2009)	36
Figure 6-3. Diurnal variation of temperature difference between land surface and air (top) and Sensible heat flux (bottom) over different land cover classes (March, 15, 2009).....	38
Figure 6-4. Comparison of average daily EF with instantaneous EF and EF calculated from daily average data for rainfed croplands (March, 15, 2009).....	39
Figure 6-5. Comparison of average daily EF with instantaneous EF and EF calculated from daily average data for irrigated croplands (March, 15, 2009).....	39
Figure 6-6. Comparison of average daily EF with instantaneous EF and EF calculated from daily average data for Sparse vegetation (March, 15, 2009).....	40
Figure 6-7. Comparison of average daily EF with instantaneous EF and EF calculated from daily average data for broadleaved deciduous forest (March, 15, 2009).....	40
Figure 6-8. Comparison of average daily EF with instantaneous EF and EF calculated from daily average data for needleleaved evergreen forest (March, 15, 2009)	41
Figure 6-9. Comparison of average daily EF with instantaneous EF and EF calculated from daily average data for mosaic croplands-vegetation (March, 15, 2009)	41
Figure 6-10. Comparison of average daily EF with instantaneous EF and EF calculated from daily average data for mosaic forest-shrubland (March, 15, 2009)	42

Figure 6-11. Comparison of average daily EF with instantaneous EF and EF calculated from daily average data for shrubland (March, 15, 2009)	42
Figure 6-12. Comparison of average daily EF with instantaneous EF and EF calculated from daily average data in the Castilla y Leon region, Spain (March, 15, 2009).....	43
Figure 6-13. The maps of temperature difference between land surface and air for daily averaged and mid day (12:00 UTC) on March, 15, 2009.....	44
Figure 6-14. Location of 10 land cover classes nearby meteorological stations used for comparison of evaporative fractions and daily AET	45
Figure 6-15. Overall comparisons of evaporative fractions using a single pixel per each land cover class near by meteorological stations.	46
Figure 6-16. Comparison of measured AET with MET (top) and variation of temperature difference between land surface and air (bottom) in the Sparse Vegetation in half hourly step (September, 01, 2009)	47
Figure 6-17. Comparison of measured AET with SEBS AET and MET in the Sparse Vegetation in hourly bases (September, 05, 2009)	47
Figure 6-18. Comparison of measured AET with MET (top) and variation of temperature difference between land surface and air (bottom) in the Sparse Vegetation in half hourly step (September, 07, 2009)	48
Figure 6-19. Comparison of SEBS estimated AET and MET (March, 15, 2009)	49
Figure 6-20. Maps of SEBS estimated AET and MET in the Castilla y Leon region, Spain (March, 15, 2009).....	51
Figure 6-21. Daily rainfall distribution over the Spain during study period that covers the Castilla y Leon region as taken from MPEF-MPE.....	52
Figure 6-22. Daily AET maps in the Castilla y Leon region for some selected dates during the study period.....	53
Figure 6-23. Variation of AET with precipitation distribution over rainfed croplands during the study period.....	54
Figure 6-24. Variation of AET with rainfall distribution over irrigated croplands during the study period.....	55
Figure 6-25. Five days cumulative AET, precipitation, and change in water storage over rainfed croplands during the study period	55
Figure 6-26. Cumulative AET and rainfall over rainfed crop lands during the study period (March, 15 – September, 15-2009)	55

List of tables

Table 4-1. Land surface products from EUMETSAT LSA SAF	11
Table 4-2. Real time meteorological data types from 40 stations in the study area	13
Table 4-3. Meteorological data from NNDC and WMO	14
Table 4-4. Land cover data collected during field work	15
Table 4-5. Land cover classes, vegetation height and number of collected points for each land cover class	15
Table 4-6. Detail Crop calendar for crops growing in Spain	18
Table 5-1 Calculation of land surface emissivity	25
Table 5-2. Land cover types and associate physical information	26
Table 5-3. The standard and absolute error of both interpolation methods for air temperature in °C ...	28
Table 6-1. Land cover classes with associate bio-physical information	37
Table 6-2. Comparison of daily AET from eddy covariance measurement and MET in the Sparse vegetation	46
Table 6-3. Input data for SEBS and MET algorithm for estimation of AET	50

1. Introduction

1.1. Background

Water use strategy and water resources management require scientifically sound information on water availability, which includes the quantification of the spatial and temporal changes of water balance components like actual evapotranspiration (AET) and rainfall. These components are inextricably linked with climate, so the prospect of global climate change has serious implications for water balance, particularly in arid and semi-arid regions. In order to adopt or mitigate such situation, it is important to investigate the best meteorological input data to hydrological and surface energy balance models that are the central support for hydrological decision making.

The group of geostationary weather satellites (MSG, MET-7, GEOS-E/W) with 15-30 minute temporal resolutions form the backbone of the near real time global observing systems, supported by other polar or skew orbiting sensors (METOP, MODIS, AVHRR, etc.). The atmospheric and land surface data from these satellites can be obtained through an earth observation data and product dissemination system (GEONETCast system for earth observation data) which embraces free and open source tools for easy access to satellite data and products for water, climate and environmental studies. This system is able to provide relevant meteorological and bio-physical input data to hydrological and surface energy balance models for near real time water balance estimations in poorly gauged catchments, and water limited environments.

Good estimates of precipitation from meteorological satellites are achieved using a range of techniques, like the combined passive microwave (PM) and infrared (IR) technique (Kidd et al., 2003), and using vertical profiles of a reflectivity factor estimated from data of the precipitation radar (PR) on the Tropical Rainfall Measuring Mission (TRMM) satellite, at which the rainfall rate is the function of reflectivity factor using a power law (Iguchi et al., 2000). Both methods have great potential in improving short duration rainfall estimates.

A tremendous number of methods have been used and developed by researchers to estimate surface energy fluxes using combined remote sensing and ground based observations, for example Surface Energy Balance Algorithm for Land (SEBAL) (Bastiaanssen et al., 1998a; Bastiaanssen et al., 1998b), two-source energy balance model (TSEB) (Norman et al., 1995), Soil-Vegetation-Atmosphere transfers (SVAT) (Calvet et al., 1998) and surface energy balance system (SEBS) (Su, 2002). Most of these models estimate ET as a residual of the energy balance at the earth's surface, which contain uncertainties from both the sensible heat flux and net radiation. Therefore, atmospheric forcing and land surface input parameters for these models play a crucial role for better estimation of AET over heterogeneous land cover classes. Also, these models require explicit characterization of numerous physical parameters, many of which are difficult to determine for a large area. Some of these uncertainties can be reduced by making use of combined high temporal resolution (geostationary

satellites) and better spatial resolution (polar/skew orbiting satellites) to get better estimation of land surface parameters over large area in near real time bases.

This study focuses on use of combined geostationary and polar orbiting satellites images and products in conjunction with ground based meteorological data for estimation of daily AET and climatological water balance. The main task of this research comprises the estimation of instantaneous and daily average evaporative fraction, actual evapotranspiration, and a simple water balance over different land cover classes in the semi arid region of Spain called “Castilla y Leon region” located in the western part of Europe. This region is characterized as dry with high evaporation and low rainfall where runoff is very low.

1.2. Problem Statement

Accurate quantification of water balance components like AET and rainfall over large area from satellite remote sensing and ground based observations is a challenging task due to the heterogeneity of land surface properties (land cover type, moisture condition, topography, temperature and other bio-physical parameters), none uniformity of atmospheric parameters (wind speed, wind direction, air temperature, humidity and pressure) and uncertainties in retrieval of land surface properties and radiation from remote sensing observations. But both AET and rainfall are extremely an important water cycle components need to be estimated as accurate as possible, particularly in arid and semi-arid areas for scare water resource management.

Increasing human population, rapid climate change and water availability are the most challenging problems next generations will face. Currently, lack of relevant hydro-meteorological information hinders the deep knowledge of water cycle at the continent and basin levels in developing countries. This represents a critical problem to understand the current status of water resources in continents or basins, and to identify the impacts of climate change on water availability. Generally, information on impact of climate change and the status of hydrological networks in developing countries are inadequate to satisfy the minimum needs for water information (The TIGER Initiative, 2009-2011). In this context, water is one of the most endangered resources of the continents, while at the same time it is one of the main critical elements for society and development. Therefore, use of earth observation technologies with available ground based data can help to fill the water information gap in the developing countries from local to regional to continental scales.

Satellite remote sensing (SRS) is the only method capable of providing wide area coverage of environmental variables at economically affordable costs. However, a major difficulty to the use of SRS for monitoring AET at regional and global scale is that the phase change of water produces neither emission nor absorption of an electromagnetic signal (Gellens-Meulenberghs et al., 2008). Therefore, AET is not directly quantifiable from satellite observations. It has to be assessed by taking advantage of information gained through the satellite about surface variables influencing evapotranspiration (Menenti, 1993). In addition, Su (2002) and Kinoti Mutiga et al. (2008) mentioned that the problems associated with large scale estimation of energy fluxes are surface meteorological parameters, surface geometrical and thermal conditions, which are neither homogenous nor constant. This means that classical remote sensing flux algorithms based on surface temperature measurements in combination with spatially constant surface meteorological parameters

may be suitable for assessing the surface fluxes on a small scale, but they require surface meteorological and geometrical input parameters pixel wise over heterogeneous surface.

Using the advantage of high temporal resolution of geostationary satellites data in combination with polar orbiting satellites for estimation of AET with SEBS model is not tested yet, but the products from geostationary satellites also provide good estimation of near real time meteorological data that can be used as input to AET algorithms (LSA SAF RMI Team, 2008). In addition, Ferguson et al. (2009) found for the major river basins in the United State of America that the selection of source of input parameters to AET models has a large impact on remote sensing based estimation of evapotranspiration. They did a comparison of different sources of input data to AET models, and concluded that LAI has the most (27%) and land surface albedo and emissivity have the least (1.9%) impact on estimation of evapotranspiration using remote sensing observations. They also added that other uncertainty which contribute about 19% is from sources of net radiation used to extrapolating instantaneous to daily by assuming that evaporative fraction is constant throughout the day.

1.3. Research Objectives and Questions

To fill the water information gap, particularly in the developing countries, exploiting the advantages of earth observation technologies are the best alternative way due to lack of ground-based hydrological network. In this research, a region in Spain was selected due to its suitability for ground based data collection and availability of some data to execute the research work.

The general objectives of this research are to estimate actual evapotranspiration and climatological water balance “Precipitation minus Evapotranspiration” in large area by combined use of remote sensing and ground-based meteorological data.

The specific objectives are:

1. To compare the daily and instantaneous evaporative fraction over a large area using the surface energy balance systems model SEBS.
2. To compare SEBS estimated AET with MET and measured AET
3. To investigate the role of model input parameters derived from both geostationary and polar orbiting satellites.
4. To investigate the performance of SEBS over a large area
5. To carry out a water balance estimation using AET estimated by SEBS and a rainfall product derived from remote sensing observations.

These objectives are planned to answer the following research questions:

1. What are the advantages of combined use of geostationary and polar orbiting satellites in estimating AET?
2. Are the daily averages of remote sensing and ground based meteorological data can be used for estimation of daily AET with SEBS model in an area with scarce instantaneous ground-based meteorological data?
3. Is it possible to use SEBS model over a large area with different land cover classes?
4. Is it possible to make water balance estimation over land surface from remote sensing observations?

1.4. Research Output

The outputs of this study are:

1. Multi-scale comparison of daily and instantaneous evaporative fraction
2. Maps of daily averaged EF, instantaneous EF and EF from daily averaged data over different land cover classes in the study area
3. Some maps of rainfall distribution and AET over the study area during the study period
4. Statistical comparison of SEBS estimated AET, AET estimated from eddy covariance measurements and Meteosat second generation evapotranspiration (MET)
5. Graphs showing the variations of AET, rainfall and change in water storage over rainfed cropland during the study period.
6. A detailed description of the role of input parameters for SEBS model derived from geostationary satellites.
7. Personal scientific skills and the technical capacity to make the best use of earth observation technology to better understand assess and monitor the status of scarce water resources.

1.5. Software Employed

The following software used in this study

- Integrated land and water information system (ILWIS)
- SEBS model integrated to ILWIS
- GEONETCast toolboxes and batch files in ILWIS scripts
- HDF-EOS to GeoTIFF (HEG) tool
- Matlab and SPSS
- Microsoft offices

1.6. Assumptions and Source of errors

Although both the remote sensing and ground based data are collected from reliable sources, they are not quality checked, except the land cover classification map. This is due to large number of data were used (340 images are processed for each day, approximately more than 8500 images were used for the whole study period) which is beyond the scope of this thesis to check the quality of individual products. Therefore, the following assumptions are made while using these products:

- The validation reports provided in the metadata of all operational products are reliable and all products approach to reality in the field.
- The pre-operational products like MET can also represent the actual phenomena with acceptable error as mentioned in the validation reports

Apart from the errors induced from the data source, the followings are the main sources of errors that can generate during the processing of the data;

- Interpolation of point data (all ground based meteorological data)
- Measurement height of meteorological data
- Estimation of roughness height for momentum transfer

2. Literature Review

2.1. Remote Sensing of Evapotranspiration

Evaporation of water is like a commercial transaction in which a wet surface sells water vapour to its environment in exchange for heat (Gash and Shuttleworth, 2007). Therefore, water lost to the atmosphere through evapotranspiration has the effect of cooling the earth's surface. Particularly, in arid and semi arid areas, recycling of moisture through evapotranspiration appears to be responsible for more than 90% of the rainfall (Savenije and G.Hubert, 1995). This means that knowledge of evapotranspiration is crucial for climatic studies, weather forecasts, ecological monitoring, hydrological surveys, and water resource management (Bastiaanssen et al., 2000).

Remote sensing provides a means of observing hydrological state variables over large areas (Schmugge et al., 2002). Indeed, large scale estimation of AET has many challenges and requires good estimation of surface bio-physical parameters involved in the exchange of energy between the land surface and atmosphere. In the past decades, large scale estimation of evapotranspiration was achieved using the two source (soil and canopy) called atmosphere-land exchange inverse (ALEXI) model (Anderson et al., 1997; Mecikalski et al., 1999). This model estimates surface fluxes of heat and water vapour on the 5-10km scale using primarily satellite-derived input data, including surface radiometric temperature, down-welling short -wave and long-wave radiation, and vegetation indices. For particular applications, the coarser resolution of ALEXI output can be disaggregated to desired resolution by applying disaggregation algorithm called DisALEXI with additional model input, such as higher resolution thermal and shortwave imagery from satellite platforms like ASTER, Landsat or airborne (Norman et al., 2003).

Efforts have been undertaken by Tang (2007) as well to estimate land surface evapotranspiration from remote sensing data with special interest to achieve a near real-time crop water use estimation at the spatial scale ranging from a small basin to a region. In addition, Mu et al. (2007) developed a global remote sensing evapotranspiration algorithm based on Cleugh et al., (2007) which considers both the surface energy partitioning process and environmental constraints on evapotranspiration. The result reveals that the spatial pattern of the MODIS ET agrees well with that of the MODIS global terrestrial gross and net primary production (MOD17), with the highest ET over tropical forests and the lowest ET values in dry areas with short growing seasons. They also concluded from the result that MODIS ET product can provide critical information on the regional and global water cycle and resulting environmental change.

Recently, Minacapilli et al. (2009) made a comparison between two different energy balance models (SEBAL and TSEB) in Mediterranean perennial crops. This research was done due to the fact that the agricultural practice in the study area is converting from rainfed to irrigated crops. For this reason, the selection of the best energy balance model became an important issue for the region. Both are widely used models to estimate evapotranspiration. SEBAL is a one-source model, where soil and vegetation are considered as the sole source (mostly appropriate in the case of uniform vegetation coverage) and TSEB a two sources model, where soil and vegetation components of the surface energy balance are treated separately. Actual evapotranspiration estimates by means of the two surface energy balance

models were compared with the outputs of the agro-hydrological SWAP model, which was applied in a spatially distributed way to simulate one-dimensional water flow in the soil-plant-atmosphere continuum. The results of this investigation appeared to prove better agreement between SWAP and TSEB for some fields of the study area. This agreement reveals that separate treatment of soil and vegetation components of land surface energy balances may provide good estimation of surface fluxes.

Regional scale water cycle estimates have been made by Pan et al. (2008) using multiple satellite remote sensing data (Tropical rainfall measurement mission (TRMM), TRMM microwave imager (TMI), and moderate resolution imaging spectroradiometer (MODIS)) with the support of previously developed assimilation techniques, such as the ensemble Kalman filter (EnKF), the particle filter (PF), the water balance constrainer, the copula error model, and physically based models, including the variable infiltration capacity (VIC), the land surface microwave emission model (LSMEM), and the surface energy balance system (SEBS). They found that a land surface model driven by the bias corrected TRMM rainfall produces reasonable water cycle states and fluxes. The estimates are also moderately improved by assimilating TMI 10.67 GHz microwave brightness temperature measurements that provides information on the surface soil moisture state, while they mentioned that it remains challenging to improve the results by assimilating evapotranspiration estimated from satellite-based measurements. But they also successfully validated the evapotranspiration estimated using SEBS over the region. In addition, Wenjing et al (2006) found in Hebei Plain, Northern China, a good agreement between AET estimated by SEBS and Lysimeter, but big differences were observed when SEBS estimated AET was compared to AET derived from empirical equation using a locally derived coefficient. Therefore, there are indications of the possibility of estimating AET over large area using those energy balance models which gave good estimation of AET over relatively homogenous land surface.

2.2. Meteosat Second Generation Evapotranspiration

The methodological approaches selected in the framework of the LSA-SAF to estimate evapotranspiration intends to be applicable at regional to global scales, to be able to provide a monitoring at short time step to follow the diurnal cycle evolution and to obtain results continuously for all nebulosity conditions. Most of proposed methods use satellite remote sensing derived data combined with models of different degrees of complexity ranging from empirical direct methods to complex deterministic models based on SVAT modules that compute the different components of the energy budget (Courault et al., 2005). Similarly, the AET algorithm developed in LSA-SAF targets the quantification of the flux of water vapour released from the ground surface (soil and canopy) into the atmosphere using input data derived from MSG satellite and other source like numerical weather perdition (Gellens-Meulenberghs et al., 2006). The elementary spatial unit of the model is an MSG pixel. The dimension of the surface represented by a pixel varies in function of its location (longitude and latitude) and is 3x3 km at MSG sub satellite point. Since the vegetation cover influences most of the surface atmospheric processes over land, the estimation of AET is made by reference to a land cover map which provides the fraction of vegetation types within each MSG pixel. This primary vegetation types are called “tiles”, and each pixel may be composed of several tiles. In practice, a maximum of four tiles (3 vegetation tiles + bare soil) are allowed in a pixel. AET is calculated separately for each tile in pixel and the pixel value is obtained by a weighted contribution of all tiles composing the pixel (LSA SAF RMI Team, 2008).

2.3. Rainfall Estimation from Satellite Observation

There is high demand for improved rainfall estimates from satellite systems throughout the entire range of scales in time and space, from global to local resolutions (Kidd et al., 2003). Applications requiring rainfall products cover a range of hydro-meteorological sciences, including water resources, flood forecasting and moisture budgets. A range of techniques has been developed to produce estimates of rainfall from satellite data. For example, GOES precipitation index (GPI) (Arkin and Meisner, 1987) uses the fraction of cloud colder than 235 K in the IR with a fixed rain rate. More complex algorithms have been developed with varying degrees of success, such as GOES IR rainfall estimation technique (auto-estimator) by Vicente et al. (2002) and the GOES multispectral rainfall algorithm (GMSRA) by Ba and Gruber (2001). A number of inter-comparison projects have taken place to assess the validity of satellite estimates at different spatial and temporal scales (Ebert et al., 1996; Adler et al., 2001). Results showed that the passive microwave (PM) estimates produced the best instantaneous results and the IR based estimates provided the best long-term estimates. Adler et al. (1993) noted that the combined use of the frequent observations of the IR with the accuracy of the instantaneous PM data would be advantageous. For this reason, recently combined passive microwave (PM) and infrared (IR) technique was developed by Kidd et al. (2003) that provide better spatial and temporal resolutions of rainfall estimate. A similar method is implemented by EUMETSAT meteorological product extraction facility (MPEF) using special sensor microwave / imager (SSM/I) onboard of the US defense meteorological satellite program (DMSP) and METEOSAT satellites (<http://www.eumetsat.int>).

2.4. EUMETSAT Land Surface Products

The land surface analysis (LSA) is part of the satellite application facility (SAF) network, a set of specialised development and processing centres, serving as European Organization for the Exploitation of Meteorological Satellites (EUMETSAT) distributed applications ground segment. The LSA SAF is taking full advantage of remotely sensed data, particularly those available from EUMETSAT sensors, to measure land surface variables. Most EUMETSAT land surface products are from spin-stabilised Meteosat Second Generation (MSG), which has an imaging-repeat cycle of 15 minutes. The Spinning Enhanced Visible and Infrared Imager (SEVIRI) radiometer embarked on the MSG platform encompasses unique spectral characteristics and accuracy, with a 3 km resolution (sampling distance) at nadir (1km for the high-resolution visible channel), and 12 spectral channels (Schmetz et al., 2002). The following products are categorized as operational and pre-operational in LSA SAF that can be used with surface energy balances models: down-welling surface short-wave flux (DSSF), downwelling surface long-wave flux (DSLW), land surface temperature (LST), leave area index (LAI), Surface albedo, and fractional vegetation cover (FVC). These products have the temporal resolution of 15 minute to one day with MSG spatial resolution. The detailed description of the algorithms of all products, including atmospheric correction and generating procedures, can be found on the LSA SAF website (<http://landsaf.meteo.pt>).

Among the products, land surface temperature plays an important role in the physics of land surface, as it is involved in the processes of energy and water exchange with the atmosphere. This means that it is the primary variable determining the upward thermal radiation and one of the main controllers of sensible and latent heat fluxes between the surface and the atmosphere. Accurate values of LST are of special interest in a wide range of areas related to land surface processes. Satellite remote sensing is

the only means to provide estimates of land surface temperature (LST) for large areas. LST estimations from remotely sensed data are generally obtained from one or more channels within the thermal infrared atmospheric window from 8 to 13 μm (Dash et al., 2002). It is mainly dependent on land surface emissivity which in turn estimated independently from satellite derived fractional vegetation cover (Trigo et al., 2008). LSA SAF system largely follows previous developments achieved at Météo-France (Brisson et al., 1999) by make use of split-window algorithms (Prata, 1993; Wan and Dozier, 1996), the formulation initially developed for AVHRR and MODIS by Wan and Dozier (1996) adapted to SEVIRI split-window channels centered on 10.8 and 12.0 μm . A detailed formulation of the algorithm and product information can be found on <http://landsaf.meteo.pt>.

2.5. Aerodynamic Roughness and Displacement Heights

The most challenging problem in estimating evapotranspiration is the calculation of correct aerodynamic roughness (z_{0m}) and displacement (d_0) height. Roughness is often separated in different complexities related to its effects on land surface–atmosphere dynamics. The complexities are (1) vegetation and urban roughness, where the horizontal scale is relatively small, (2) transition roughness between landscape patches (i.e., plowed field next to a forest), and (3) topographic roughness due to changing landscape elevations. These complexities and scales have different effects on wind, heat, and water movement and are difficult to measure in the field at large scales (Prueger et al., 2004). The traditional way to calculate z_{0m} is based on the Monin-Obukhov similarity by extrapolating wind profile observations at several levels under neutral condition. For non-neutral conditions, it is necessary to solve the wind profile relationship iteratively to obtain a fitted solution (Lu et al., 2009). Furthermore, z_{0m} can also be obtained with an eddy covariance system observation at a single level.

Many studies have focussed on estimating the roughness height of different land cover types like forest, crop, grass, shrubs, built-up areas, etc. (Borak et al., 2005; Champeaux et al., 2000; Lu et al., 2009; Lyra and Pereira, 2007; Prueger et al., 2004; Su et al., 2001). According to these studies, the variation of z_{0m} over different surfaces is large, from 0.7-2.3m over tropical forest or urban areas and mountainous areas to an order of 0.1 mm or occasionally 0.01 mm over smooth water body surfaces, ice and snow surfaces (Wieringa, 1993). Other researchers (Brutsaert, 1982; Waters et al., 2002) have proposed some parameterizations between the aerodynamic roughness length and displacement height and the land surface physical properties e.g., vegetation height, leaf area index (LAI) and normalized difference vegetation index (NDVI). The most commonly used relationship is to assume d_0 and z_{0m} proportional to the roughness element height (h). Large variations in the ratio of z_{0m}/h over different land surfaces are found in the literature. For example, z_{0m}/h is 0.04 for sparse sorghum (Azevedo and Verma, 1986); 0.14 for small cotton (Kustas et al., 1989), and 0.8 for cotton of intermediate foliage density (Hatfield, 1989). Matthias et al. (1990) and Garratt (1992) found $z_{0m}/h = 0.1$ as a rough estimate from a review of literature even though Garratt noted that the ratio can range from 0.02 to 0.2 for natural surfaces. In many land surface models, z_{0m} and d_0 are taken as a constant according to vegetation type (Dickinson et al., 1993; Dorman and Sellers, 1989). Dai et al. (2003) took z_{0m} as a constant ratio of vegetation height, i.e., $z_{0m} = 0.07h$, and Matthias et al. (1990) derived $d_0/h = 0.5$ for small cotton. In the remote sensing models that used to estimate the regional evapotranspiration, for instance, in SEBS NDVI and h were used to estimate z_{0m} and d_0 (Liu et al., 2007; Su, 2002; Su and Jacobs, 2001), SEBAL uses an empirical relationship between NDVI and z_{0m} (Bastiaanssen, 1995; Waters et al., 2002).

3. Study Area

The study area of this research is the main land of Spain in **Iberian Peninsula**, or **Iberia** region, which is located in the extreme southwest of Europe. However, the study addressed the situations in the most part of Spain; particular attention was made in Castilla y Leon region (see Fig. 3-1) due to the availability of real time meteorological data in the region. The geographic location of Spain extends from the southernmost extremity at 36°00'15"N 5°36'37"W the northernmost extremity at 43°47'38"N 7°41'17"W westernmost extremity at 42°55'1.07"N 9°17'10.28"W to the easternmost extremity at 42°19'09"N 3°19'19"E with approximate area of 505,000 km². The Castilla y Leon region has approximate area of 23400 km². Generally, the Iberian Peninsula is dominated by the Meseta (central plateau); a great uplifted fault block (average elevation 610 m) ringed and crossed by mountain ranges (http://en.wikipedia.org/wiki/Iberian_Peninsula).

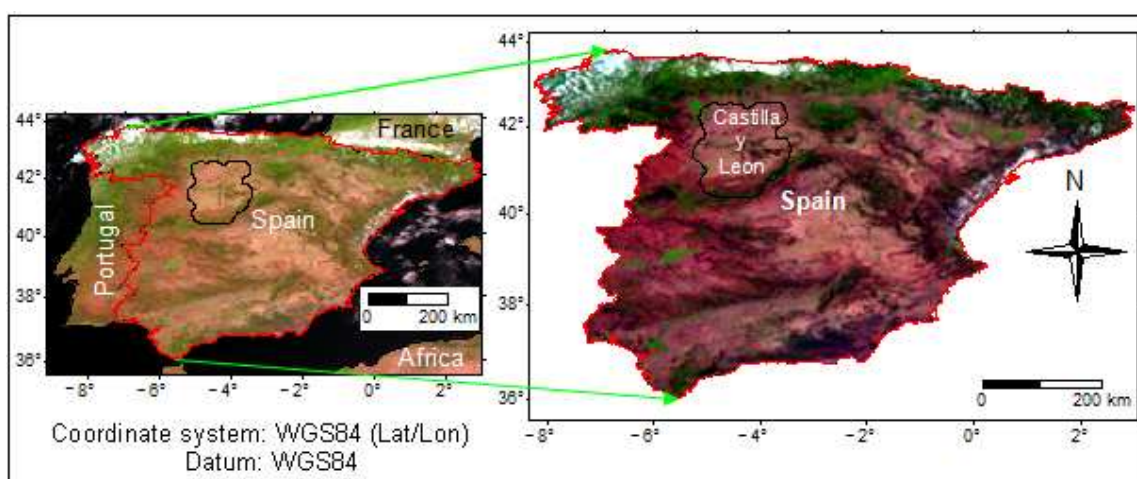


Figure 3-1. The RGB (channel 1, 2 and 3) color composite of MSG images covering the study area (July, 15, 2009 at 11:15 UTC)

3.1. Climate

Spain is dominated by Mediterranean climates which are characterized by winter rains - with some months of excess rainfall over evapotranspiration, warm and dry summer months with moisture deficits-drying out soils and their annual vegetation (xeric moisture regime). Generally, Spain has hot summers, cold winters, and limited precipitation (Peel et al., 2007). The climates of the region are divided into three main climatic zones Fig. 3-2.

1. Atlantic climate (oceanic climate) of northern coast: Average temperatures here are 9°C in winter and 18°C in summer. This is the wettest part of the peninsula with annual rainfall between 800-1500mm.
2. Continental climate of interior central plateau (mesetas). It covers the majority of Spain. Continental winters are cold at -1 to -15 °C with strong winds and high humidity, despite the low precipitation. Summers are warm and cloudless, producing average daytime temperatures that reach 21 °C to 27 °C and nighttime temperatures range from 7 °C to 10 °C. The annual precipitation is 300- 640 mm, and heavy snowfalls occur in winter.

3. Mediterranean climate region: This region roughly extends from the Andalusian Plain along the southern and eastern coasts up to the Pyrenees. The average temperatures in the region are 11°C in winter and 23°C in summer. The annual precipitation is between 250 mm and 600 mm.

In addition to the above mentioned climate zones, there are two small zones characterized by mountainous and semi-arid climate zones Fig. 3-2. The mountain climate is in areas with sizeable mountain ranges. These areas are characterized by cold winters and mild summers, with a predominance of cold temperatures. The semi-arid climate zone takes up southeast of Spain in Almeria. This area of Spain is characteristically hot and dry, with very little rainfall.

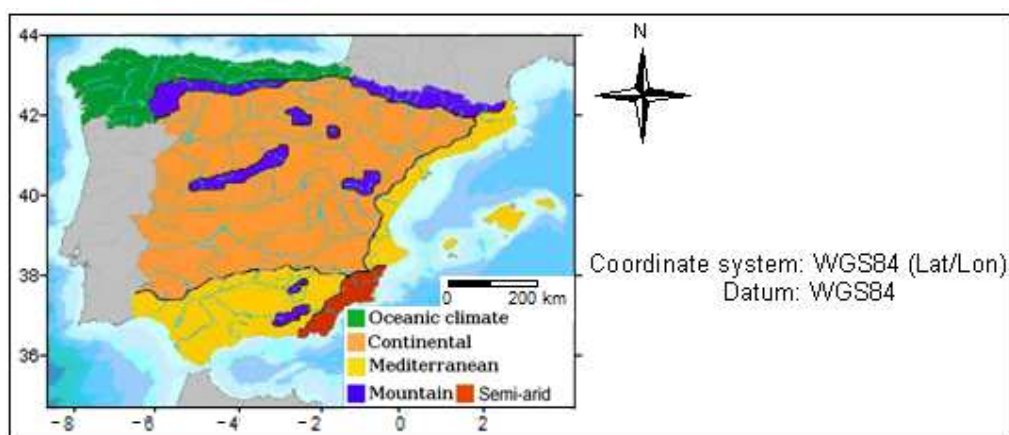


Figure 3-2. Spain climate zones (source: <http://www.worldweather.org/083/m083.htm>)

3.2. Geology

Studies show that the geology of Spain is extremely variable with sites. In order to give a general idea of the geological constitution of the region, it has three principal divisions, viz. the Crystalline or Gneissoid formations; the Transition formations; and the Secondary. Generally, researches believed that the Spanish physical geography directly reflects the underlying geology with the present geomorphology (Door and Teresa, 2002). Fig. 3-3 shows the dominant soil types in the geography of Spain.

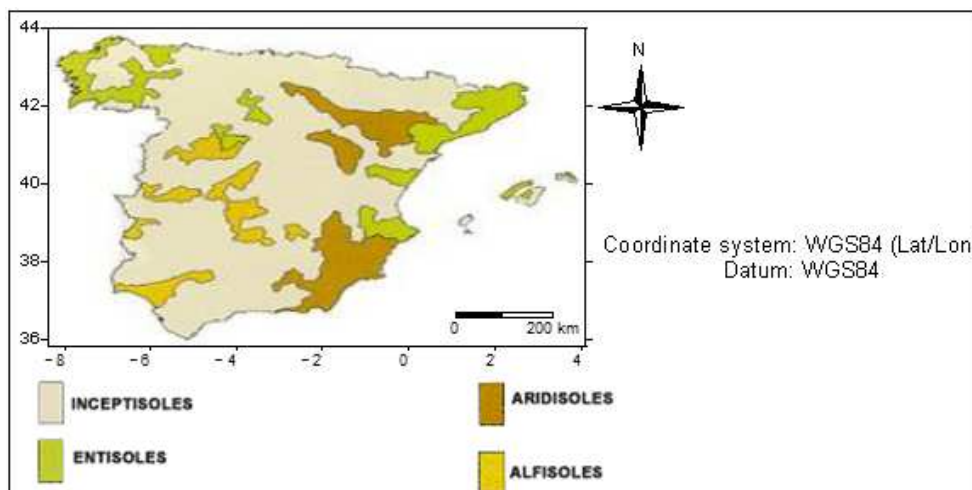


Figure 3-3. Soil Map of Spain, Source: Spanish system of water information (<http://hispagua.cedex.es>)

4. Materials

4.1. General

In this research, both ground-based and remote sensing data were collected for estimation of actual evapotranspiration using SEBS model. Apart from that, the finished products of evapotranspiration and rainfall were collected for comparison and water balance estimation respectively. Both remote sensing and ground-based data collected for this work cover the study period of seven months from March, 15 – September, 15 2009. Except rainfall data, all data described in this chapter were collected for 3-4 days per month for a total of 22 days during the study period. The rainfall product was collected for the whole study period. The selection of days in each month was based on the daily rainfall occurrence and clear sky over the study area.

4.2. Remote Sensing Data

4.2.1. EUMETSAT Land Surface Products

In this research, the main input data from remote sensing observation were taken from GEONETcast data stream of European organisation for the exploitation of meteorological satellites on land surface analysis satellite application facility (EUMETSAT LSA SAF) and meteorological product extraction facility-Multi-sensor precipitation estimate (MPEF-MPE) via <http://landsaf.meteo.pt> and <http://www.eumetsat.int> respectively. Table 4-1 summarizes the detail information of these data. All products from are derived from spinning enhanced visible and infrared imager (SEVIRI) radiometer embarked on the Meteosat second generation (MSG) platform and other European satellite systems within the area covered by the MSG disk for European window with MSG spatial resolution.

Table 4-1. Land surface products from EUMETSAT LSA SAF

Product name	Acronym	Unit	Temporal resolution
Land surface temperature	LST	°C	15 Minute
Down-welling surface short-wave radiation	DSSF	W/m ²	30 minute
Down-welling surface long-wave radiation	DSLRF	W/m ²	30 minute
Land surface Albedo	Albedo	-	daily
Fraction of Vegetation cover	FVC	-	daily
Leave Area Index	LIA	m ² /m ²	daily
MSG Evapotranspiration	MET	mm/hr	30 minute

These data are in HDF5 file format which were converted to raster via GEONETCast toolbox and batch file processing in ILWIS. According to the validation report of all products, there is a good agreement between the satellite estimates and the in-situ data when comparing in instantaneous and daily time series. Therefore, it is convenient to use all products for research purposes. Detailed descriptions of the products including validation reports and algorithms of all data streams can be found on the website <http://landsaf.meteo.pt/algorithms.jsp>.

4.2.2. MODIS Land Surface product

The 16 days NDVI products with 250m spatial resolution of Moderate-resolution Imaging Spectroradiometer (MODIS)-Terra satellite and Level-1B images were downloaded from U.S geological survey land processes distributed active archive center (LA DAAC) and level 1 and atmospheric archive and distribution system (LAADS) via their website (<https://lpdaac.usgs.gov>). All images and land surface product data are in HDF format which were converted to raster using HDF-EOS to GeoTIFF (HEG) tool. The NDVI product is grid vegetation-index maps use as input MODIS-Terra surface reflectances, corrected for molecular scattering, ozone absorption, and aerosols, and adjusted to nadir and standard sun angles with bidirectional reflectance distribution factor (BRDF) models. A detailed description of the product and related algorithms can be found in the “MODIS Vegetation index Algorithms theoretical basis document” at link <http://modis.gsfc.nasa.gov/data> and other literature such as; Deering (1978), Huete et al (1999), Colwell (1974), and (Huete et al., 1994). The three tile products were mosaicked to get the whole coverage of the study area during this work.

4.2.3. Digital Elevation Model

The SRTM data is available as 3 arc second (approx. 90m resolution) DEMs. The vertical error of the DEM's is reported as less than 16 m. The data is currently being distributed as finished product contains no data holes where water or heavy shadow prevented the quantification of elevation. For this study, three tiles of 5*5 degree SRTM DEM maps were taken from the consultative group for international agriculture research-consortium for spatial information (CGIAR-CSI) via <http://srtm.csi.cgiar.org/>. It available in both ArcInfo ASCII and GeoTiff format which facilitate their ease of use in a variety of image processing and GIS applications. The DEM of the entire study area (see Fig. 4-1) was obtained by making the mosaic of the three tiles.

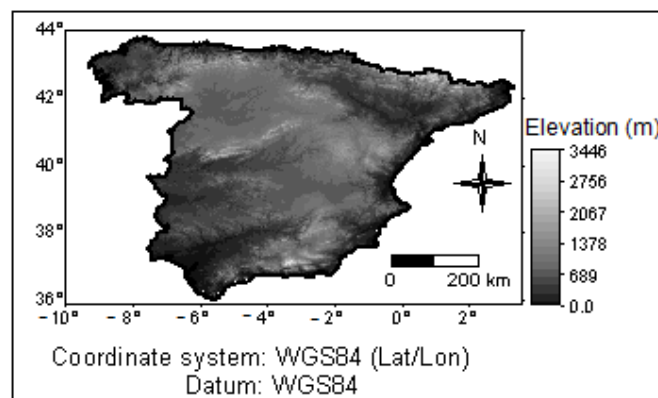


Figure 4-1. SRTM digital elevation model of Spain

4.2.4. Precipitation Products

Currently, precipitation products from Meteosat-7, Meteosat-8 and Meteosat-9 are produced in near real-time by EUMETSAT MPEF. For this thesis, the multi-sensor precipitation estimate (MPE) from Meteosat-9 which consists of the rain rate in mm/hr was used. It has the temporal resolution of 15 minute. This product is currently aggregated to daily rain rate at the ITC (personal computer of Dr. Ben Maathuis).

4.3. Meteorological Data

4.3.1. Spain Online Climate Data (Inforiego)

Inforiego is the climate information tool from Spain local meteorological organization which supplies climate data and water use by crops through internet for Castilla y Leon region. It contains near real time data measured at dense ground meteorological stations for only Castilla y Leon region (Fig. 4-2). This data has the temporal resolution of 30-minutes. Information on how to download the data online and the geographic locations of the stations was collected from local meteorological organization and inforiego website (http://www.inforiego.org/opencms/info_meteo). Additional information on the data type and spatial distribution of the stations are given in the Table 4-2 and Fig. 4-2 respectively. This data was used to calculate the instantaneous and daily evaporative fraction (EF) for Castilla y Leon region.

Table 4-2. Real time meteorological data types from 40 stations in the study area

Parameter	Unit	Time Resolution	Data Access
Wind speed	m/s	30 minute	Online by request
Air Temperature	°C	30 minute	Online by request
Relative Humidity	%	30 minute	Online by request
Precipitation	mm	30 minute	Online by request
Solar Radiation	W/m ²	30 minute	Online by request
Sunshine hours per day	hrs	Daily	Online by request

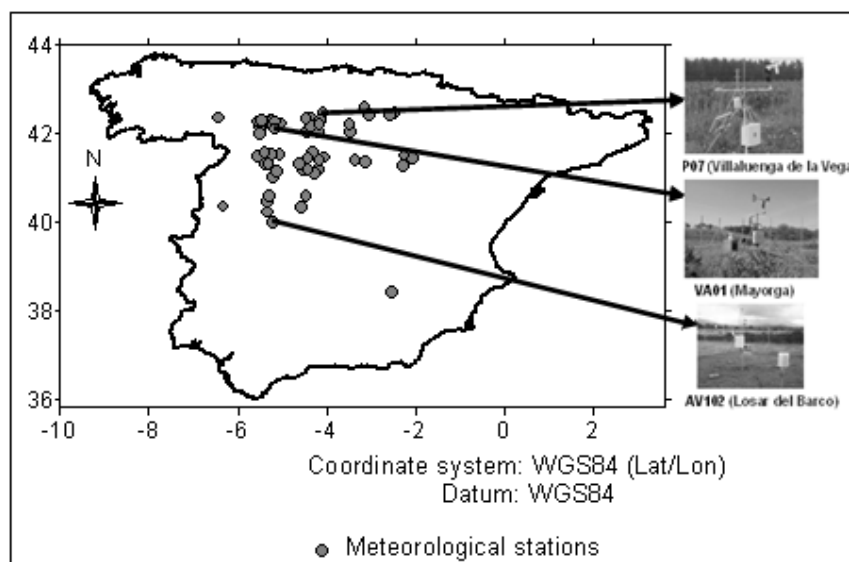


Figure 4-2. Spatial distribution of near real time data from Inforiego

4.3.2. NOAA National Climate Data Center (NNDC)

The national climatic data centre (NCDC) is part of department of national oceanic and atmospheric administration (NOAA), which provides daily global climate data, and other weather related data free of charge. This weather data is representative of world meteorological organization (WMO)-resolution 40, the world data centre system, and other international scientific programs. Accordingly, the daily meteorological data for the whole Spain was downloaded from their website

(<http://www7.ncdc.noaa.gov/CDO/cdo>). This data was used to estimate EF from daily averaged data to compare with instantaneous EF and daily averaged EF. Table 4-3 and Fig. 4-3 show the data type and the spatial coverage of the data respectively.

Table 4-3. Meteorological data from NNDC and WMO

Parameter	Unit	Time Resolution	Data Access
-Wind speed -Max. wind speed	Knot	Daily	Online by country
-Air Temperature -Max. Temperature -Min. Temperature -Dew point Temperature	°F	Daily	Online by country
Precipitation	mm	Daily	Online by country
Air Pressure	mb	Daily	Online by country
Sea level Pressure	mb	Daily	Online by country
Visibility	Km	Daily	Online by country
Snow depth	in	Daily	Online by country
Number of observations used to calculate the daily values for all parameters	count	Daily	N/A

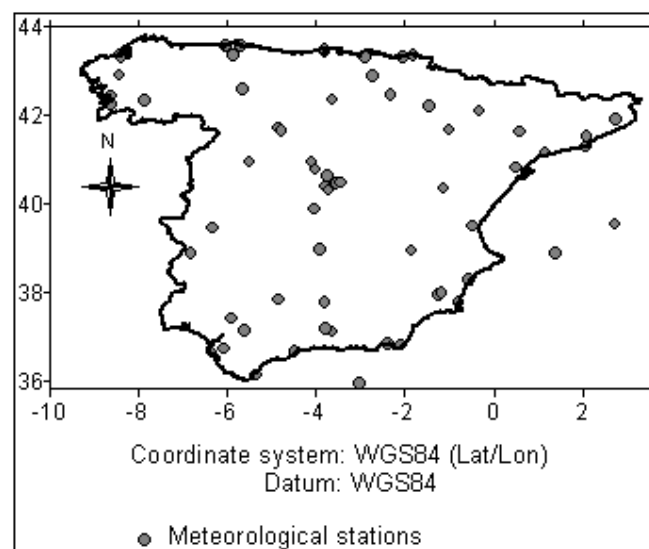


Figure 4-3. Spatial distribution of stations with daily averaged data

4.4. Field Data

Field work was carried out in the month of September from 1-14, 2009 in some part of the study area (approx. 70 x 70 km). The main objective of this field work was to collect the data required for the validation of land cover product and other land cover physical parameters and meteorological data.

4.4.1. Land Cover Classification

During the field work some required land cover information were collected. The collected land cover types with associated information and methods used during the work are summarized in Table 4-4.

Table 4-4. Land cover data collected during field work

S.No.	Collected data	Methods/Equipment used
1	Land cover type	Physical observation
2	Vegetation Height (H)	Tape measurement and clinometer
3	Picture of the site	Digital Camera
4	Geographic location	GPS

The land cover classification product of the whole of Spain was taken from European space agency (ESA), prepared by Globcover land cover classification project. This product contains detailed product description and validation report. It is the latest land cover classification product available as of 2008-12-10 and can easily be accessed at <http://www.esa.int/due/iona/globcover>. This product was generated by automated processing chain from the 300m spatial resolution of environmental satellite's (ENVISAT's) medium resolution imaging spectrometer (MERIS) time series images which is unsupervised type of classification that need to be checked before use (Bicheron et al., 2008).

As recommended by distributor, this product was validated against the ground truth collected during field work. Table 4-5 illustrates the naming of land cover type and associated information for validation of this product.

Table 4-5. Land cover classes, vegetation height and number of collected points for each land cover class

ID.	Field name	Equivalent name in ESA land cover product	Av.canopy height(m)	No.of points
11	Maize, sun flower and alfalfa	Irrigated crop lands, irrigated shrub three crops, irrigated herbaceous crop.	2.3,1.2, 0.35	13
14	Wheat and barley	Rainfed crop lands, rainfed shrub or three crops, rainfed herbaceous crop	0.65	10
20	Mixed maize, grass, three, harvested wheat	Mosaic cropland (50-70%) / Vegetation (grassland/shrubland/forest) (20-50%)	2.4	3
30	Shrubs, small trees, wine yard	Mosaic vegetation / grassland/shrubland/forest (50-70%) cropland (20-50%)	2.1	3
40	Mixed forest needle and broad leaved	Closed to open (>15%) mixed broadleaved and needleleaved forest (>5m) Closed to open (>15%) broadleaved or needleleaved, evergreen or deciduous, shrubland (<5m)	7 3.5	2

50	Broad leaved Forest	Closed (>40%) broadleaved forest or shrubland	7	
		Closed (>40%) broadleaved deciduous forest (>5m)	8.5	3
60	Open broadleaved forest	Open (15-40%) broadleaved deciduous forest/woodland (>5m)	8	2
70	Needleleaved forest	Closed (>40%) needleleaved evergreen forest (>5m)	7.5	4
90	Open needle leaved forest	Open (15-40%) needleleaved deciduous or evergreen forest (>5m)	6	2
150	Sparse vegetation	Sparse (<15%) vegetation	6	5
190	Built up area	Artificial surfaces and associated areas (Urban areas >50%)	7.0	4
110, 120	Mixed forest, grass, shrubs	Mosaic forest or shrubland (50-70%) / grassland (20-50%) Mosaic grassland (50-70%) / forest or shrubland (20-50%) Closed to open (>15%) grassland or woody vegetation on regularly flooded or waterlogged soil	3.5	3
210	Water body	Water body	0	1
200	Bare areas	Bare area	0.009	3

The processes of validation involved generation of a point map showing different land cover classes collected during field work. The point map is then overlaid on ESA globcover land cover classification for a small part of the study area (Fig. 4-4).

The comparison was done manually by checking whether the location of point on the ESA land cover classification product is agreed with collected land cover information according to the naming system in the Table 4-5.

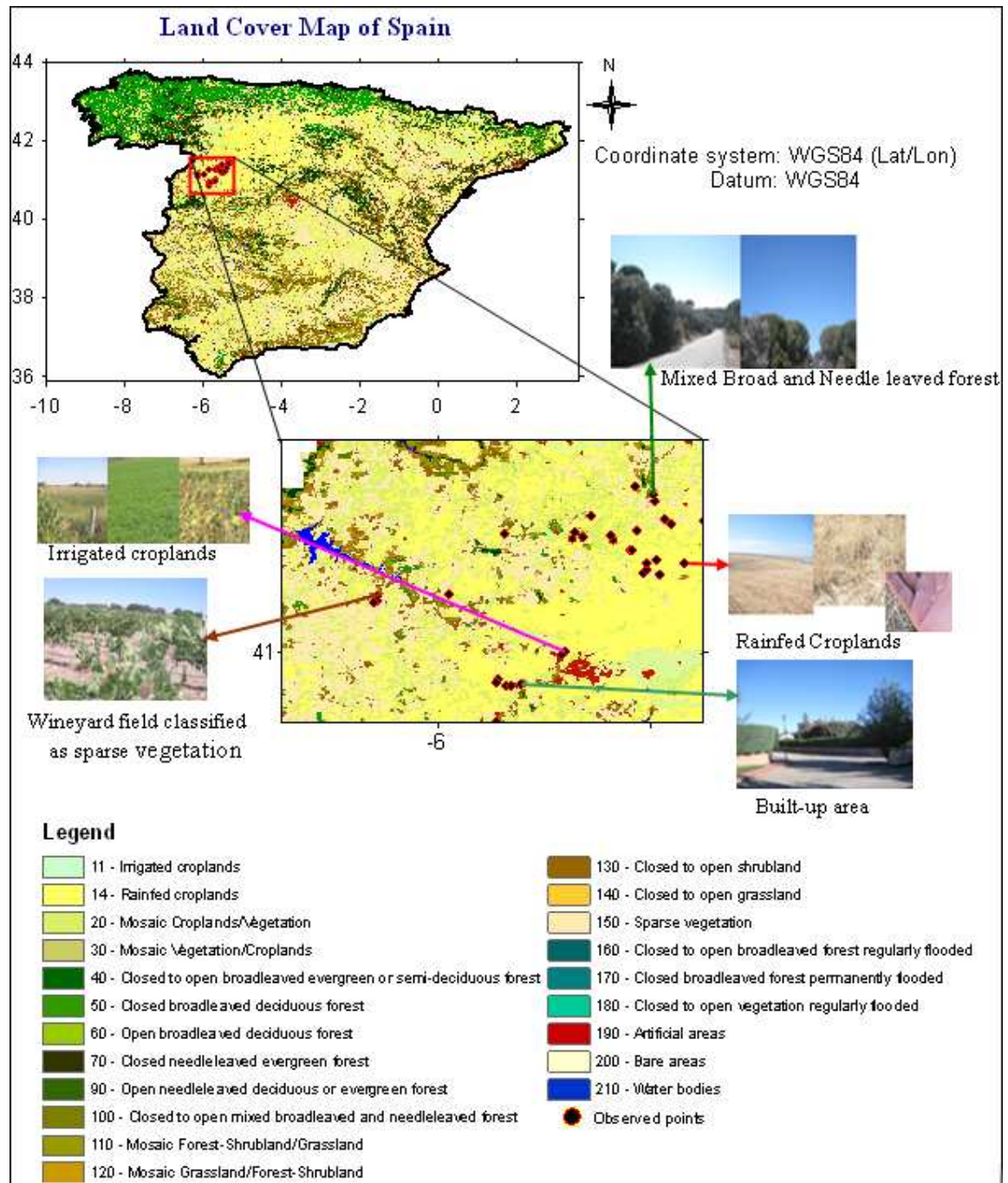


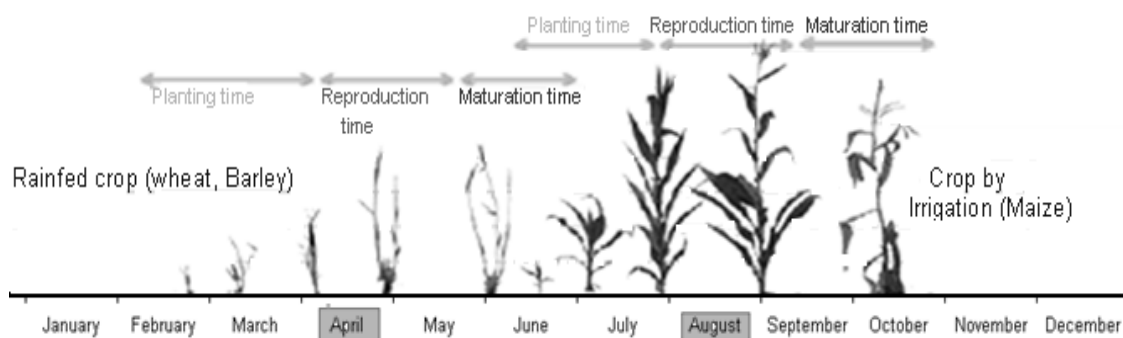
Figure 4-4. ESA land cover classification map overlaid with point map of observed locations

4.4.2. Crop Calendar

The crop calendar used in this study contains the recent information on growing seasons of different crops in Spain during rainy season and by irrigation. This data was taken from Martín (2009) in Spanish language which was translated into English in this work (see Table 4-6 and Fig. 4-5). The main purpose of this crop calendar is to assign the crops height to land cover classification map to have right information of surface roughness in the cropland during the study period.

Table 4-6. Detail Crop calendar for crops growing in Spain

Regimen	Crop Type	Planting time	Maximum	Harvesting time
Summer irrigation	Potatoes	April-May	June-July	September-October
	Maize	April	August	October-December
	Beetroot	March	July	October-November
	Alfalfa	April	May-August	Not specified
	Sunflower	April-May	July	October
Spring irrigation	Short-cycle cereal crops (wheat, barley), industrial crops(rape)	February	May	June-July
	Vegetables	May	June-July	August-September
Rainfed long cycle	Cereals (wheat, rye, oats, triticale, barley)	October-November	May	July
	Legumes(peas and lentils)	October	May	July
Rainfed short cycle	Cereals	February	May	July
	Legumes(chickpea)	March	May-June	July
Variable	Grapevine	Not specified	June	September


Figure 4-5. Schematic representation of growing stages and seasons for the two main crops in Spain

4.4.3. Eddy Covariance Data

An eddy covariance system of 10m high tower was installed in June, 2009 in the Sardon catchment, Trabadillo area (see Fig. 4-6) by WRS-ITC staff members. The land cover class of the tower site is sparse vegetation, dominated by two oak (*Quercus*) tree species. This site is relatively homogenous land cover class over large area that can represent MSG spatial resolution. The data from the system was collected during field work and used to validate the performance of the model over sparse vegetation only. The raw data was processed to equivalent latent heat flux at every 30 minute time by Rwasoka (2010).

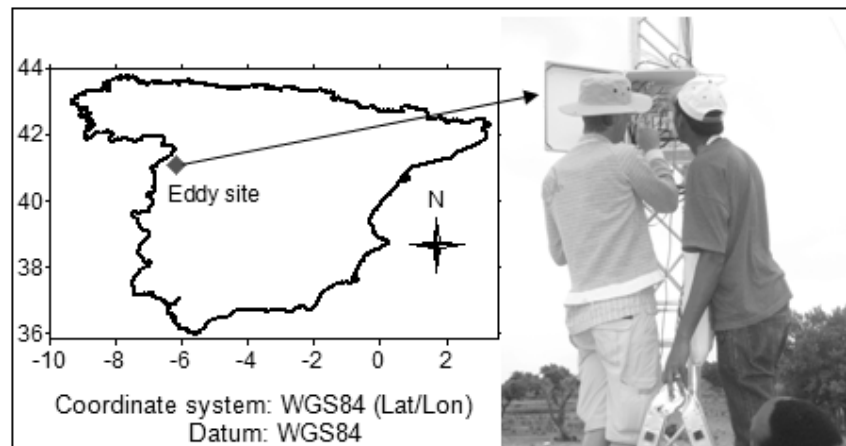


Figure 4-6. Location of an eddy covariance tower in the study area

4.4.4. Radiosonde data

The radiosonde data recorded twice a day at 00:00 and 12:00 UTC at seven locations in Spain. This data was obtained from university of Wyoming department of atmospheric science via their web site <http://weather.uwyo.edu/upperair>. The data was used to determine the height of atmospheric boundary layer (ABL). Fig. 4-7 shows the spatial distribution of the stations over the study area.

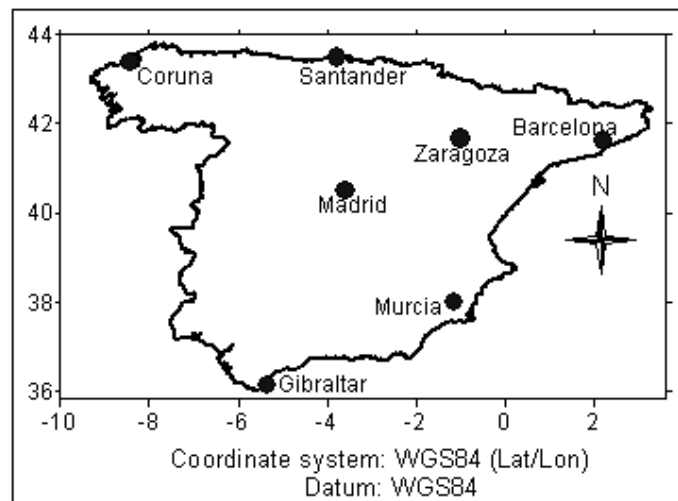


Figure 4-7. The spatial distribution of radiosonde stations in Spain

5. Methodology

5.1. General

In this research, the surface energy balance system (SEBS) model derived by Su (2002) for the estimation of atmospheric turbulent fluxes was used. Most surface energy balance models are based on the conservation of energy principle; likewise SEBS model is based on the energy involved in the soil-vegetation-atmosphere interface, which can be given as energy balance equation;

$$R_n = H + LE + G_0 \quad (5-1)$$

where, R_n is the net radiation [W m^{-2}], H is the sensible heat flux [W m^{-2}], LE is the latent heat flux [W m^{-2}], and G_0 is the soil heat flux [W m^{-2}].

In order to estimate these energy balance components, SEBS model requires remote sensing data (land surface temperature (LST), Albedo, Emissivity (ϵ), Down-welling surface short-wave flux (DSSF), leave area index (LAI), Fraction of vegetation cover (FVC), normalized difference vegetation index (NDVI), and Digital elevation model (DEM)), ground-based meteorological data (air temperature, wind speed, specific humidity and air pressure) at standard height, ground geometrical data (displacement height and roughness height or vegetation height) and other data (Solar zenith angle, sunshine hours per day and height of atmospheric boundary layer). All these data used in this study are either estimated or collected from trusted sources with required temporal resolution and resampled to the required spatial coverage. The detail procedures are explained in the previous and this chapter. The products from EUMETSAT LSA SAF were resampled to 300m to fit with the higher resolution products (MODIS and MERIS). A detailed description on calculation and formulation of each energy balance components and other related parameters can be found in Su (2002).

The analysis in this thesis was done for two seasons (wet and dry) from March to September, 2009 in the Castilla y Leon region. The main purpose of considering these seasons are to check weather we are able to estimate reasonable daily AET over different land cover classes in the study region using SEBS model at different climate conditions. In this region, February – July is the growing season of short cycle rainfed crop and for crops growing by spring irrigation. Similarly, April-September is the growing season for crops with summer irrigation. The rainfed crops and crops by irrigation reach their maximum coverage (reproduction time) in May and August respectively. Therefore, we expect relatively high evaporation in these two land cover classes in the month of May and August. Generally, four sets of analysis were done; each analysis was targeting different objectives.

The first set of analyses was done for 15th, March, 2009. It comprised the estimation of instantaneous EF from 07:00 – 18:00 UTC at an hourly time step, daily average EF and EF from daily averaged data. This analysis was done for different land cover classes in the study area. Its aim was to compare the daily average EF with instantaneous EF and EF from daily data for different land cover classes. However, the possibility of using average daily data in SEBS model is not clear for me; the main objective of estimating EF from daily data was to test whether the daily averaged data can be used to estimate daily AET with SEBS model when instantaneous meteorological data are not available.

The second analysis was estimation of hourly AET (07:00 – 18:00 UTC) on 05th, September, 2009 over sparse vegetation located in the Sardon catchment, Trabadillo. The purpose of this task was to compare the measured AET with SEBS estimated AET and MET in sparse vegetation

Estimation of daily AET for selected days per month was the third analysis. It involved the selection of dates in each month (from 15, March, 2009 to 15, September, 2009) according to the rainfall distribution in the study area, particularly on the rainfed and irrigated croplands. Accordingly, the estimation of daily AET was done for a total of 22 days (March, 15, 25; April, 05, 11, 15, 26; May, 01, 05, 15, 27; June, 05, 11, 15, 25; July, 05, 14, 21; August, 03, 16, 25 and September, 05, 15, 2009). These days are after and before the rainy day or sometimes the rainy day itself if the sky is cloud free at the time of interest (Mid day). The main reason for selecting the specific days in each month was due to time constraints of the research work to carry out the analysis for the whole study period (214 days) in these two seasons. In addition, the instantaneous EF was used in calculating the daily AET for selected days in each month. The objectives of this analysis were to compare daily AET estimated by SEBS model with MET at regional as well as local scale, and to estimate the time series of ET in the seasons over different land cover types.

The final analysis was estimation of water balance over rainfed croplands (see the location of selected pixel on Fig. 6-14). The main objective of this analysis was to test whether we are able to estimate a simple water balance “precipitation minus actual evapotranspiration ($P - AET$)” using products from geostationary satellites and SEBS model for a specified pixel throughout the study period. This principle of water balance estimation is known as “climatologically water balance” in agricultural research which often used to forecast whether or not irrigation is required at a specific site (Böhm et al., 1998). It is also referred to the net flux of water from the atmosphere to the earth’s surface. In this research, it was used to identify the wet and dry days of the selected pixel in the rainfed cropland. The analysis was done using SEBS estimated daily AET and precipitation products from MPEF-MPE, by assuming that AET varies linearly between carefully selected days during the study period.

Finally, comparisons were made at different scales within results, with ground data, and with similar product from EUMETSAT. In these comparisons, the following simple statistical methods were used; (1) coefficient of determination /square of correlation coefficient (R^2), it provides a measure of how well outcomes are likely to be predicted by the model or it is the measure of how well the regression line represent the data, (2) correlation coefficient (r), it measures the strength and the direction of a linear relationship between two variables (3) standard error, it is a measure of the amount of error in the prediction of variables for an individual measured values, (4) absolute error (abs. error), it is the magnitude of the difference between the measured value and the approximation, (5) percentage error (% error), when the relative error is expressed in percentage (see the formula of all parameters in Appendix F).

The flow chart in Fig.5.1 outlines the general workflow of the thesis that was followed during data preparation, analysis, and displaying of the results. In addition, the detailed descriptions of the procedures followed when determining each parameter including calculation procedures and formulations are given in the next sub topics.

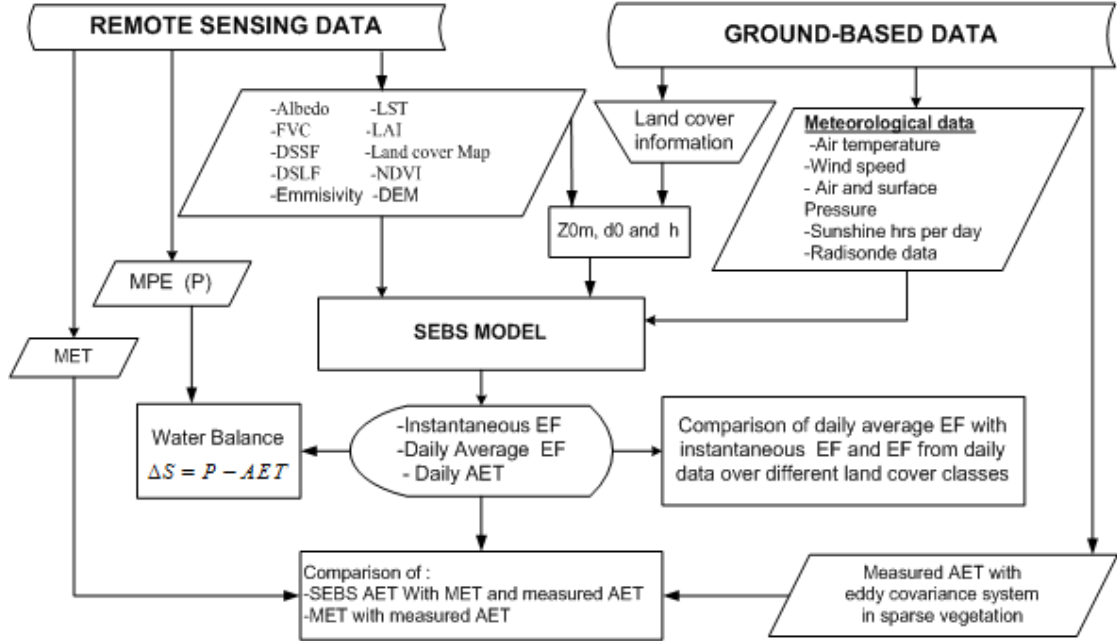


Figure 5-1. A simplified flow chart of the research methodology – the main operational steps

5.2. Atmospheric Parameters

5.2.1. Air and Surface Pressure

The sea level pressure and air pressure were collected from NOAA Notational climate data centre (NNDC). It was corrected for elevation using the following formula after interpolation of point sea level pressure to grid.

$$P = P_o \cdot \left(\frac{293 - 0.0065Z}{293} \right)^{5.26} \quad (5-2)$$

where P is the air pressure at the reference height [Pa] and P_o the air pressure at sea level [Pa], and Z the elevation above sea level [m], It is the elevation of the terrain (from a DEM).

5.2.2. Air Temperature

The air temperature record over the study area was obtained from NNDC and Inforiego. It was converted to Kelvin and corrected for elevation using the following routine formulas:

$$T_{air} = 5/9 \cdot (T_F - 32) + 273.16 \quad (5-3)$$

$$\Theta = T_{air} \cdot \left(\frac{P_o}{P} \right)^{0.286} \quad (5-4)$$

Where P is the air pressure [hPa], T_{air} the air temperature in [K], Θ is the potential temperature [K], and T_F is air Temperature [°F].

The potential temperature at sea level was interpolated to calculate the air temperature by considering the effect of elevations as follows:

$$T_{air} = \Theta \cdot \left(\frac{P}{P_o} \right)^{0.286} \quad \text{by substituting } P \text{ with equation (5-2):} \quad (5-5)$$

$$T_{air} = \Theta \cdot \left(\frac{293 - 0.0065 \cdot Z}{293} \right)^{1.50436} \quad (5-6)$$

5.2.3. Wind Speed

The real time wind speed from Spain online climate data was directly used without applying any correction. But, the daily average wind speed data obtained from NNDC was used after conversion to m/s unit using the following simple unit conversion (1 international knot = 0.514 meters per second). No effect of elevation applied due to its complexity.

5.2.4. Specific Humidity

Neither specific nor relative humidity is directly available from online NOAA Notational climate data centre (NNDC). The specific humidity was estimated from actual vapour pressure and air pressure using the following formula:

$$q = \frac{0.622 \cdot e_a}{P - 0.378 \cdot e_a} \quad (5-7)$$

where e_a actual vapour pressure [hpa], P air pressure [hpa], and q specific humidity [kg/kg]

$$e_a = a_0 + T_{dew} \cdot (a_1 + T_{dew} \cdot (a_2 + T_{dew} \cdot (a_3 + T_{dew} \cdot (a_4 + T_{dew} \cdot (a_5 + T_{dew} \cdot a_6)))) \quad (5-8)$$

where T_{dew} = Dew point temperature in Kelvin, and

$$\begin{aligned} a_0 &= 6984.505294 & a_1 &= -188.903931 & a_2 &= 2.133357675 & a_3 &= -1.288580973 \cdot 10^{-2} \\ a_4 &= 4.393587233 \cdot 10^{-5} & a_5 &= -8.02392 \cdot 10^{-8} & a_6 &= 6.136820929 \cdot 10^{-11} \end{aligned}$$

Since the dew point temperature is not available for the data from Spain local meteorological organization (Inforiego), the daily actual vapour pressure was calculated from saturated vapour pressure and relative humidity using the following formulas adopted from (Allen et al., 1998):

$$e_a = \frac{e_s(T_{\min}) \cdot \frac{RH_{\max}}{100} + e_s(T_{\max}) \cdot \frac{RH_{\min}}{100}}{2} \quad (5-9)$$

$$e_s(T) = 0.6108 \exp \left[\frac{17.27 \cdot T}{T + 237.3} \right] \quad (5-10)$$

where e_s saturation vapour pressure at the air temperature T [Kpa], T the maximum and minimum air temperature of the day [°C], RH the maximum and minimum relative humidity of the day [%], and e_a is actual vapour pressure [Kpa].

For instantaneous specific humidity, the instantaneous actual vapour pressure was estimated as;

$$e_a = \frac{RH \cdot e_s}{100} \quad (5-11)$$

where e_s is instantaneous saturation vapour pressure at the air temperature T [Kpa], RH is instantaneous relative humidity [%], and e_a is instantaneous actual vapour pressure [Kpa].

5.3. Solar Information

5.3.1. Sun Zenith Angle

The solar zenith angle (θ) was calculated using the following equation:

$$\theta = \cos^{-1}[\sin(\phi) \cdot \sin(\delta) + \cos(\phi) \cdot \cos(\delta) \cdot \cos(\omega)] \quad (5-12)$$

where ϕ is latitude of the area, δ is solar declination, and ω is hours angle. The detail calculation of all parameters can be read from Iqbal (1983).

5.3.2. Sunshine hours per day

Sunshine hours per day are available at some stations which shows more or less similar records at all stations. For this reason, average values of the station records are used. A small variation of sunshine hours per day has a negligible effect on the large scale estimation of AET (Bormann et al., 1996; Hanna and Siam, 1981).

5.4. Estimation of Land Surface Emissivity

The land surface emissivity (ϵ) for the study area was derived from an empirical formula developed by Sobrino et al. (2003; 2001). This empirical formula is relating NDVI threshold, proportion of vegetation, and red band surface reflectance with land surface emissivity as shown in the Table 5-1.

Table 5-1 Calculation of land surface emissivity

Pixel type	Mixed pixel ($0.2 \leq \text{NDVI} \leq 0.5$)	Pixels covered by vegetation ($\text{NDVI} > 0.5$)	Bare soils pixels $\text{NDVI} < 0.2$	Water body Albedo < 0.035
Algorithm	$\epsilon = 0.971 + 0.018 P_v$	$\epsilon = 0.990 + de$	$\epsilon = 0.9832 - 0.058 \rho_{\text{red}}$	$\epsilon = 0.995$

Where P_v is proportion of vegetation, given by $\frac{(\text{NDVI} - 0.2)^2}{0.09}$, de is the emissivity difference of

MODIS Band 31 and 32, equal to 0.005 for pixels covered by vegetation, and ρ_{red} is Land surface reflectance of red band (MODIS Band1).

5.5. Estimation of Aerodynamic Roughness and Displacement Heights

Most studies use look-up tables, NDVI, vegetation height or from measurements of friction velocity under neutral stability condition to determine aerodynamic roughness height (z_{0m}) and displacement height (d_0) (Borak et al., 2005; Brutsaert, 1982; Gellens-Meulenberghs et al., 2008; Lin et al., 2008; Lu et al., 2009; Su and Jacobs, 2001).

In this research, the estimated vegetation height (h_c) was collected during field work. The crop calendar of the study area and FAO irrigation and drainage manual (Allen et al., 1998) are also used to estimate the crops height at different growing seasons in Spain. The detailed land cover classifications used for the assignment of vegetation height is given in Appendix D. Based on these data, the displacement height, and aerodynamic roughness height are estimated as the function of vegetation height, normalized difference vegetation index (NDVI), leave area index (LAI) using empirical formulas and look-up tables.

First, the equations of Brutsaert (1982) and Su and Jacobs (2001) were used. These empirical formulas are widely used for croplands (Eq. 5-13 and 5-15) and for forests and built-up area (Eq. 5-13 and 5-14) in regional scale estimation of evapotranspiration (Lin et al., 2008; Liu et al., 2007; Tsouni et al., 2008):

$$d_{o1} = 2/3 * h_c \quad (5-13)$$

$$Z_{om1} = 0.136h_c \quad (5-14)$$

$$Z_{om2} = 0.005 + 0.5 * \left(\frac{NDVI}{NDVI_{max}} \right)^{2.5} \quad (5-15)$$

Second, the parameterization proposed by Choudhury and Monteith (1988) was used. They used the second-order closure model results of Shaw and Pereira (1982) to estimate d_o and z_{om} :

$$d_{o2} = h_c [\ln(1 + X^{1/6}) + 0.03 \ln(1 + X^6)] \quad (5-16)$$

$$Z_{om3} = \begin{cases} Zos + 0.28 * h_c * X^{1/2} & \text{for } 0 \leq X \leq 0.2 \\ 0.3 * h_c * (1 - d_{o2} / h_c) & \text{for } 0.2 \leq X \leq 2 \end{cases} \quad (5-17)$$

Where $X = 0.2LAI$, Zos is soil roughness which can be taken as 0.009m for unvegetated substrates and $0.1 * h_s$ for vegetated substrates, h_s is the height of vegetation understory, which is indeed less than h_c . This method accounts for the effect of canopy density on roughness length. For this reason, these parameterizations Eq. (5-16 and 5-17) were selected for mosaic forest-shrubland, mosaic croplands-vegetation, shrubland, and sparse vegetation. In addition, the detail literature review made by Wieringa (1993), and work of Champeaux et al. (2000) for vegetations in Western Europe agree with the results obtained from these empirical formulas (see Table 5-2). In this table, single values are from Champeaux et al (2000) and the ranges of values are from Wieringa (1993).

Table 5-2. Land cover types and associate physical information

Land cover type	h_c (m)	d_{o1} (m)	d_{o2} (m)	Z_{om1} (m)	Z_{om2} (m)	Z_{om3} (m)	Wieringa (1993) and Champeaux et al (2000) Z_{om} (m)
Sparse Vegetation	6	4	2.93	0.78	0.07	0.44	0.206
Closed needleleaved evergreen Forest	7.5	5.0	4.51	1.16	0.24	0.74	0.8-1.6
Closed broadleaved deciduous forest	8.5	5.67	5.02	1.08	0.20	0.75	1.0-2.3
Summer crops (Maize)	2.4	1.6	2.20	0.48	0.16	0.39	0.13-0.2
Winter crops (Wheat)	0.6	0.43	0.10	0.03	0.14	0.21	0.10-0.16
Mixed broadleaved and needleleaved forest	7	4.67	2.22	0.748	0.21	0.38	1.0
Low mature crops	0.4	0.27	0.08	0.02	0.06	0.02	0.04-0.09
Mosaic forest - shrubland	3.5	2.33	2.78	0.68	0.17	0.52	0.5
Artificial surfaces	7	4.67	3.64	0.91	0.09	0.64	0.7-1.5
Shrubland	3.5	2.33	2.19	0.61	0.16	0.39	0.35-0.45

5.6. Determination of Height of Atmospheric Boundary Layer

The height of atmospheric boundary layer (ABL) can be derived with the help of two different measuring systems and methods; from radio soundings using parcel method and by temperature and humidity gradients, and from lidar backscatter measurements using the combination of averaging variance method and the high-resolution gradient method (Hennemuth and Lammert, 2006). In this work, the height of atmospheric boundary layer was estimated roughly using radiosonde data taken at mid night (00:00 UTC) and mid day (12:00 UTC) every day at stations distributed over the study area (see Fig. 4-7). The determination of this height was based on vertical profile of atmospheric variables like potential temperature, wind speed, and specific humidity. Only the vertical profile of potential temperature for Madrid station is shown as an example in the Fig. 5-2 and 5-3.

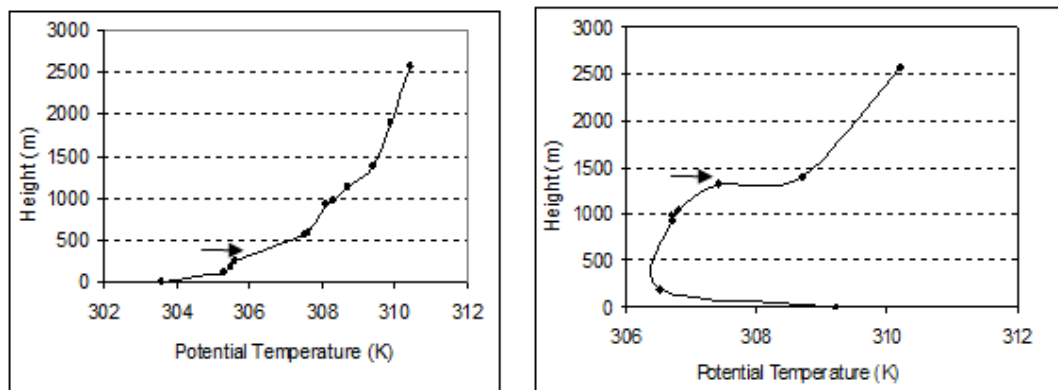


Figure 5-2. Profile of potential temperature for Madrid station on August, 15, 2009, at 00:00 (left) and 12:00 (right) UTC. **Note:** The arrows indicate the location of inversion height

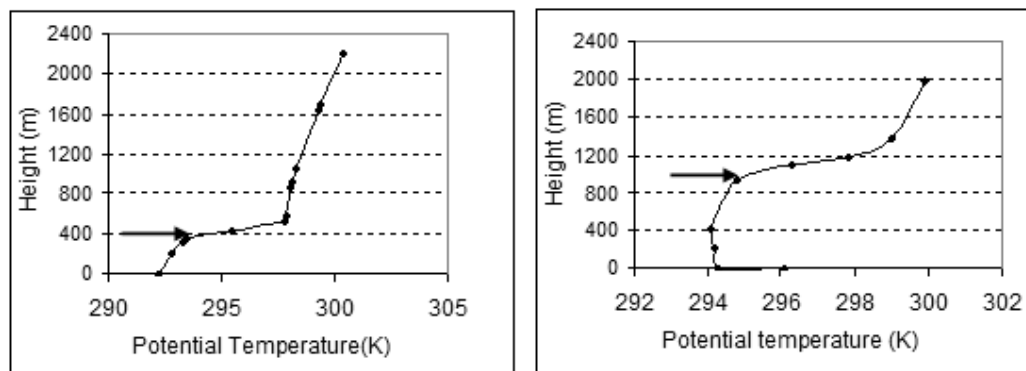


Figure 5-3. Profile of potential temperature for Madrid station on March, 15, 2009, at 00:00 (left) and 12:00 (right) UTC. **Note:** The arrows indicate the location of inversion height

5.7. Interpolation of Point Data to Grid

All atmospheric parameters (air temperature, wind speed, air pressure and specific humidity) are point measurements which need to be interpolated to the required spatial coverage. The moving average is used in this work after some comparison has been made with nearest point. The comparison was done by removing some nearby stations before interpolation and compares the outputs after interpolation has been done with remaining stations.

this work to reduce the weight of far points due to the assumption that small local variations is desired for all point values). Then, for each output pixel, an output value is calculated as given below;

$$\text{Output pixel value} = \frac{\sum (W_i * P_i)}{\sum W_i} \quad (5-19)$$

where P_i is value of point i .

5.8. Instantaneous to Daily Average

5.8.1. Land Surface temperature

Theoretically, a total of 96 images per day are available, if the processing system is not interrupted over 24hrs. Aggregating 15 minute LST product to daily values involves systematic approach using scripts and small programming in ILWIS. The average daily LST for cloud free pixels which are observed by the satellite 96 times per day (every 15 minute for 24 hours) is given by;

$$LST_{daily} = \frac{\sum_{i=1}^{i=96} LST_i}{96} \quad (5-20)$$

where LST_{daily} daily land surface temperature, LST_i instantaneous land surface temperature (every 15 minute for 24 hrs). Such simple averaging technique is not suitable for pixels with undefined values at some time interval due to cloud cover and other effects during LST retrieval. It is common in hyper temporal resolution remote sensing that most pixels are observed many times either midnight/evening/midday/morning/afternoon or at the combination of two or more of these periods. The traditional method of averaging does not give the correct average daily LST under above mentioned conditions. To overcome this problem, the 24 hrs LST products were divided in to four periods according to their time of observation (morning-midday (06:00-12:00), midday-evening (12:00-18:00), evening-midnight (18:00-00:00), and midnight-morning (00:00-06:00)) local time. In this division, the start and end of down-welling surface short-wave flux (DSSF) is used to identify the start of day and night time. This division is useful to discover whether every pixel is more or less observed by the satellite uniformly throughout the day. The pixels that are not observed consistently through out the whole periods are rejected and undefined values are assigned in the average daily LST map. According to the above division, every pixel is observed 0-24 times in each period. The number of observation of each pixel during these periods depends on the number of LST image available, which is dependent on cloud cover and other effects during retrieval. This number of observations is called N in next equations. In this method N refers to the number of pixels in each block of input pixels that are not undefined (i.e. the number of pixels that have LST value in the input maplist, or the number of observation of a pixel throughout the day).

The general expression for this averaging technique is:

$$LST_{daily} = \frac{\sum_{i=1}^{i=96} LST_i}{N} \quad \text{or} \quad LST_{daily} = \frac{\sum_{i=1}^{i=96} LST_i}{N1 + N2 + N3 + N4} \quad (5-21)$$

where LST_{daily} daily land surface temperature, LST_i instantaneous land surface temperature, $N = N1 + N2 + N3 + N4$, is the total number of pixels in the maplist with LST value which are not undefined, $N1$ number of pixels that have LST value out of 24 observations from morning to midday, $N2$ number of pixels that have LST value out of 24 observations from afternoon to evening, $N3$ number of pixels that have LST value out of 24 observations from evening to midnight, $N4$ number of pixels that have LST value out of 24 observations from midnight to morning. The threshold was developed for the number of counts to be valid for a pixel during each period to get better estimation of daily averaged LST for a pixel. Appendix C shows the pattern of LST missing data at different periods for randomly selected pixels. In these graphs a pixel with complete data (observed 96 times per day, $N=96$) is used to see the change of daily average LST value by taking the missing pattern of randomly selected pixels. As it can be seen from the graphs in appendix C, large N value does not guarantee the accuracy of daily average LST. Instead, the uniformity of N values in each period or availability only half day data give better estimation of average value (Appendix C, b, d, h, and i). Therefore, pixels that were neither uniformly nor totally observed throughout the day were rejected.

Treating the consistency of small count at each period is a tedious activity and need advanced programming which is not the objective of this research. For this reason, the minimum of 15 counts out of 24 possible counts at each period (four periods per day) was used, which is the possible thresholds that can give good estimation of daily average LST.

5.8.2. Down-welling Surface Short-wave Flux

Down-welling surface short-wave fluxes (DSSF) are generated at every 30 minute for both cloudy and cloud free pixels. Therefore, a total of 48 images are available per day. During the daylight, only 24-28 images have DSSF values. The number of available images depends on the length of the day. By taking zero DSSF during the night time, the daily DSSF is derived by averaging all images using simple averaging techniques as follows:

$$DSSF_{daily} = \frac{\sum DSSF_i}{48 - 2 * n} \quad (5-22)$$

where n is the number of missing data during the day which can be given by $48-N$, N is the number of observations of a pixel per day in the maplist that are not undefined, $DSSF_i$ is the instantaneous down-welling surface short-wave flux during the day.

5.8.3. Wind speed and Air temperature

The average of 24 hrs record of wind speed and air temperature was used to calculate the evaporative fraction from daily averaged data.

5.9. Estimation of Evaporative Fraction and Actual Evapotranspiration

5.9.1. Calculation of Instantaneous and Average Daily Evaporative Fraction

The instantaneous evaporative fraction was calculated for March, 15 and September, 05, 2009 from 7:00-18:00 hrs at every one hour steps and at mid day (12:00) for the other selected days using SEBS model. The purposes of these calculations were to compare the daily average EF with mid day EF for

different land cover classes shown in the Fig.5-5, and for estimation of daily actual evapotranspiration in the region. The evaporative fraction (EF) is given by:

$$EF = \frac{\lambda E}{R_n - G_0} \quad (5-23)$$

But in SEBS model, the instantaneous evaporative fraction (EF_{inst}) is calculated as;

$$EF_{inst} = \frac{\Lambda_r \cdot \lambda E_{wet}}{R_n - G_0} \quad (5-24)$$

$\Lambda_r = \frac{\lambda E}{\lambda E_{wet}} = 1 - \frac{H - H_{wet}}{H_{dry} - H_{wet}}$, where Λ_r is the relative evaporation [-], H_{wet} is the sensible heat flux at wet limit [$W m^{-2}$], H_{dry} is the sensible heat flux at dry limit [$W m^{-2}$], λE_{wet} is the latent heat flux at wet limit [$W m^{-2}$], R_n is the instantaneous net radiation [$W m^{-2}$], H is the instantaneous sensible heat flux [$W m^{-2}$], λE is the instantaneous latent heat flux [$W m^{-2}$], and G_0 is the instantaneous soil heat flux [$W m^{-2}$]. In SEBS, the calculation of actual sensible heat flux is based on Monin-Obukhov similarity (MOS) by solving the system of non-linear equations Su (2002). The daily average evaporative fraction (EF_d) was calculated after inverting Eq.(5-23) to estimate the instantaneous latent heat flux from 07:00 – 18:00hrs as given below;

$$\lambda E = EF_{inst} * (R_n - G_0) \quad (5-25)$$

and daily average EF is calculated as;

$$EF_d = \frac{\lambda E_d}{R_{nd} - G_{0d}} \quad (5-26)$$

where λE_d is the daily average latent heat flux [$W m^{-2}$]. The daily average latent heat flux was estimated by assuming that little evaporation during the night that can be neglected, R_{nd} is the daily average net radiation [$W m^{-2}$], G_{0d} is the daily average soil heat flux [$W m^{-2}$]. In this work, the instantaneous net radiation at one hour steps was calculated using the products from EUMETSAT LSA SAF as follow;

$$R_n = (1 - \alpha) \cdot DSSF + \varepsilon \cdot DSLF - \varepsilon \cdot \delta \cdot LST^4 \quad (5-27)$$

where $DSSF$ is the down-welling surface short-wave flux [$W m^{-2}$], $DSLF$ is the down-welling surface long-wave flux [$W m^{-2}$], LST is the land surface temperature [K], α is the land surface albedo [-], ε is the land surface emissivity [-], δ is the Stefan-Boltzmann constant [$5.670400 \cdot 10^{-8} W m^{-2} K^{-4}$]. The instantaneous G_0 was calculated as the function of net radiation and fraction cover as used in SEBS as follow:

$$G_0 = R_n \cdot [\Gamma_c + (1 - FVC) \cdot (\Gamma_s - \Gamma_c)] \quad (5-28)$$

where Γ_c and Γ_s is the ratio of soil heat flux to net radiation for fully vegetated canopy and bare soil respectively. They usually have taken as 0.05 for Γ_c and 0.315 for Γ_s . FVC is the fraction of vegetation cover [-] that was used to interpolate between the two limiting cases.

Finally, another EF fraction called evaporative fraction from daily data was calculated using the daily averaged data as input to the model with Eq. (5-24). The purpose of this calculation is to test whether

the daily data can be used in SEBS model to estimate the daily AET when near real-time data is not available.

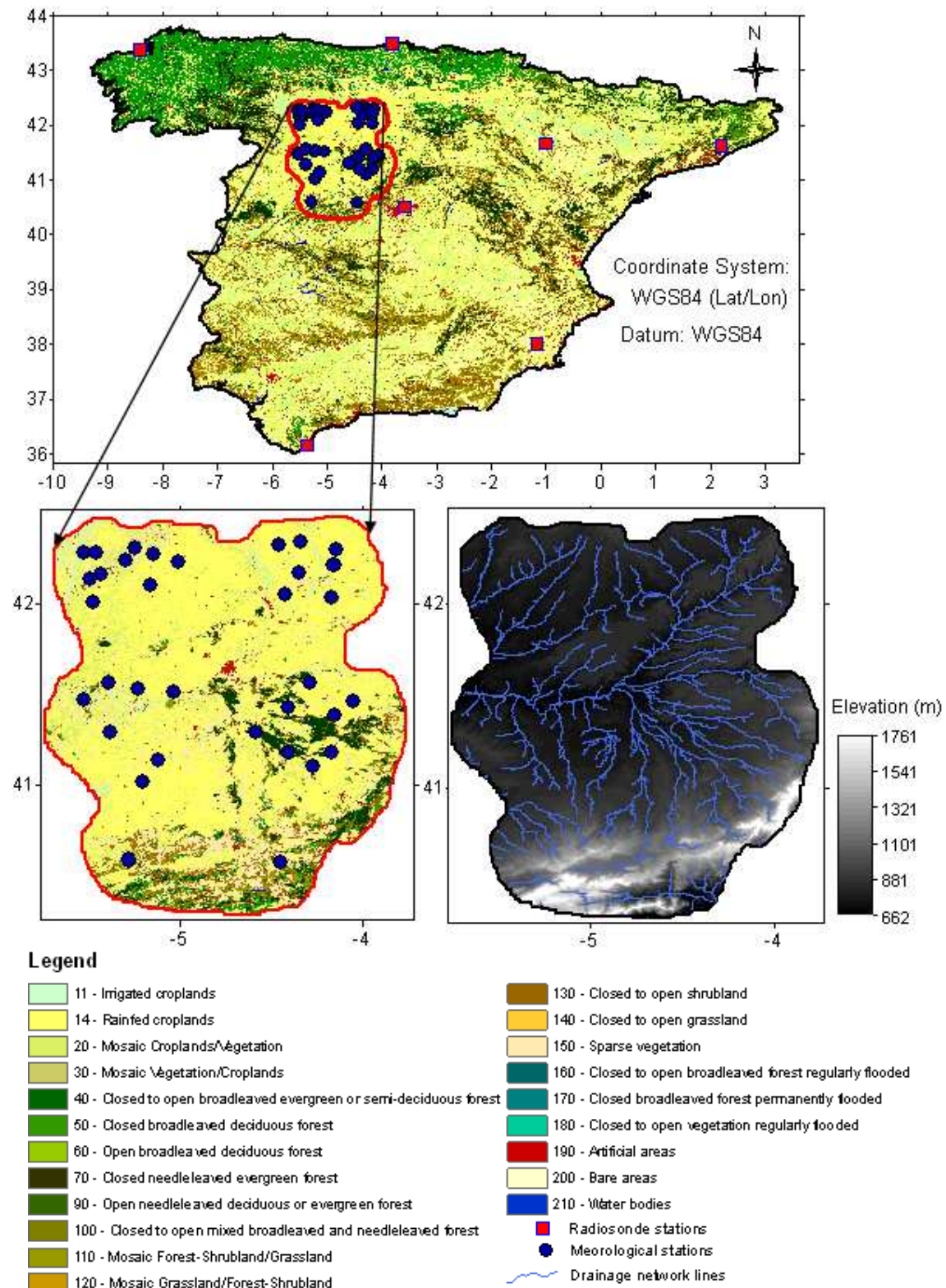


Figure 5-5. Meteorological stations, land cover classes and drainage network of Castilla y Leon region, Spain

5.9.2. Estimation of Daily Actual Evapotranspiration

The daily AET was estimated using two methods;

First, the method in SEBS model was used with instantaneous data. In this case, the daily AET was calculated at 12:00 solar time for the selected days during the study period, and at every an hour step (07:00-18:00) on September, 05, 2009.

$$AET_{daily} = 86400.EF_{inst} \cdot \frac{R_{nd} - G_{0d}}{\lambda} \quad (5-29)$$

Secondly, daily AET was calculated using daily average evaporative fraction or daily average latent heat flux as follow;

$$AET_{daily} = 86400.EF_d \cdot \frac{R_{nd} - G_{0d}}{\lambda} \text{ or } AET_{daily} = 86400 \cdot \frac{\lambda E_d}{\lambda} \quad (5-30)$$

where AET_{daily} is the daily actual evapotranspiration [mm d^{-1}], λ is the latent heat of vaporization [$\approx 2.5 \cdot 10^6 \text{ J Kg}^{-1}$], other parameters are as defined in section 5.9.1.

5.10. Water Balance Estimation from Remote Sensing Observations

The surface water balance of the study area was estimated using a simple water balance method so-called, "climatological water balance", defined as precipitation (P) minus actual evapotranspiration (AET). In this work, both P and AET were estimated from remote sensing observations. Indeed, the complete land surface water balance in water resource management includes the quantification of actual evapotranspiration, rainfall and runoff. Therefore, this water balance estimation is not a complete but it was applied due to the fact that the study area is very dry with low rainfall where surface runoff is too low to consider in the water balance of the region during this study period.

The general water balance equation is given by;

$$-\frac{\partial W}{\partial t} + Q = P - AET = \frac{\partial S}{\partial t} + R_o + R_u \quad (5-31)$$

where $\partial w / \partial t$ represents change in perceptible water with time (change in column storage of water vapour with time), Q is the convergence of water vapour flux in the atmosphere, $\partial S / \partial t$ is the change of total water storage with time, P is precipitation, AET is actual evapotranspiration, R_o is surface runoff, and R_u is the groundwater movement.

By excluding runoff and ground water movement, the surface water balance of the region was estimated using the precipitation product from EUMETSAT and AET estimated by SEBS model during the study periods. Therefore, Eq. (5-31) is now given by:

$$\frac{\partial S}{\partial t} = P - AET = \text{excess Precipitation} \quad (5-32)$$

Due to time limit of this thesis work, the daily AET was calculated only for a few selected dates (22 days) in the study period. The selection criterion of the days was based on the rainfall occurrence during the study period. If there is no rain in a month, at least 3 days were selected. The maximum number of days in each month depends on the rainfall occurrence and cloud cover in the study area at the time of interest (12:00 solar time). Except some days in the month of May and June, the daily AET was estimated for all days just after and before rainy days, but due to cloud cover and frequent

rainfall on some days in the month of May and June, the daily AET was estimate for the cloud free days after rainy day. Finally, the daily AET for the rainy days or other days which AET is not calculated for are estimated by linear interpolation of the antecedent and descendant AET estimated by SEBS model. Its main purpose was to plot the daily AET during the study period and to make the intended simple water balance estimation from remote sensing observation that can give some information about the availability of moisture (excess precipitation) in the study period. This principle of water balance estimation is climatologically water balance in agricultural research which often used to forecast whether or not irrigation is required at a specific site (Böhm et al., 1998). It is also referees to the net flux of water from the atmosphere to the earth's surface. In this research, it was used to identify the wet and dry days of a selected pixel in the rainfed cropland.

6. Results and Discussion

6.1. Land cover Classification

The validation of ESA land cover classification for the study area was successfully done using 58 points collected during field work in Salamanca area, Spain. The comparison result shows similar classification with 55 points out of 58 collected points (Fig. 6-1). The disagreement areas might be due to deforestation problems and others that were observed during field work, like from forest to young wine yard, and change of agricultural practise from rainfed to irrigated croplands.

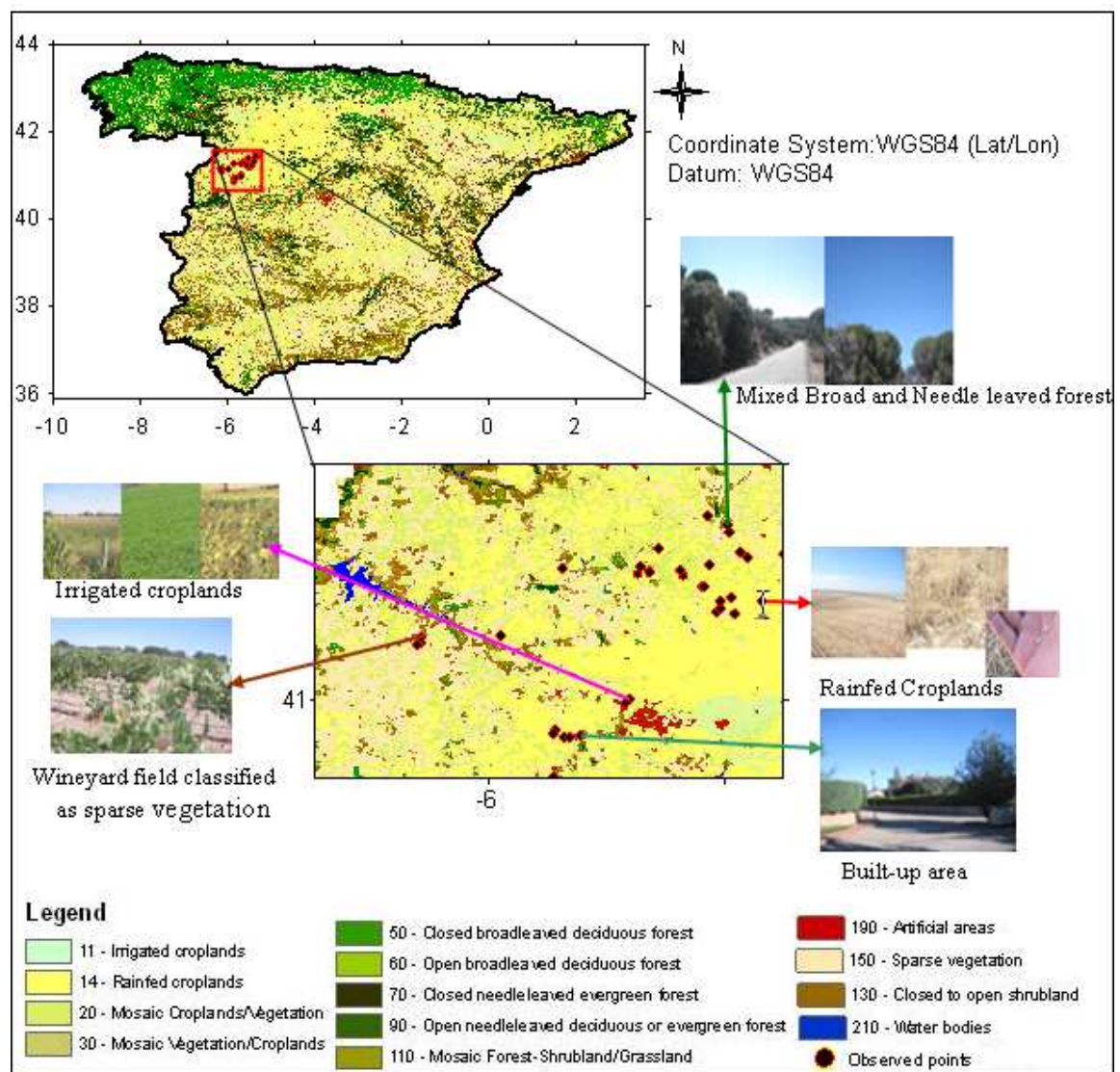


Figure 6-1. Globcover ESA land cover classification map overlaid with point map of observed locations in the study area.

6.2. Diurnal Evolution of Evaporative Fraction

The diurnal evolution of EF from 07:00-18:00 on March, 15, 2009 was estimated for different land cover classes in the Castilla y Leon region, Spain with spatial resolution of 300m. In this analysis, 10 land cover classes which are near by meteorological stations were selected (see Fig.6-14). Figure 6-2 shows the diurnal variation of EF over those land cover classes in the study area.

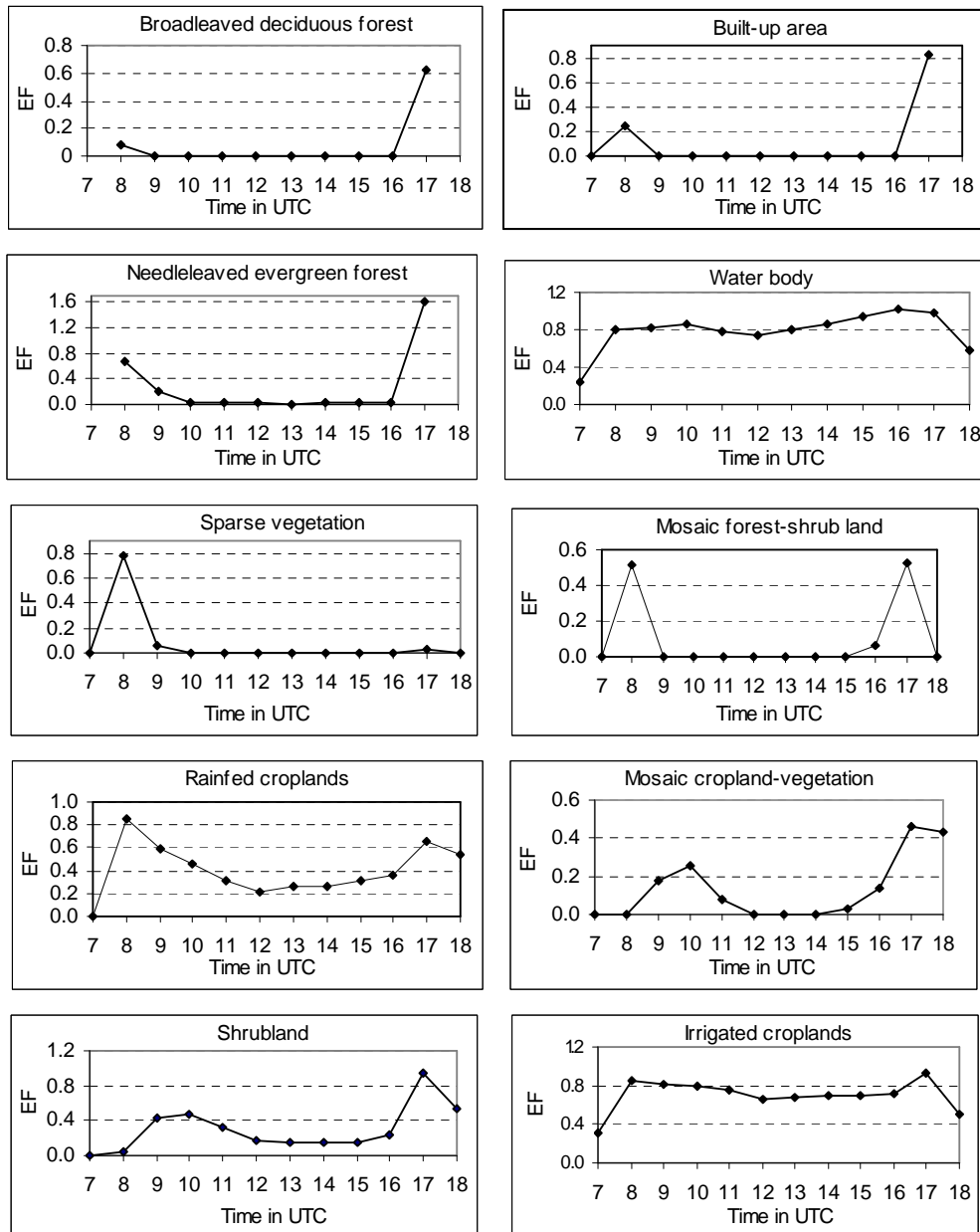


Figure 6-2. Diurnal variation of evaporative fraction for different land cover classes (March, 15, 2009)

This figure shows the instantaneous EF estimated using SEBS model with combined high temporal and spatial resolution satellites data and near-real time ground-based meteorological data. The results show that reasonable diurnal variation of EF was observed over some land cover classes. In the month of March, the study area is either dry or moderately wet during none rainy days dependent on

antecedent rainfall. There was light rainfall distributed over the area on 14 March 2009 (see Fig.6-21), but 15, March, 2009 was cloud free day. For this reason, the study area is likely to be moderately wet day on 15 March 2009. Many studies proved that EF can be stable during dry or moderately wet seasons (Carlos et al., 2009; Hoedjes et al., 2008; Lhomme and Elguero, 1999; Venturini et al., 2008). Therefore, it is useful to evaluate the diurnal stability of EF in the region, especially over land cover classes that the model performs well. Figure 6-2 shows a stable EF over the day for rainfed croplands, irrigated croplands, shrubland, and water bodies. This indicates that daily AET over these land cover classes can reasonably well be estimated using instantaneous observations by assuming EF as self-preservative during the day time, at least in a dry and moderately wet climate when the atmosphere is under unstable conditions. In addition, the higher evaporative fraction in the rainfed and irrigated croplands agreed with the crop calendar of the country given in the Fig. 4-5 and Table 4-6, which shows March, 15 is the period of planting and emerging time for short cycle rainfed crops and for crops growing by spring irrigation. In these land cover types, relatively high evaporation is expected.

In these results, zero EF was also obtained mainly from 09:00-16:00 in the built-up area, broadleaved deciduous forest, mosaic forest-shrubland, sparse vegetation, needleleaved evergreen forest and mosaic cropland –vegetations. It is unlikely that evaporation is zero over these land cover classes under normal conditions. According to Eq. (5-24), the EF can be zero when $H=H_{dry}$, it implies that all of the available energy is partitioned into sensible heat flux. At this stage, this can be explained in terms of temperature difference between land surface and air over these land cover classes on March, 15, 2009. As shown in the Fig. 6-3, the temperature difference is high over forest and sparse vegetation from 09:00 to 16:00 and low in the morning and late afternoon. In addition, as it can be seen from Table 6-1, the NDVI and LAI on March, 15, 2009 in the broadleaved deciduous forest, mosaic forest-shrubland and sparse vegetation are low. This indicates that vegetations might have few leaves (emerging just after winter) specially, for broadleaved deciduous forests, which can result in the sudden increase of surface temperature early in the morning. Therefore, the increase in land surface temperature that has similar effect on sensible heat flux could lead to zero EF (see also Fig.6-3). Such situations could also happen in dry climate due to the land surface temperature increases soon after sunrise, and the plant close their stomata early. Indeed, it is not unusual to get zero EF over woodlands even for a long period in dry environment (Farah et al., 2004). For the case of needleleaved evergreen forest and mosaic cropland–vegetation, the model either underestimates the EF or due to the increasing of canopies temperature. Generally, the above reasons are just to express the probable cause of zero EF in those land cover classes based on currently available information and results.

Table 6-1. Land cover classes with associate bio-physical information

Land cover classes	FVC	LAI	NDVI
Irrigated croplands	0.010	0.020	0.228
Rainfed croplands	0.130	0.330	0.390
Mosaic croplands-vegetation	0.120	0.310	0.346
Broadleaved deciduous forest	0.080	0.210	0.346
Needleleaved evergreen forest	0.170	0.530	0.595
Mosaic forest-shrubland	0.120	0.300	0.554
Shrubland	0.190	0.520	0.491
Sparse vegetation	0.330	0.450	0.377

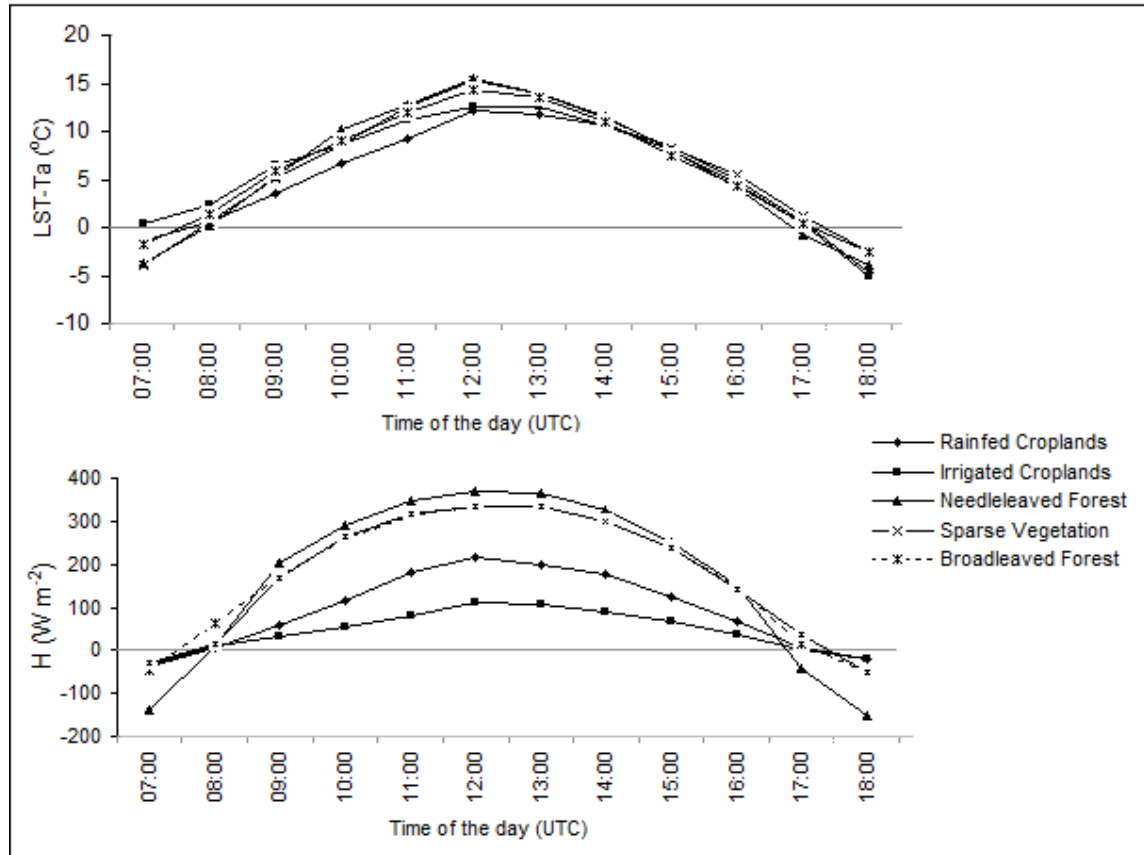


Figure 6-3. Diurnal variation of temperature difference between land surface and air (top) and Sensible heat flux (bottom) over different land cover classes (March, 15, 2009)

In the most land cover classes, EF peaked in the morning at 08:00 and late afternoon at 17:00 UTC (Fig. 6-2). This situation could be due to one or more of the following three possible reasons: Firstly, the opening and closing of stomata by vegetations. Since the area has hot climate and limited moisture, the land surface temperature might increase in the morning, as the result the newly emerging plant leaves could probably close their stomata early before 9:00 and reopen after 16:00 during this period (March, 15, 2009). The second reason might be the low temperature difference between land surface and air in the morning and late after. As it can be seen from Fig. 6-3, the variation of sensible heat flux is highly linked to the temperature difference between land surface and air. Therefore, a low temperature difference between land surface and air implies low sensible heat flux and a high EF regardless of moisture availability. The last reason could be the aerodynamic resistance. As shown in Fig. 6-3, LST-Ta is less variable than H in all land cover classes, so it perhaps the higher aerodynamic resistance that result in lower sensible heat flux and higher EF in the morning and late afternoon.

6.3. Comparison of Instantaneous and Daily Average Evaporative Fractions

Fig. 6-4 to 6-11 show the maps, error bars at 0.05 intervals (denoting the standard deviation) and scatter plot at back ground for comparison of daily average EF with instantaneous EF and EF from daily data for different land cover classes in the Castilla y Leon region. This comparison was done only on March, 15, 2009 during the study period.

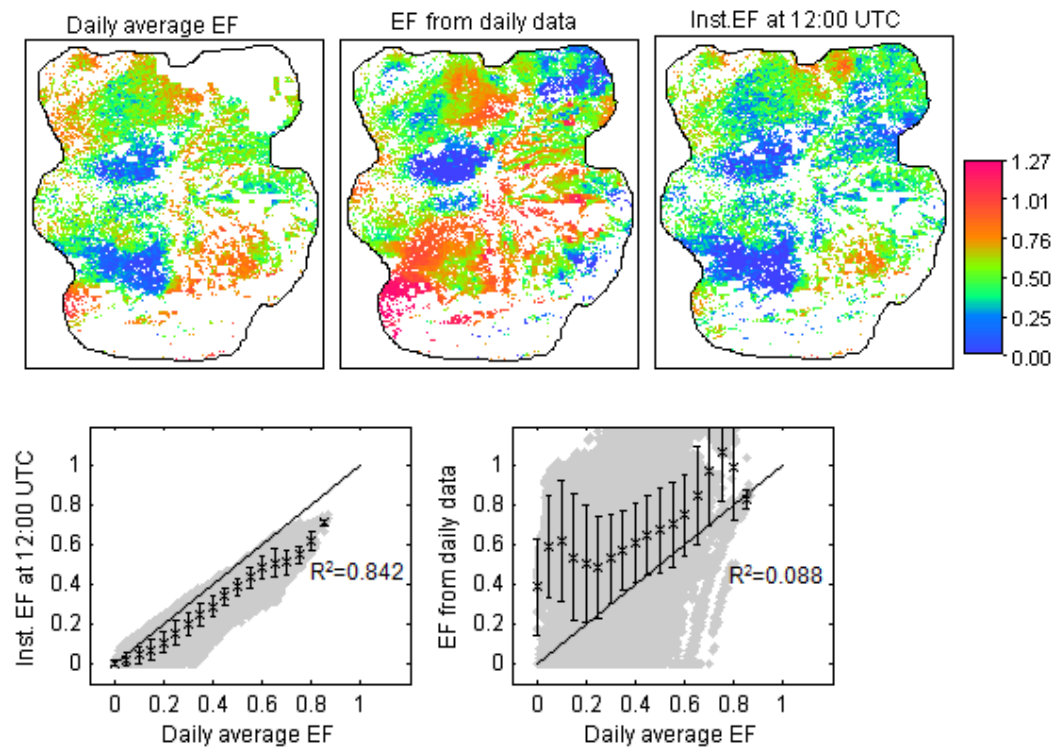


Figure 6-4. Comparison of average daily EF with instantaneous EF and EF calculated from daily average data for **rainfed croplands** (March, 15, 2009)

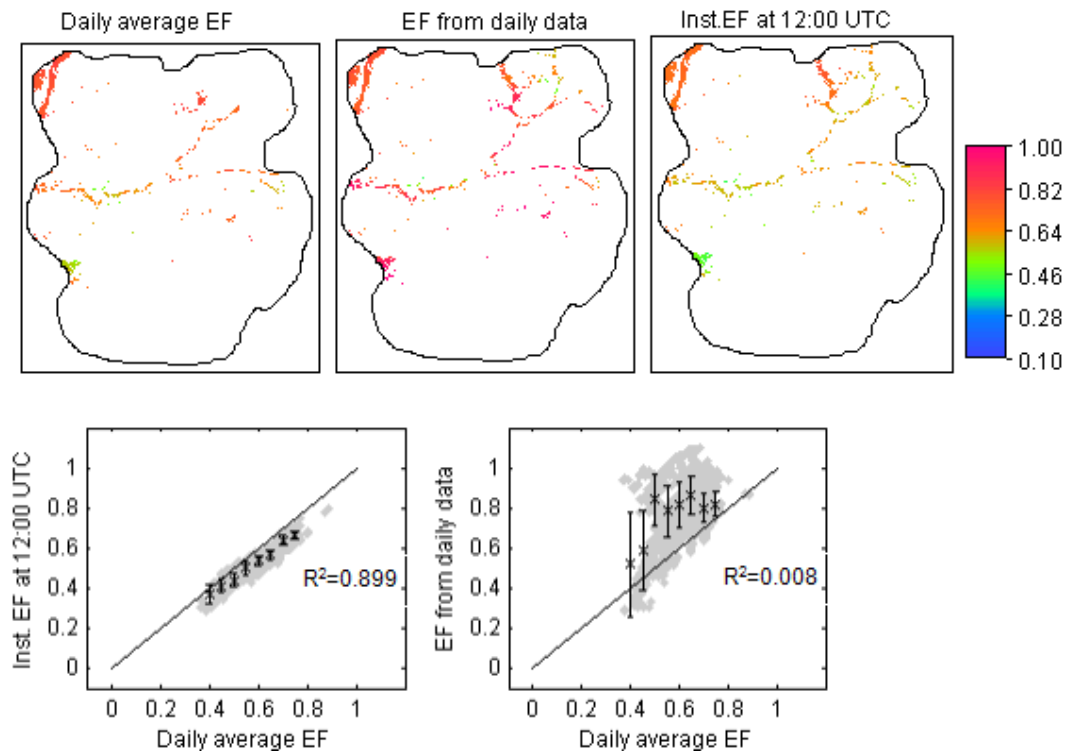


Figure 6-5. Comparison of average daily EF with instantaneous EF and EF calculated from daily average data for **irrigated croplands** (March, 15, 2009)

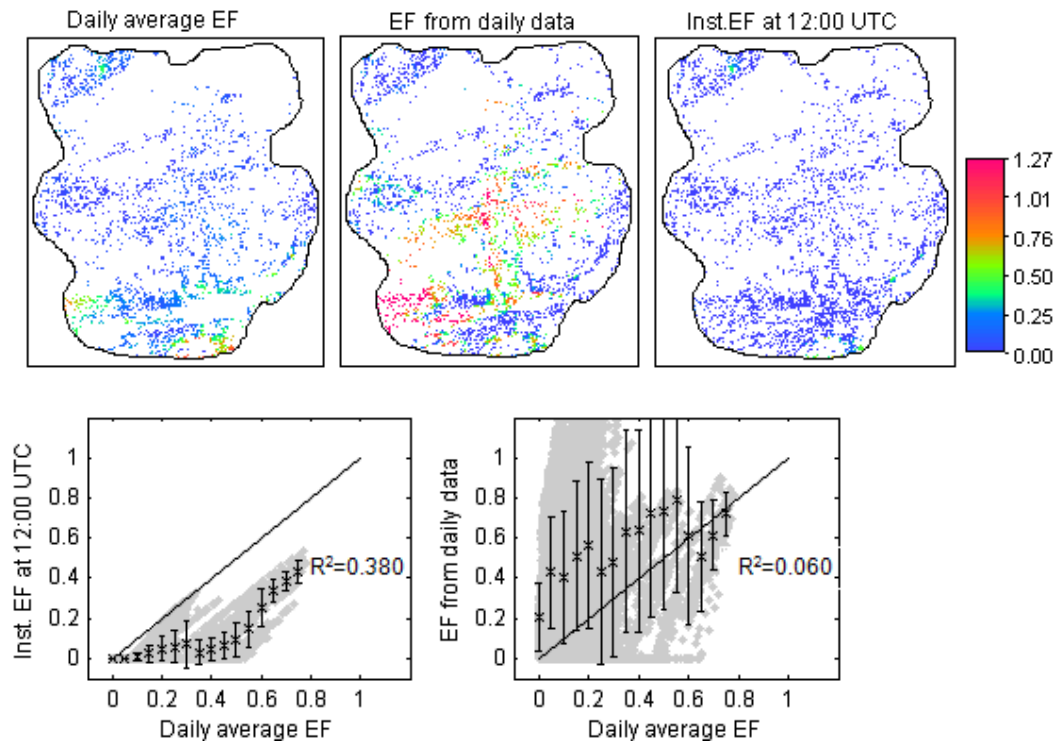


Figure 6-6. Comparison of average daily EF with instantaneous EF and EF calculated from daily average data for **Sparse vegetation** (March, 15, 2009)

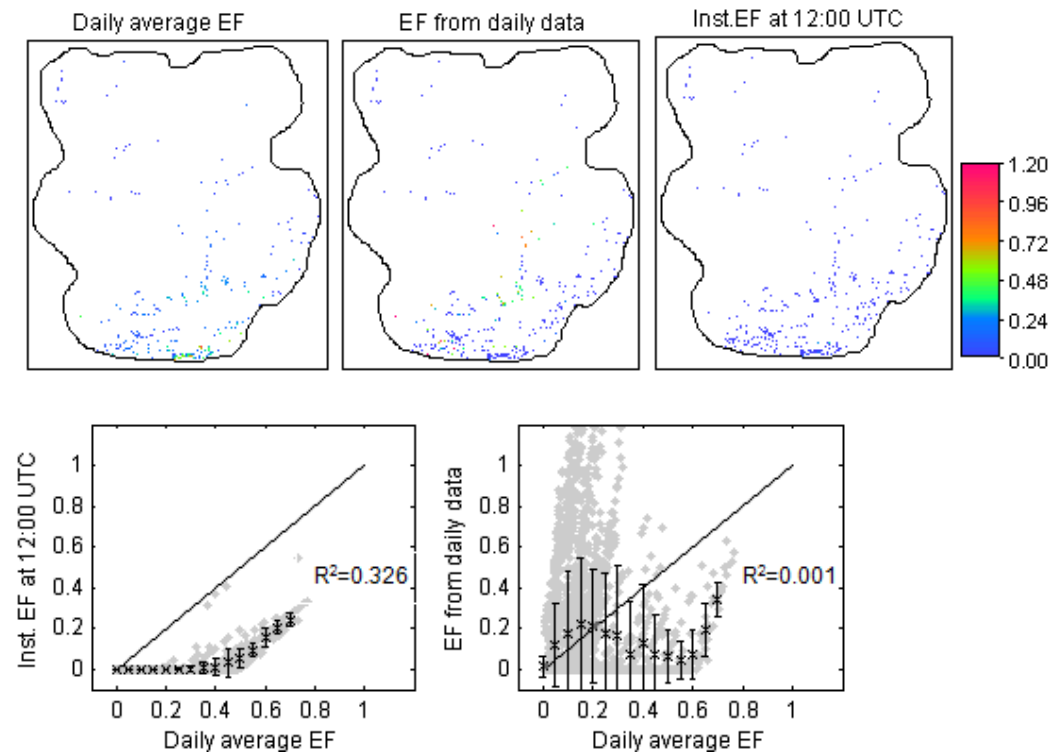


Figure 6-7. Comparison of average daily EF with instantaneous EF and EF calculated from daily average data for **broadleaved deciduous forest** (March, 15, 2009)

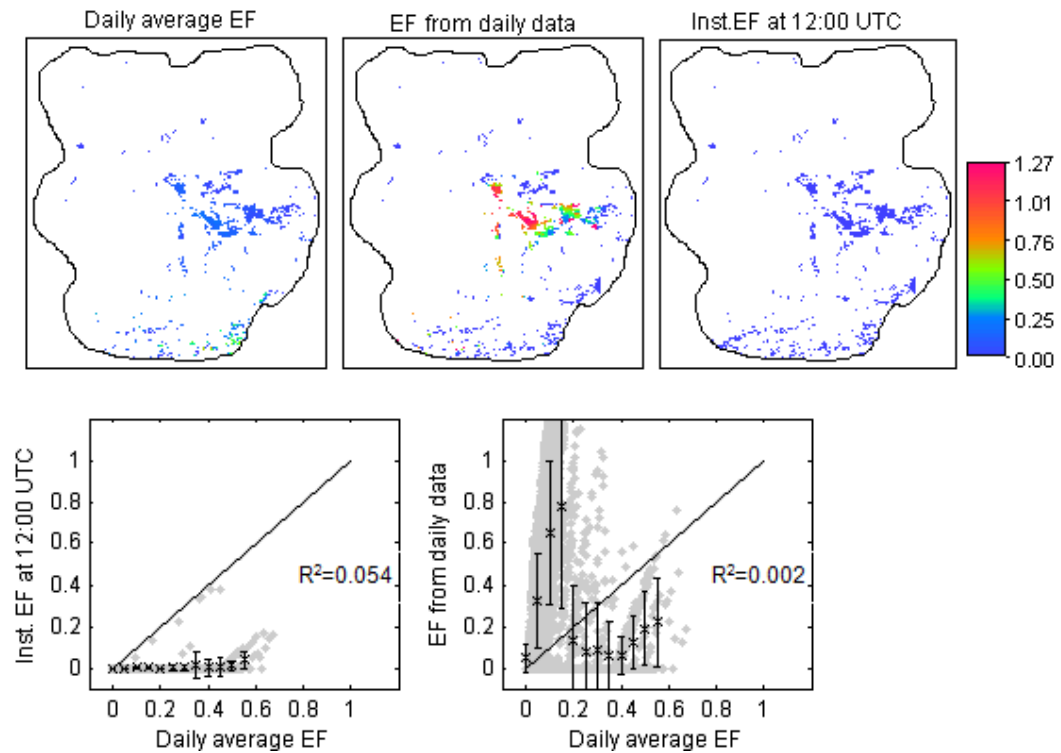


Figure 6-8. Comparison of average daily EF with instantaneous EF and EF calculated from daily average data for **needleleaved evergreen forest** (March, 15, 2009)

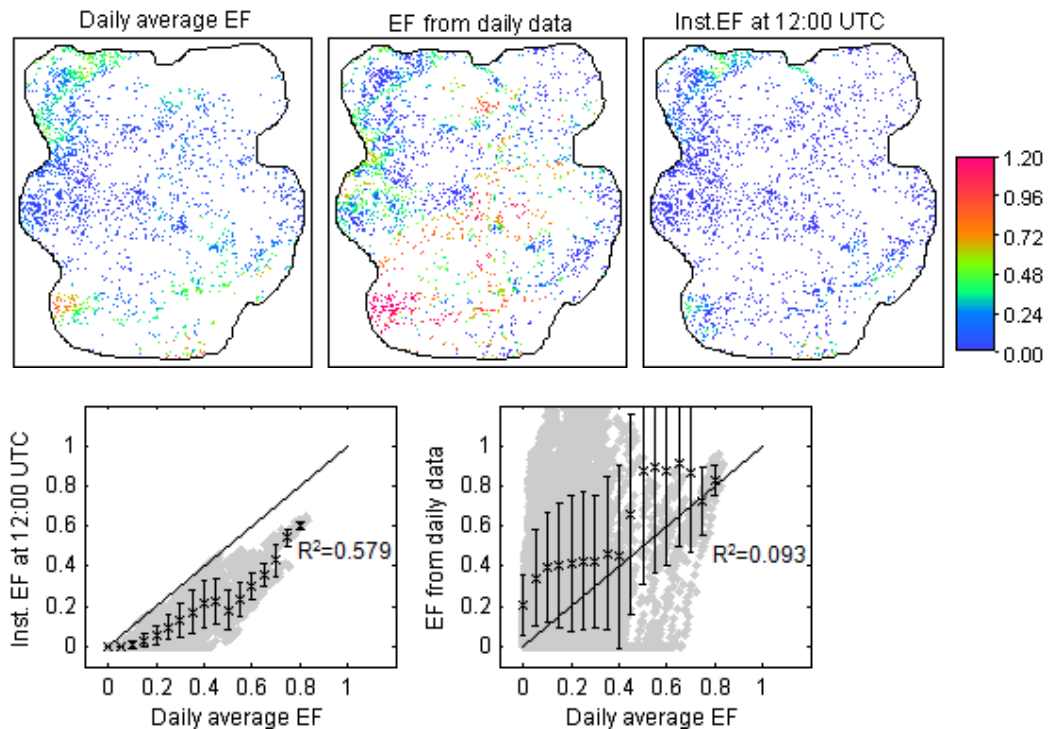


Figure 6-9. Comparison of average daily EF with instantaneous EF and EF calculated from daily average data for **mosaic croplands-vegetation** (March, 15, 2009)

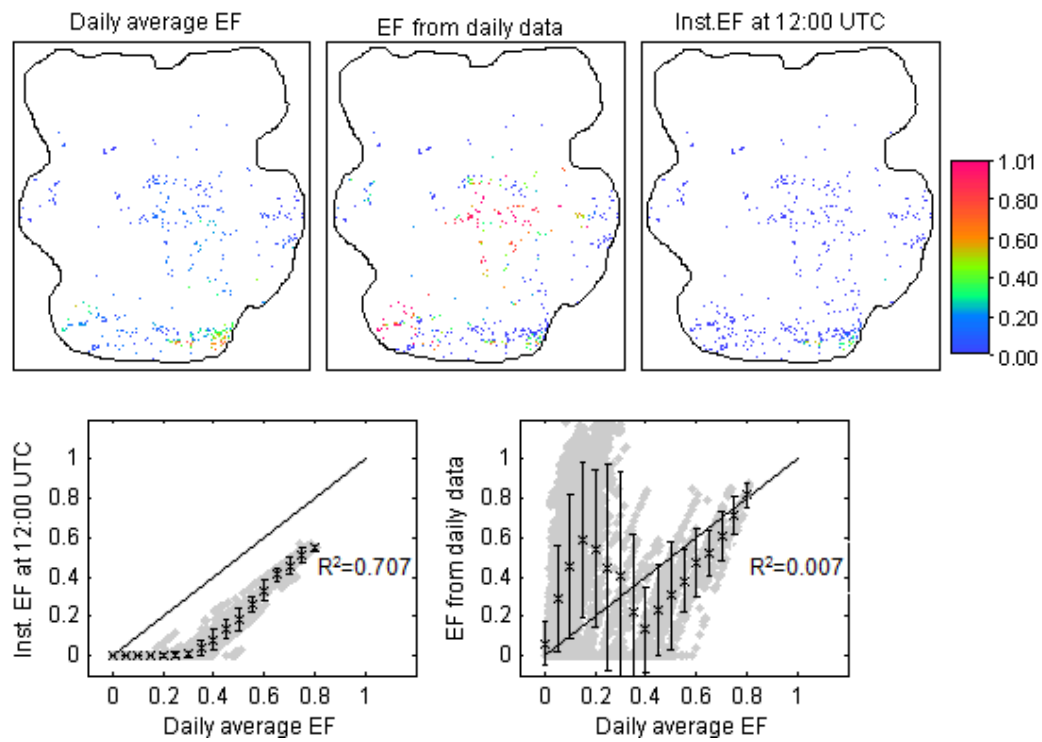


Figure 6-10. Comparison of average daily EF with instantaneous EF and EF calculated from daily average data for **mosaic forest-shrubland** (March, 15, 2009)

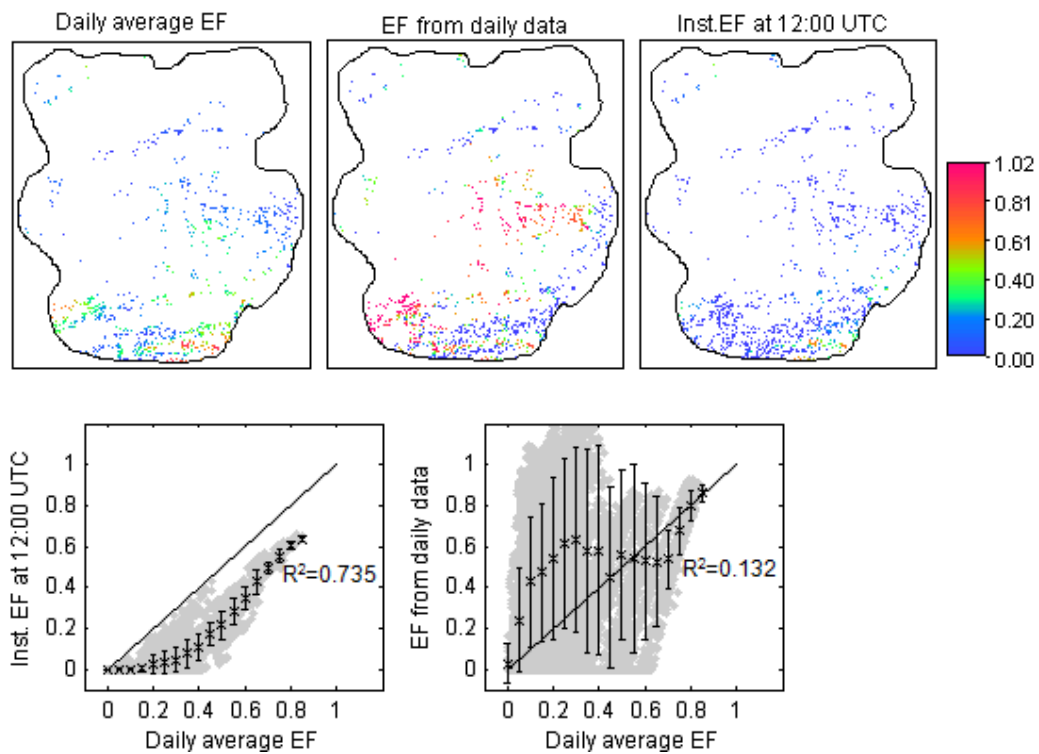


Figure 6-11. Comparison of average daily EF with instantaneous EF and EF calculated from daily average data for **shrubland** (March, 15, 2009)

The results in Fig. 6-4 to 6-11 show that the daily average EF and instantaneous EF have strong relation for irrigated croplands, rainfed croplands, shrubland, mosaic forest-shrubland and mosaic crop-vegetation respectively ($R^2=0.899$, 0.842 , 0.735 , 0.707 , and 0.579). But it exhibits poor agreement for sparse vegetation, broadleaved deciduous forest and needleleaved evergreen forest ($R^2=0.380$, 0.326 , and 0.054 respectively). This indicates that instantaneous observations can not be used to estimate daily AET in sparse vegetation, broadleaved deciduous forest and needleleaved evergreen forest. These results support the conclusion made by Farah et al. (2004) that EF is not stable in all vegetation types, soil moisture and atmospheric conditions. This could be due to the diurnal variation of surface resistance, energy and moisture advection. In addition, the daily averaged EF is almost without exception higher than instantaneous EF over all land cover classes. This indicates that use of only mid day observation for estimation of daily AET could lead to underestimation of the results. Especially for semi-arid and arid climate, the available moisture might evaporate early in the morning and it becomes dry during the mid day. There is no agreement between the daily average EF and EF estimated from daily averaged data for all land cover classes, although in some land cover classes, the lumped data for all pixels show a similar pattern. This might be due to the nonlinear relationship between the changes of atmospheric forcing parameters particularly, LST and air temperature with surface energy fluxes or atmospheric stabilities, but the comparison was done to test whether or not the daily average data can be used to estimate daily AET with SEBS model when instantaneous meteorological data are not available. Generally, if the Monin-Obukhov similarity (MOS) theory was derived only for instantaneous observations, the concept of using daily averaged data with SEBS model would be incorrect.

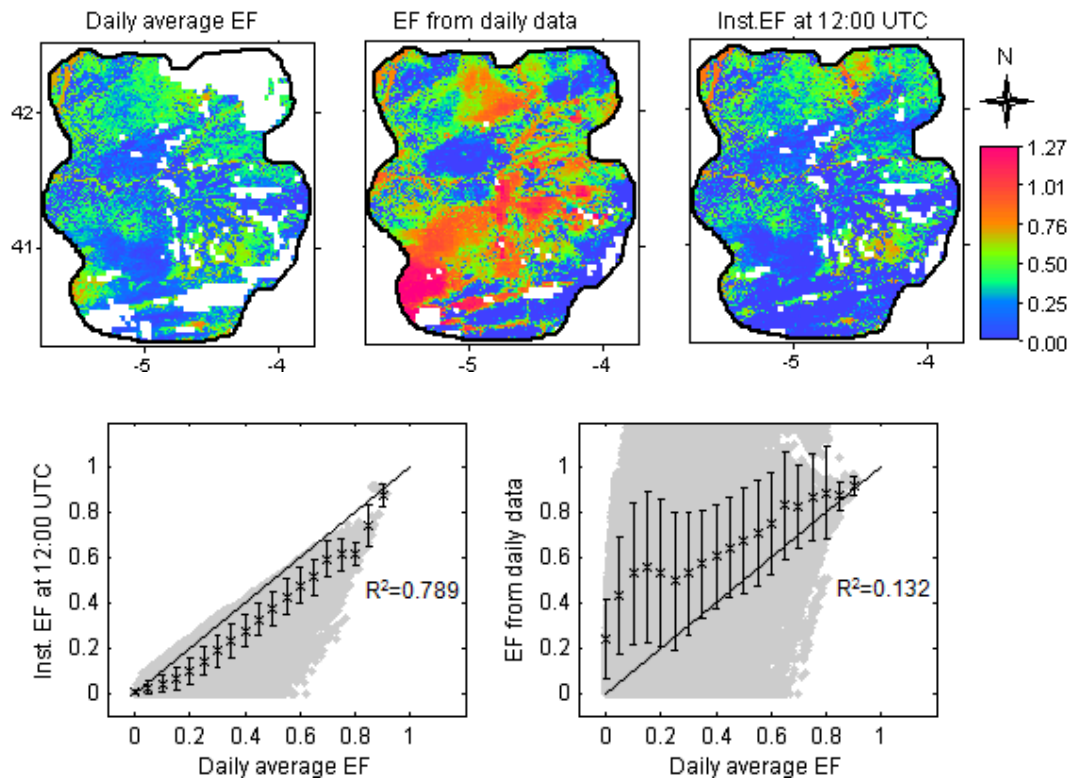


Figure 6-12. Comparison of average daily EF with instantaneous EF and EF calculated from daily average data in the Castilla y Leon region, Spain (March, 15, 2009)

Table 6-1. Correlation matrix using SPSS

	Daily average EF Npix = 356614	Instantaneous EF Npix = 356614	EF from daily data Npix = 356614
Daily average EF	1	0.888**	0.363**
Instantaneous EF	0.888**	1	-
EF from daily data	0.363**	-	1

** . Correlation is significant at the 0.01 level (2-tailed)

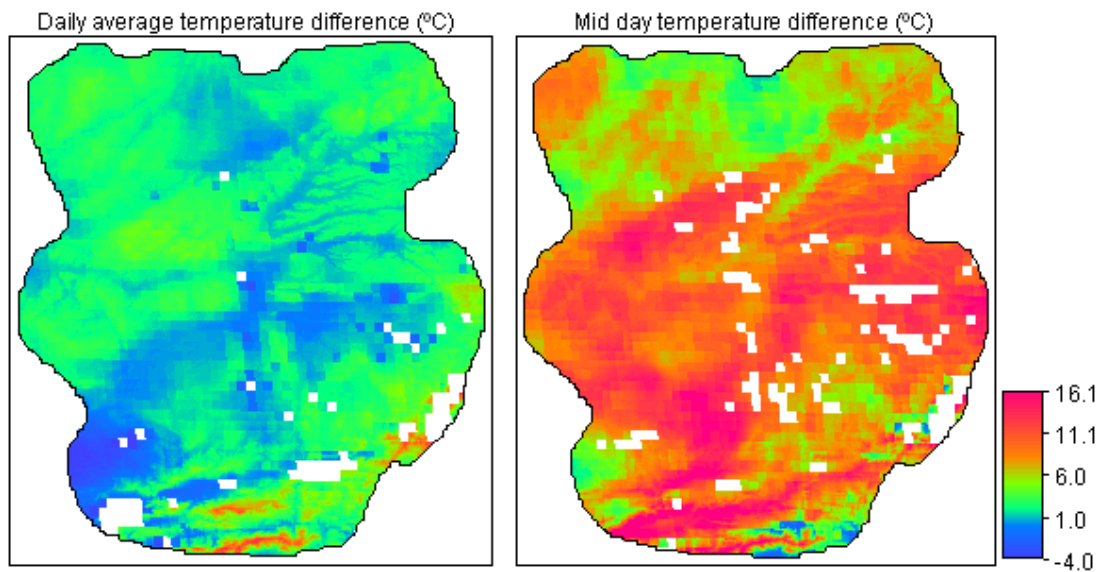


Figure 6-13. The maps of temperature difference between land surface and air for daily averaged and mid day (12:00 UTC) on March, 15, 2009

Finally, the comparison of EF over large area with mixed land cover classes was carried out (Fig. 6-12 and Table 6-1). The strong relation between daily average EF and instantaneous EF is preserved with $R^2 = 0.79$ and the correlation of 0.89 as it is for most individual land cover classes. But there is weak relation between daily average EF and EF from daily data with $R^2 = 0.132$ and the correlation of 0.363. Therefore, the instantaneous data can be used to estimate the daily AET over large area dominated by irrigated croplands, rainfed croplands, shrubland, mosaic forest-shrubland and mosaic crop-vegetation in such climate condition within acceptable error. Generally, since it is possible to estimate daily average EF from EUMESAT satellite system products and ground-based data, there is high potential of making good estimation of daily AET using this daily averaged EF in all land cover classes and weather conditions during clear sky days. Many studies (Cleugh et al., 2007; Farah et al., 2004; Gentile et al., 2007; Hoedjes et al., 2008; Lhomme and Elguero, 1999) were conducted to estimate daily AET using ground based meteorological data and one time observation from polar orbiting satellites. The results showed that evaporative fraction is more unstable during wet, cloudy and rainy periods. Therefore, they are not in favour of using the instantaneous EF to estimate daily AET over large area in all climate conditions. Likewise, this study also supports similar arguments and encourages research to test and estimate daily average EF using combined geostationary and polar orbiting satellite products in conjunction with ground based meteorological data to estimate daily AET in any climate condition.

Besides, higher values (greater than one) of EF were obtained while estimating EF using daily averaged data. This implies that actual evaporation is higher than potential evaporation which is unlikely to occur under natural conditions. From a mathematical point of view, this implies that the actual sensible heat flux is negative due to the air temperature greater than land surface temperature. However, in some cases it is reasonable to obtain higher values of air temperature than land surface temperature both in the daily bases and in instantaneous as well, especially in some land cover classes like irrigated areas and forest due to advection and cooling effect of available moisture. For the daily bases, the low temperature difference between land surface and air could be due to the contribution of low land surface temperature during night time, but there is a very low flux and high aerodynamic resistance during the night time. Therefore, the result of higher value of EF over some land cover classes can only be explained potentially in terms of temperature difference between land surfaces and air (see Fig. 6-12 and 6-13). It is clearly seen in these figures that pixels with higher evaporative fraction estimated from daily data have smaller or negative temperature difference between land surface and air. Therefore, using daily averaged data as input to SEBS model to estimate daily AET could lead to the overestimation of EF in all land cover classes. Indeed, there is no information on the formulation of SEBS model whether it is possible to use daily averaged data as in put or not.

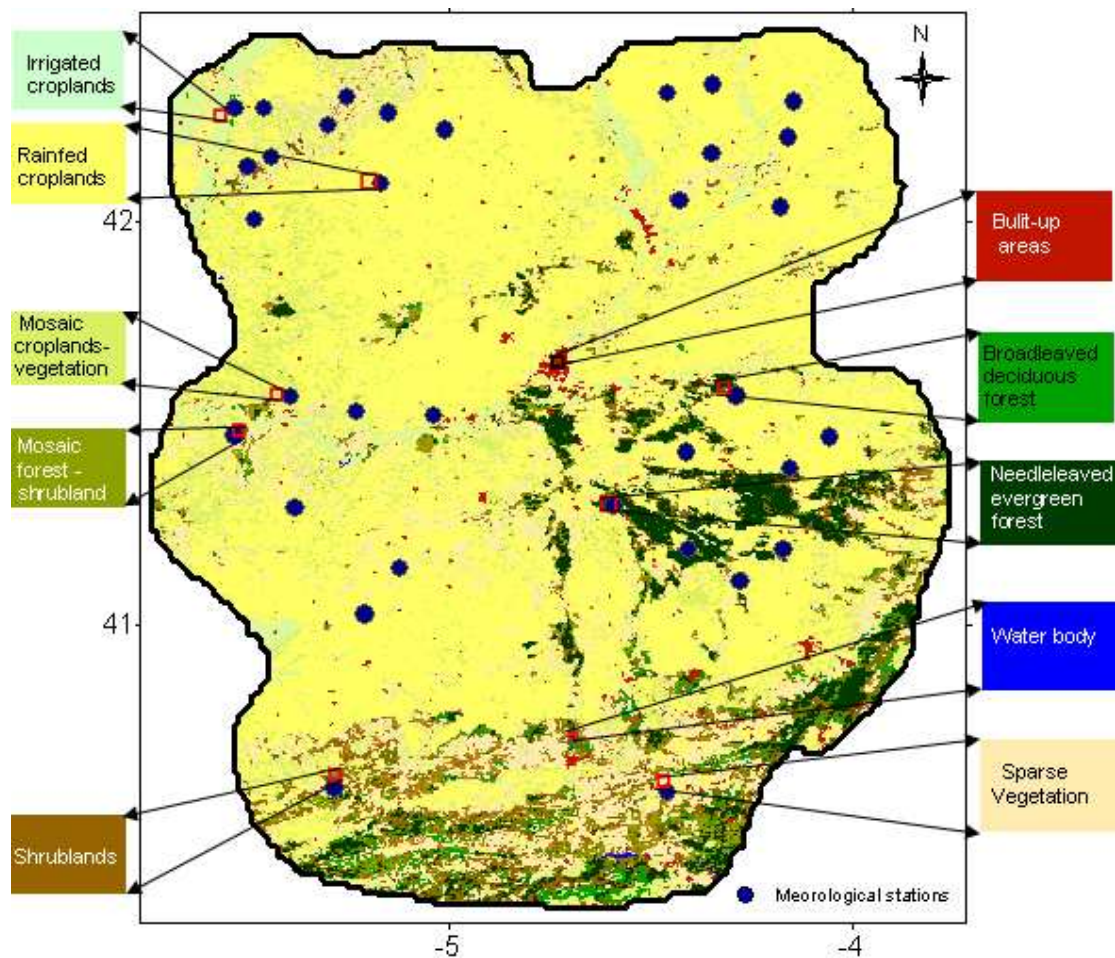


Figure 6-14. Location of 10 land cover classes nearby meteorological stations used for comparison of evaporative fractions and daily AET

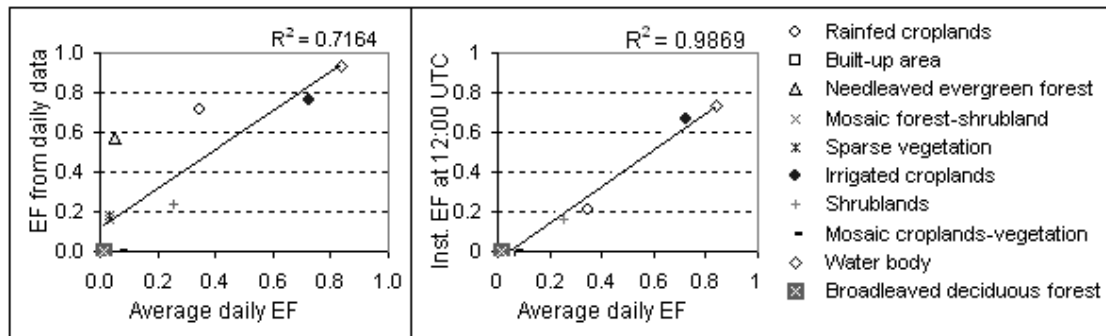


Figure 6-15. Overall comparisons of evaporative fractions using a single pixel per each land cover class near by meteorological stations

Additional comparison was done for selected single pixel per land cover classes (Fig.6-14) near by meteorological stations to reduce the effect of uncertainties induced by interpolation. As shown in Fig. 6-15, the higher square of correlation ($R^2=0.99$) between the instantaneous and daily average EF over mixed land cover was obtained. In addition, strong relation between daily average EF and EF from daily data ($R^2=0.72$) was also achieved. It is obvious that there is a considerable error generated by interpolation of point meteorological data for some land cover classes like forest or in mixed land cover. In this analysis, since the daily average EF was estimated from instantaneous EF and energy fluxes, the error might not be reflected on the square of correlation between the instantaneous EF and daily average EF. Indeed, one reason for weak correlation between daily average EF and EF from daily data could be the lower temperature difference between land surface and air in the daily bases (Fig. 6-13). In general, many uncertainties involved during estimation of evapotranspiration or EF over large area from remote sensing observations with diverse land cover classes (Abdelghani et al., 2008; Ferguson et al., 2009; Wenjing et al., 2006). These uncertainties may include but not limited to the following; **I**, selection of data set and provision of right information for individual pixels in the very mixed land cover classes, where surface meteorological parameters, surface geometrical and thermal conditions are neither homogenous nor constant **II**, the spatial distribution and measuring height of ground based meteorological data particularly in the forest **III**, estimation of roughness height for momentum transfer and displacement height (especially, in sparse vegetation and mixed land cover).

6.4. Comparson of Measured AET with MET and SEBS Estimated AET

The measured AET using an eddy covariance system over sparse vegetation was compared with SEBS AET and Meteosat second generation evapotranspiration (MET). All comparisons were done for 1-7 September 2009. Table 6-2 shows the comparison of measured AET with MET in daily bases.

Table 6-2. Comparison of daily AET from eddy covariance measurement and MET in the Sparse vegetation

Date	MET(mm)	Eddy AET (mm)	Abs. error(mm)	% error
01/09/2009	0.769	0.475	0.294	61.8
02/09/2009	0.936	0.575	0.360	62.6
03/09/2009	0.815	0.391	0.424	108.6
04/09/2009	0.935	0.304	0.630	207.1
05/09/2009	0.96	0.28	0.685	247.0
06/09/2009	0.77	0.32	0.447	140.9
07/09/2009	1.19	0.30	0.891	297.8

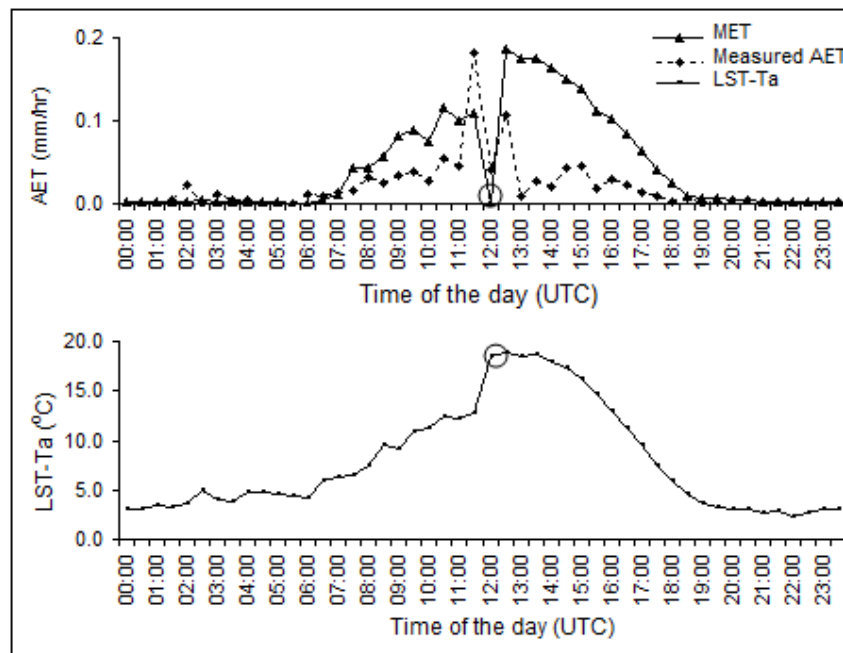


Figure 6-16. Comparison of measured AET with MET (top) and variation of temperature difference between land surface and air (bottom) in the Sparse Vegetation in half hourly step (September, 01, 2009)

As shown in Table 6-2, there is a considerable difference between the measured AET and MET on a daily bases with an error of up to 298%. This indicates that MET over estimate the actual evapotranspiration in daily bases in this specific land cover class. Even though they have big difference in value, they show similar pattern of the diurnal variations of AET, mainly before mid day (Fig. 6-16 and 6-18). Only both respond in a similar way to the abrupt changes of the temperature difference between land surface and air in the mid day as shown in circle.

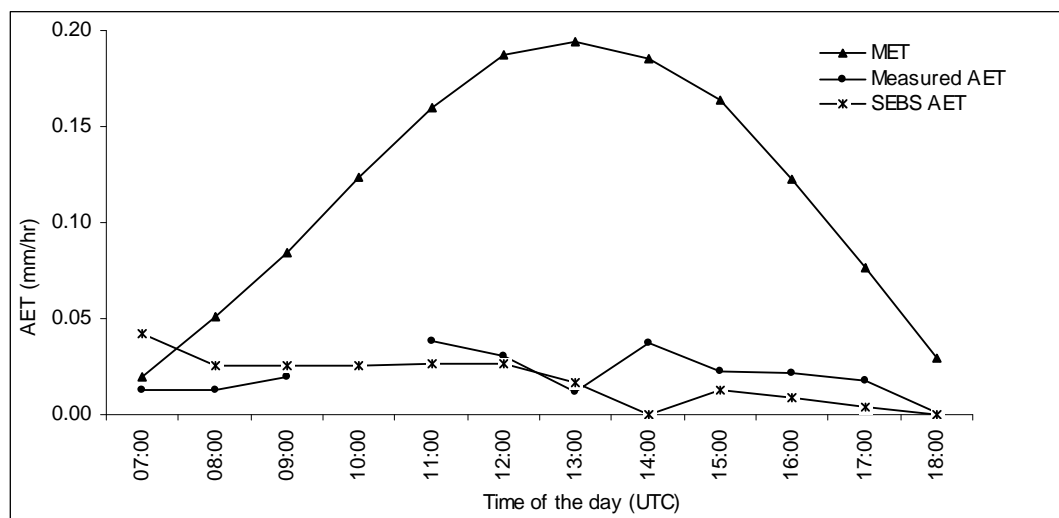


Figure 6-17. Comparison of measured AET with SEBS AET and MET in the Sparse Vegetation in hourly bases (September, 05, 2009)

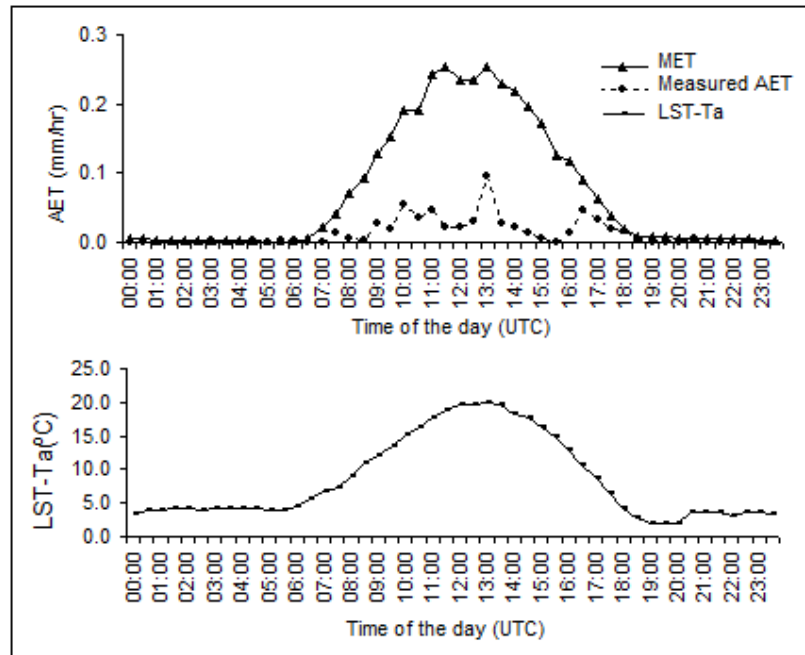


Figure 6-18. Comparison of measured AET with MET (top) and variation of temperature difference between land surface and air (bottom) in the Sparse Vegetation in half hourly step (September, 07, 2009)

The SEBS estimated AET was also compared with measured AET in sparse vegetation on September, 05, 2009 at every an hour step from 07:00-18:00. As it is clearly seen from Fig.6-17, SEBS estimated AET is close to the measured AET but it slightly over estimate in the morning and under estimate in the afternoon. The daily AET values are approached to each other (Measured AET=0.226 mm and SEBS AET=0.212mm). In addition, it was observed in Fig.6-6 that there is a poor correlation between the instantaneous EF and daily average EF over sparse vegetation. Therefore, it is not good to use SEBS to calculate daily AET using instantaneous EF over sparse vegetation. Moreover, a small error in estimation of land surface temperature results in considerable change of sensible heat flux and consequently affects the latent heat flux in SEBS model. This means, a little underestimation of land surface temperature in the morning and overestimation in the afternoon might result in over estimation and under estimation of latent heat flux respectively.

As shown in Fig. 6-16, 6-17 and 6-18, MET overestimates the actual evapotranspiration, but it has a similar pattern with measured and SEBS estimated AET. Beside its pre-operational product, MET algorithm is completely different from SEBS algorithm but they use some similar input parameters derived from MSG, except that MET use soil temperature instead of LST, and soil moisture at four layers. The next section discusses the comparison between SEBS AET and MET in more detail.

6.5. Comparison of SEBS Estimated AET and MET

Actual evapotranspiration estimated using SEBS model at different scales was compared with the Meteosat second generation evapotranspiration product from LSA SAF. This comparison was done in two ways. Firstly, by taking a single daily AET value for each land cover classes (see the selected pixels in Fig. 6-14). Secondly, by generating AET maps in both methods (Fig. 6-20).

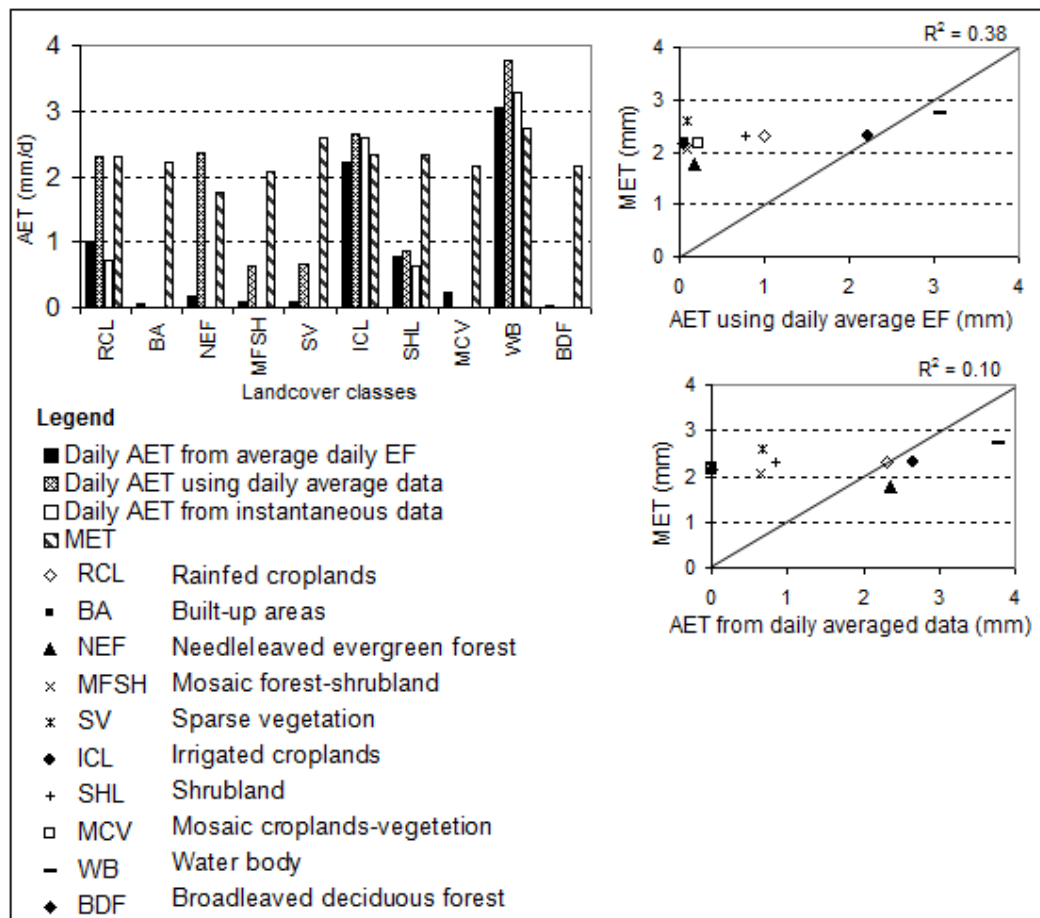


Figure 6-19. Comparison of SEBS estimated AET and MET (March, 15, 2009)

The bar graph in Fig. 6-19 shows the daily AET estimated using SEBS with instantaneous data and daily averaged data, and MET. In all methods, the SEBS estimated AET and MET have close values in irrigated croplands and water body. In addition, AET estimated from daily averaged data is also close to MET for rainfed croplands, and needleleaved evergreen forest. Generally, there is considerable difference (up to 2.59 mm) between MET and SEBS AET in other land cover classes. The scatter plots in Fig. 6-19 also shows poor square of correlation ($R^2 = 0.38, 0.10$) between MET and AET estimated using SEBS with daily averaged EF and daily averaged data respectively. On the other hand, the maps shown in Fig. 6-20 have a similar pattern of AET in most areas despite the value difference. Indeed, this pattern recognition will also help us to modify the algorithms after having long term ground based observations over different land cover classes. In addition, the daily AET values from MET are very close to each other at all land cover classes (see Fig. 6-20), but this is less likely to occur during a moderately wet day. The cause of such big value difference between MET and SEBS might be the different approach of both algorithms while estimation turbulent heat fluxes. MET is a pre-operational product that was generated using a simplified Soil-Vegetation-Atmosphere Transfer (SVAT) model modified to accept remote sensing derived data in combined with data from other sources like numerical weather prediction (NWP). In MET, the estimation of ET is made by reference to a land cover map which provides the fraction of vegetation types within each MSG pixel. This primary vegetation types are called “tiles” and each pixel may be

composed of several tiles. In practice, a maximum of four tiles (3 vegetation tiles (Forest, Crops and grass) + bare soil) are allowed in each pixel. ET is calculated separately for each tile in the pixel and the pixel value is obtained by a weighted contribution of all tiles composing the pixel. Generally, it is an energy balance model aiming to compute, for each tile i in the considered pixel, the partition of net radiation (Rn_i), sensible heat flux (H_i), latent heat flux (LE_i) and heat conduction flux into the ground (GO_i). The latent and sensible heat fluxes are obtained via called resistance approach (LSA SAF RMI Team, 2008).

According to the validation report of MET (<https://landsaf.meteo.pt>), the MET algorithm is able to reproduce the temporal evolution of observed ET. No systematic bias has been discovered for the different vegetation classes, except for a boreal coniferous forest site and a Mediterranean evergreen broadleaved forest site. The report also mentions that very good agreement is found for stations over grassland and mixed forest. For stations over other types of land cover, good agreement is found when a close correspondence exists between the land cover types and the effective cover type at the station.

Both SEBS and MET algorithms use some similar products from LSA SAF and ground meteorological data. In MET, the ground meteorological data are originally gathered at European centre for medium-range weather forecasts (ECMWF) spatial resolution. This data is again transposed into MSG grid and spatially interpolated.

Table 6-3. Input data for SEBS and MET algorithm for estimation of AET

Input data used in SEBS Algorithm	Input data used in MET Algorithm
Down-welling surface short-wave flux [$W m^{-2}$]	Down-welling surface short-wave flux [$W m^{-2}$]
Down-welling Surface long-wave flux [$W m^{-2}$]	Down-welling Surface long-wave flux [$W m^{-2}$]
Land Surface Albedo [-]	Land surface Albedo [-]
Land surface temperature [K]	Soil temperature for 4 soil layers [K]
Specific Humidity [$kg kg^{-1}$]	Dew point temperature [K]
Air temperature [$^{\circ}C$]	Air temperature [K]
Wind speed [$m s^{-1}$]	Wind speed [m/s]
Air and surface pressure [Pa]	Atmospheric pressure at sea level [Pa]
Emissivity [-]	Soil moisture for 4 soil layers [$m^3 m^{-3}$]
NDVI [-]	
Vegetation Proportion [-]	
Leave area index [$m^2 m^{-2}$]	Leave area index [$m^2 m^{-2}$]
Sun Zenith angle [$^{\circ}$]	
DEM [m]	
Displacement height [m]	Canopy resistance [$s m^{-1}$]
Surface roughness [m]	Aerodynamic Resistance [$s m^{-1}$]
Reference height [m]	Reference height [m]
Height of PBL [m]	
Sunshine hors per day [hrs]	
Julian day number[-]	

As shown in the Table 6-3, both algorithms work completely in different ways that could probability cause the big difference between them. Both MET and SEBS algorithms consider the basic input parameters like land surface parameters in different way. The different approach of both methods can significantly affect the AET estimate, and can bring considerable value differences. MET algorithm uses skin temperature which might be slightly less than surface temperature under normal condition. Apart from land surface temperature, MET algorithm used soil moisture at different depth which is not considered in SEBS model. It is also mentioned in MET product user manual that there are the deficiencies of soil moisture forecasts by the ECMWF model due to the 4D-var assimilation processes for southern part of Europe, but it is considered as the main limiting factors to evapotranspiration in the region. For this reason, the manual recommended independent estimates of soil moisture to assess a correct evaluation of ET in dry regions. Moreover, a gap filling procedure is applied on MET images to fill the non-processed pixels by an approximate estimate using similar vegetation composition and meteorological conditions with surrounding pixels in small regions.

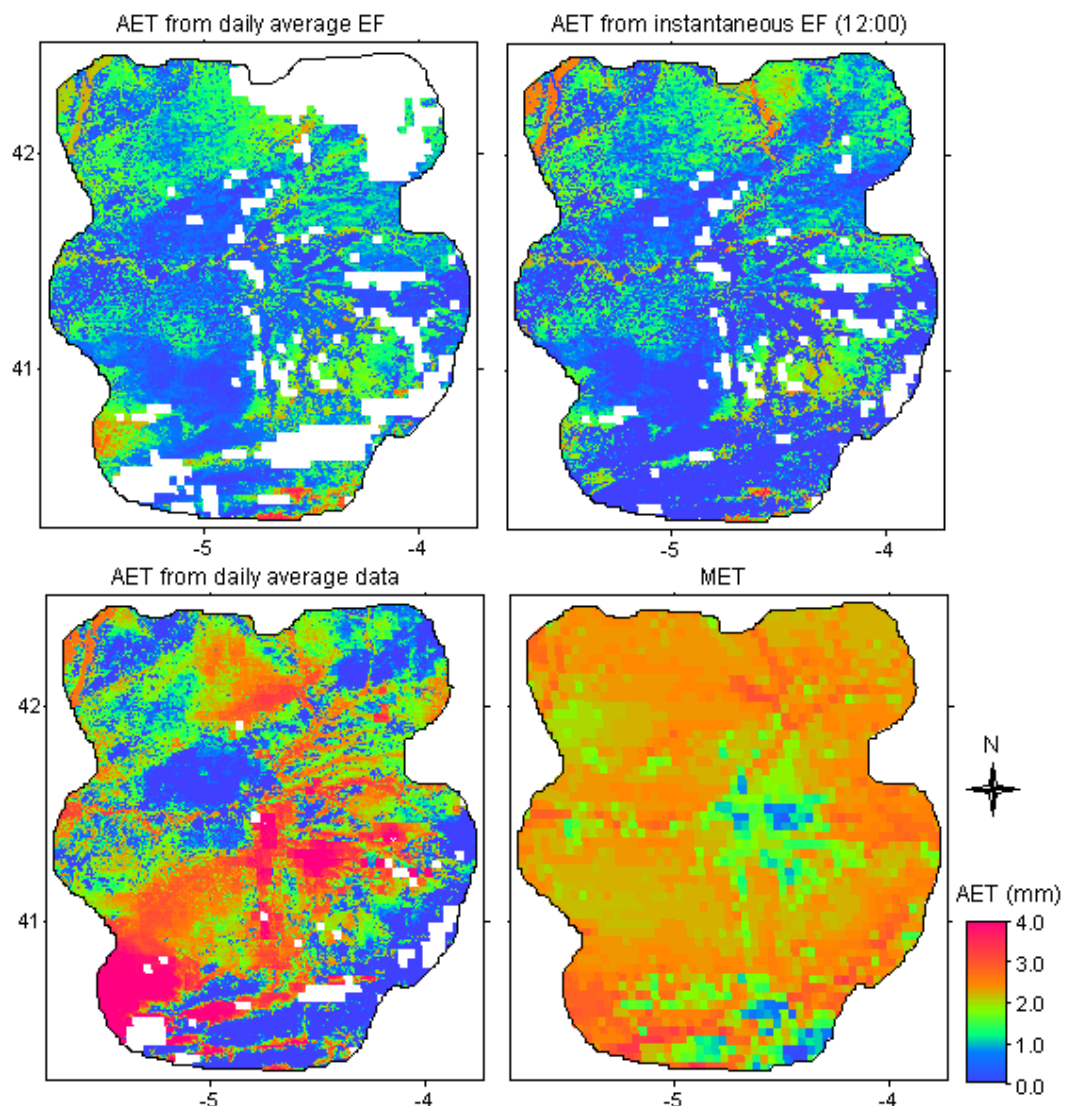


Figure 6-20. Maps of SEBS estimated AET and MET in the Castilla y Leon region, Spain (March, 15, 2009)

6.6. Water Balance Estimation

The rainfall distributions over the whole Spain and AET estimated from instantaneous data with SEBS over Castilla y Leon region during the study period are shown in Fig. 6-21 and 6-22 respectively.

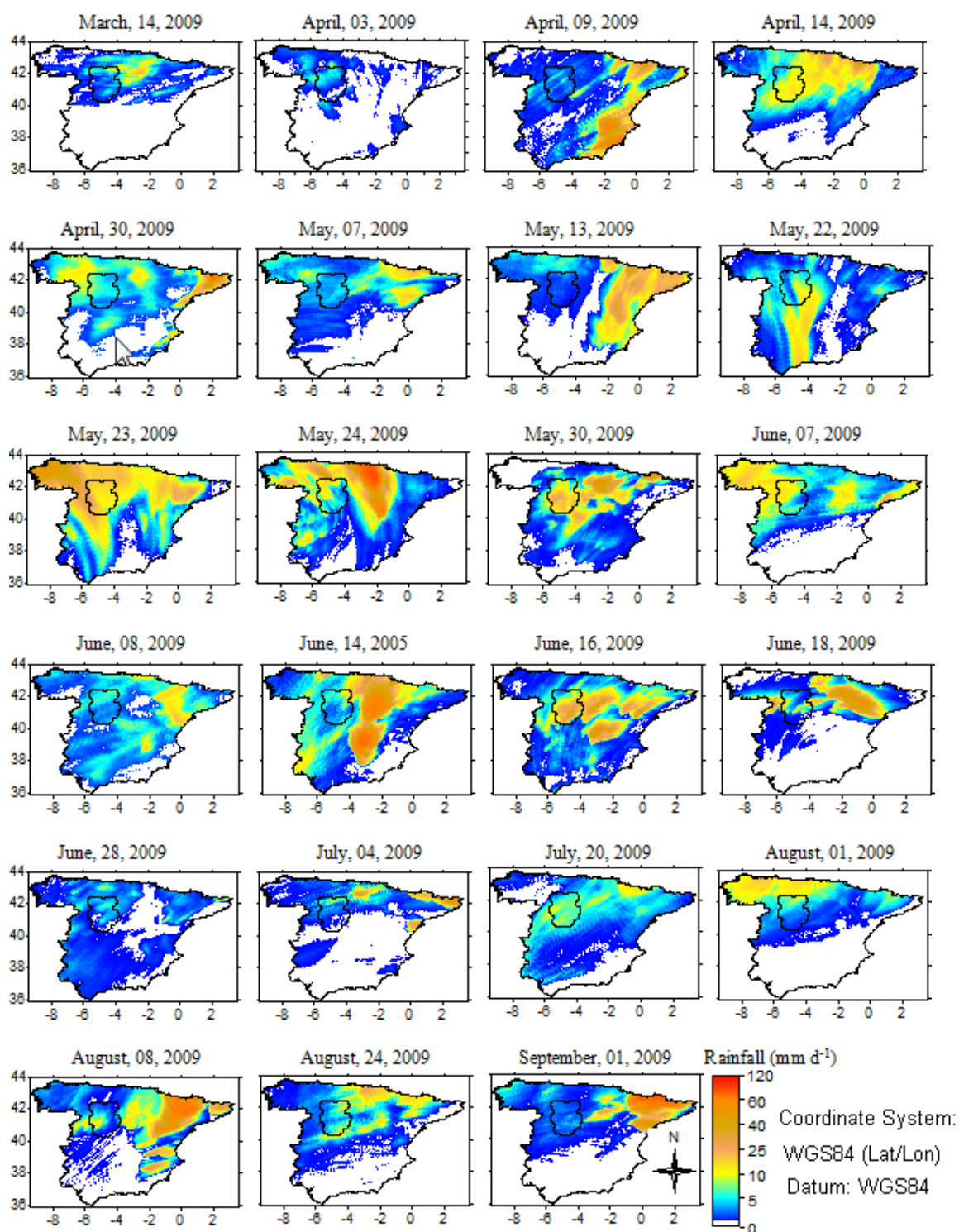


Figure 6-21. Daily rainfall distribution over the Spain during study period that covers the Castilla y Leon region as taken from MPEF-MPE

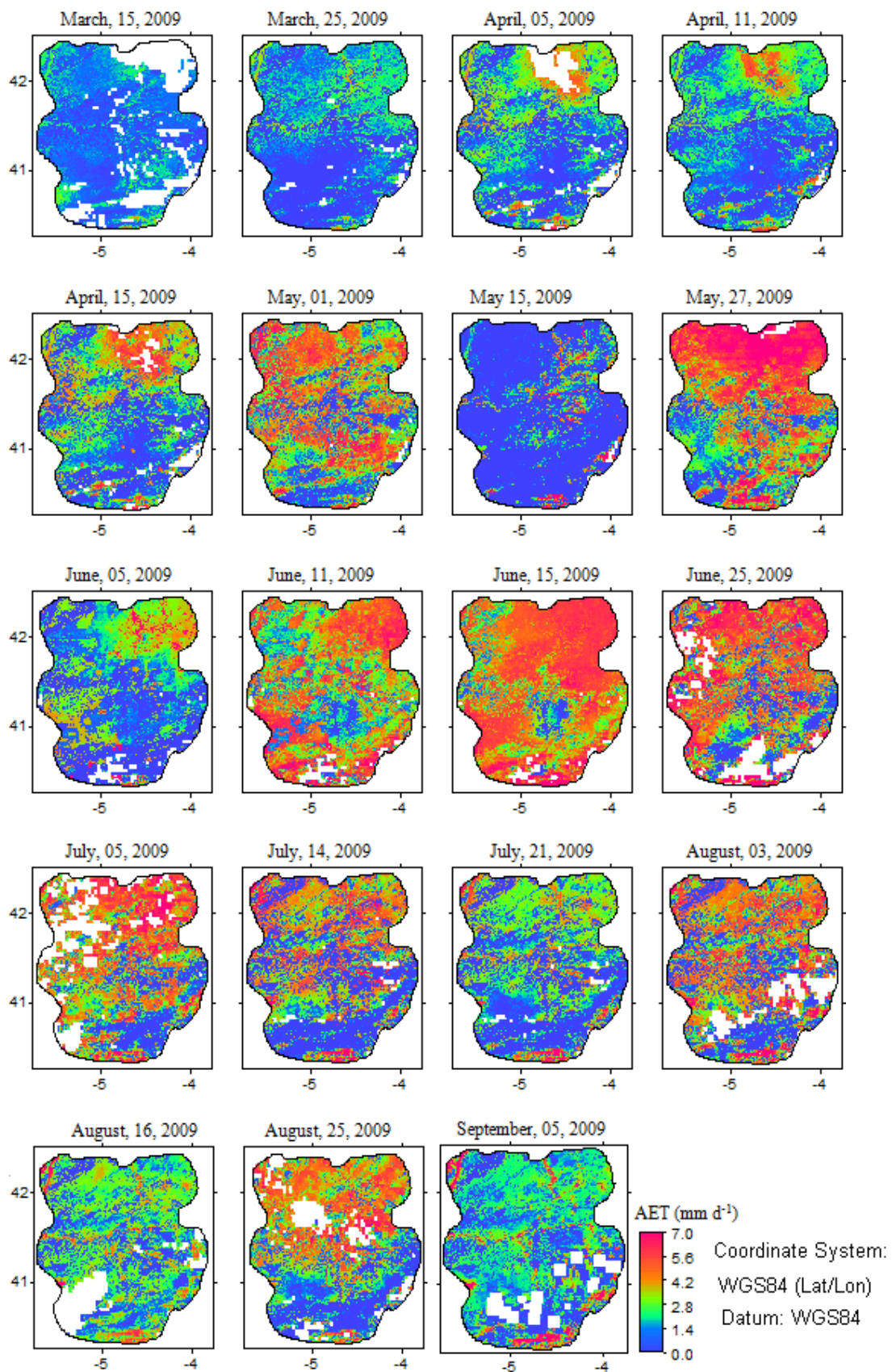


Figure 6-22. Daily AET maps in the Castilla y Leon region for some selected dates during the study period

In the map of daily evapotranspiration over Castilla y Leon region (Fig. 6-22), the undefined areas are pixels covered by cloud which persisted for more than one hour at the time of interest (11:30-12:30 UTC). As shown in the Fig. 6-21, the study area has few rainy days during active season in the region. In addition, the region is receiving light rainfall through out the study period except few days in the month of May and June.

Since the selected dates for estimation of AET are either dry or moderately wet (before or after rainy days), reasonable AET values were observed over most land cover classes. This indicates that SEBS can be used in most land cover classes to estimate the daily AET with acceptable error. Similarly, studies (Su, 2002; Su and Jacobs, 2001; Wenjing et al., 2006; Pan et al., 2008) have proven that SEBS can give good estimation of AET over some land cover class (cotton field, shrubland, wheat and other crops). Besides, high loss of rain water by evaporation has been observed in the region (Fig. 6-22 and 6-21). In addition, the daily evapotranspiration over irrigated croplands and forest were easily identifiable during the dry seasons (see September, 05 and August, 16 in Fig. 6-22), but there are still considerable evaporation values up to 2-4 mm per day from rainfed croplands and other minor land cover classes, when the area is still dry and the rainfed croplands are without crops. This indicates that overestimation of the model during dry season.

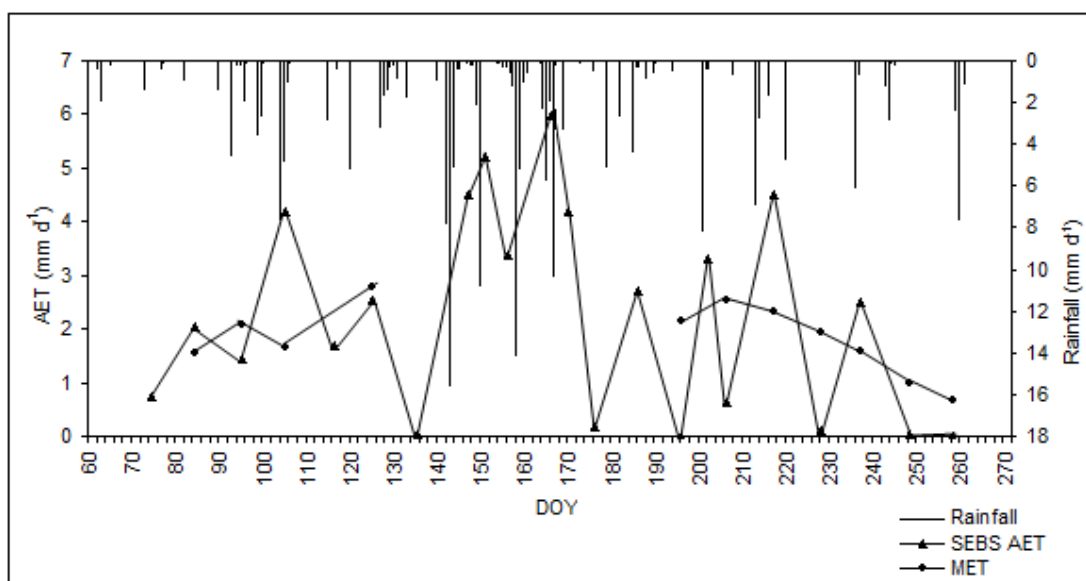


Figure 6-23. Variation of AET with precipitation distribution over rainfed croplands during the study period

A simple water balance estimation called climatological water balance (precipitation minus evapotranspiration) and variation of daily evapotranspiration during the study period were done over a main land cover class (rainfed croplands) in the study area. In addition, the daily variation of AET over irrigated croplands during the study period was also seen (Fig. 6-24). The selected pixels for this analysis are as shown in the Fig. 6-14. A linear interpolation was made between carefully selected days based on rainfall distribution to plot the daily variation of AET for the whole study period (Fig. 6-23 and 6-24). Due to the absence of MET products from the middle of April to the beginning of July, 2009, only some days of MET data were used to plot the daily variation of AET during the study period. As shown in Fig. 6-23 and 6-24, MET weakly responded to rainfall during the study period both in rainfed and irrigated croplands. Therefore, MET looks radiation driven products. For the case

of irrigated croplands, the variation of daily AET does not consistently depend on the occurrence of rainfall (see Fig.6-24). This is what we expected due to the application of water, especially during dry season. The daily AET over rainfed cropland is varied much more with rainfall distribution (Fig.6-23).

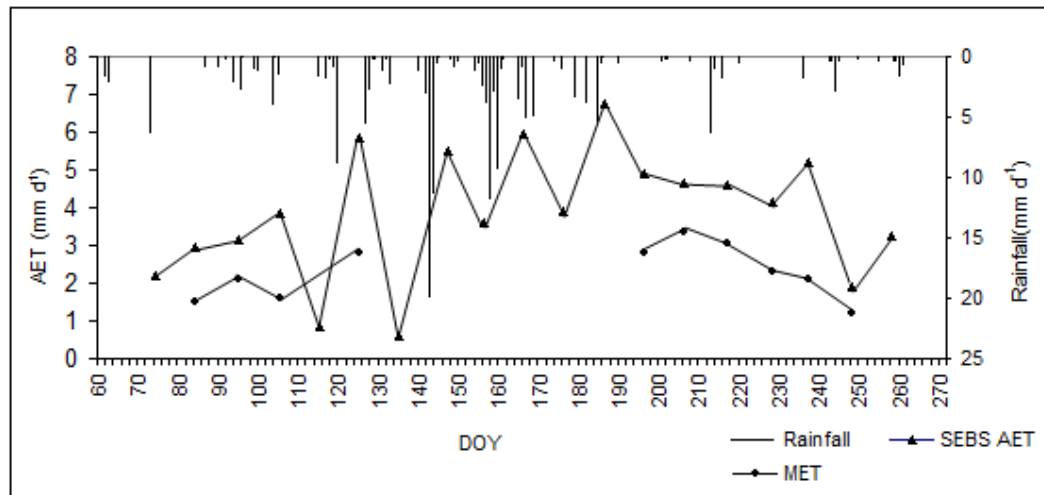


Figure 6-24. Variation of AET with rainfall distribution over irrigated croplands during the study period

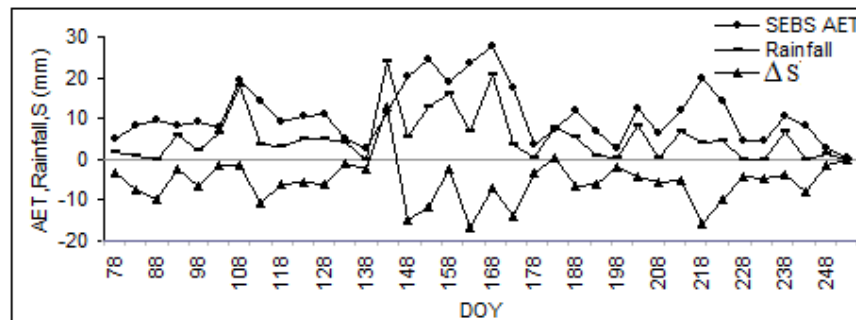


Figure 6-25. Five days cumulative AET, precipitation, and change in water storage over rainfed croplands during the study period

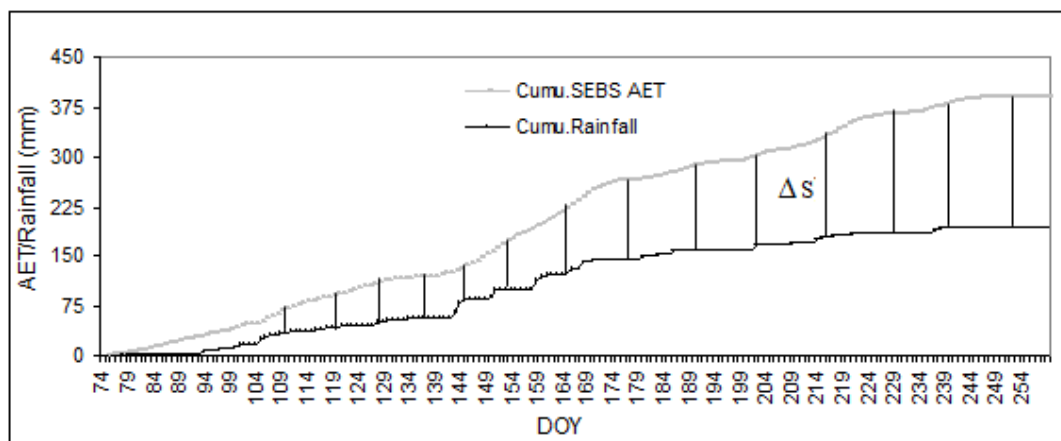


Figure 6-26. Cumulative AET and rainfall over rainfed crop lands during the study period (March, 15 – September, 15-2009)

Fig 6-25 shows the five days cumulative precipitation, actual evapotranspiration and change in water storage (precipitation minus evapotranspiration or excess precipitation) in rainfed croplands. As shown in this figure, no a month or half a month which has excess precipitation to sufficiently support crop growth. It indeed depends on the crop water requirements. Only few days in the month of May and June have excess precipitation but the remaining study period was dry with occasional rainfall. However, there is over estimation of daily AET by the model during the dry season, Fig. 6-26 shows that the region experiences high evaporation, but getting very low rainfall during the whole study period. At the end of the study period the cumulative AET is almost twice of the available precipitation. That is why the farming system of the region is gradually changing from rainfed croplands to irrigated croplands since more than a decade.

This water balance estimation method can be applied to any types of land cover classes in the study area except irrigated croplands as long as we are able to generate good estimation of rainfall distribution and daily AET maps of the region from remote sensing observation . Therefore, it is possible to estimate a simple water balance using SEBS estimated AET and rainfall product from EUMESAT. In this work, since daily AET for the rainy days or other days which AET is not calculated for are estimated by linear interpolation of the previous and the next day AET, there are high probabilities of under or overestimation of the daily AET between the days. Particularly, this is the problem in dry climate at which the time of the rain in a day affect the linear interpolation between the days. This is due to the fact that evaporation during the rainy days itself may much more than the surrounding days. Therefore, the best way to make good estimation of climatological water balance “Precipitation minus Evapotranspiration” from remote sensing observation is by calculating the daily AET for all days in the study period. But, this is practically difficult due to cloud cover. Therefore, estimating AET for all cloud free days during the study period by considering the diurnal variability of rainfall in the study area might give reliable interpolation results. This could potentially minimize the possible uncertainties in the interpolations of AET between the days.

7. Conclusions and Recommendations

7.1. Conclusions

In this work, combined geostationary and polar orbiting satellite products in conjunction with ground based meteorological data were employed to estimate the instantaneous EF, daily average EF, EF from daily averaged data, daily and instantaneous AET, and a simple water balance over different land cover classes in the Castilla y Leon region, Spain. The advantage of high temporal resolution products from EUMETSAT geostationary satellite systems and the relatively high spatial resolution products from MODIS and MERIS were fully utilized in this research. The combined uses of both products were enabled us to get all model input parameters with required temporal and spatial resolution, which were used to estimate the instantaneous EF and turbulent heat fluxes at every an hour step for different land cover classes using SEBS model, and then extended to daily averaged EF and daily AET. Therefore, the use of combined geostationary and polar orbiting satellite products have great advantage to estimate daily average EF instead of traditionally used instantaneous EF for estimation of daily AET. Generally, this approach will potentially reduce the uncertainty induced by use of one time observation (instantaneous EF) to estimate daily actual evapotranspiration from polar orbiting satellites.

The analysis results showed that reasonable diurnal variation of EF over some land cover classes in the study area. EF is also relatively stable during the day time, particularly from 11:00-16:00 solar time in irrigated croplands, shrubland, water body and rainfed croplands. The comparison was made between daily average EF and instantaneous EF over different land cover classes in the region. The results depict that daily average EF and instantaneous EF (at 12:00) have strong relation in irrigated croplands, rainfed croplands, shrubland, mosaic forest-shrubland and mosaic crop-vegetation, but it exhibits poor agreement for sparse vegetation, broadleaved deciduous forest and needleleaved evergreen forest. This indicates that we can not use instantaneous observations to estimate daily AET in sparse vegetation, broadleaved deciduous forest and needleleaved evergreen forest with SEBS model during such period. Moreover, the daily averaged EF was higher than instantaneous EF over all land cover classes. This shows that use of one time observation in the mid day for estimation of daily AET could lead to the underestimation of the results.

In addition, the daily averaged data was used to test the possibility of estimating daily actual evapotranspiration from daily averaged input data to the model. There was poor correlation between daily averaged EF and EF from daily averaged data in all land cover classes. In general, using the daily averaged data in SEBS model for estimation daily AET could lead to overestimation of the results. Therefore, daily averaged data can not be used as in put to SEBS model to estimate daily AET.

SEBS estimated AET and Meteosat second generation evapotranspiration (MET) were compared with measured AET in sparse vegetation. The result shows that SEBS estimated AET is very close to

measured AET. There is a considerable difference between the measured AET and MET in half hourly and daily bases. In both cases, MET overestimated the actual evapotranspiration in this specific land cover class. Even though they have big difference in value, they show similar patterns of diurnal variation of AET, particularly before mid day. In addition, the SEBS estimated AET was compared with MET over different land cover classes. They have close values in irrigated croplands and water body, but MET overestimated in the remaining land cover classes. The cause of such value differences might be due the fact that MET is a SVAT model which estimate evaporation from soil and vegetation independently using soil moisture, soil temperature and other vegetation and weather information, while SEBS is an energy balance model that uses surface temperature, surface biophysical parameters, and weather information to estimate turbulent heat fluxes. In addition, MET is a pre-operational product under development at LSA SAF.

The daily actual evapotranspiration of Castilla y Leon region was estimated using SEBS model for 22 selected days in the study period. During the estimation AET for carefully selected days, a clear pattern of AET values were observed over most land cover classes according to our expectations. This pattern indicates that SEBS model can be used to estimate daily AET over mixed land cover classes dominated by irrigated croplands, rainfed croplands, shrubland, mosaic forest-shrubland and mosaic crop-vegetation with acceptable error. Similarly, studies (Su, 2002; Su and Jacobs, 2001; Wenjing et al., 2006; Pan et al., 2008) have proven that SEBS can give good estimation of AET over some land cover class (cotton field, shrubland, wheat and other crops). Moreover, the daily actual evapotranspiration over irrigated croplands and broadleaved deciduous forest were easily identifiable during the dry season, but there are still considerable evaporation values up to 2-4 mm per day in rainfed croplands and other minor land cover classes, when the area is still very dry and the rainfed croplands are without crops. This shows that the model overestimate during the dry season. Generally, since it is possible to estimate daily average EF from EUMESAT satellite system products and ground-based data, there is high potential of making good estimation of daily AET using this daily average EF in all land cover classes and weather condition during clear sky days.

The behaviour of daily rainfall distributions during the whole study period and the daily AET for 22 selected days in the Castilla y Leon region was studied. According to the rainfall distribution maps obtained from EUMETSAT, the study area has few rainy days during active season in the region. The region receives only light rainfall throughout the study period, except few days in the month of May and June which have heavy rainfall. The results also show that high loss of rain water by evaporation during the study period in the region. In addition, it was observed that the daily variation of MET is weakly responded to rainfall occurrence both in irrigated and rainfed croplands during the study period. Therefore, MET looks radiation drive product. In contrary, SEBS estimated AET varied considerably with rainfall distribution in both rainfed and irrigated croplands, but in case of irrigated croplands, the variation of daily AET is not consistently dependent on the occurrence of rainfall.

Finally, a simple water balance estimation called “climatological water balance” was carried out for rainfed croplands in the study area. During water balance estimation, it was observed that no a month or half a month which has excess precipitation (e.g exceeding ET) during the growing season of the region. Only few days in the month of May and June have excess precipitation but the remaining study period were dry with high evapotranspiration and occasional light rainfall. This water balance estimation method can be applied to any types of land cover classes in the study area except irrigated

croplands as long as we are able to generate good estimation of rainfall distribution and daily AET maps of the region from remote sensing observations. Therefore, it is possible to estimate climatological water balance (Precipitation minus actual evapotranspiration) over land surface using remote sensing observations.

7.2. Recommendations

The method of combined geostationary and polar orbiting satellite products to estimate daily average EF was employed for the first time using SEBS model. However, reasonable results were observed during this work, the results were not validated over all land cover classes except sparse vegetation. Therefore, additional research can be conducted in the future to identify the potential source of input data to models for accurate quantification of AET at local to regional scales with acceptable spatial and temporal resolution. From this work the following recommendations can be drawn:

1. Doing similar research in all climate condition (wet, moderately wet and dry) after having;
 - Ground based flux measurements in all land cover classes
 - Quality checked products from both geostationary and polar orbiting satellites

This will potentially assess the performance of the model in any land cover types and climate zone.
2. Modifying SEBS interface to directly accept all products from geostationary satellites, and measurement height as a map. This will enable us to run the model at global scale using meteorological data from other source like from European centre for medium-range weather forecasts (ECMWF) or numerical weather prediction (NWP) that provide some meteorological information used by SEBS. Indeed, data from ECMWF has a course resolution, but it might be better than using simple interpolation techniques.
3. In the future, EUMETSAT satellite application facility on climate monitoring (CM-SAF) will supply all meteorological data required by SEBS model at any height above the ground surface, so that any one can use such data and test the performance of the model completely independent of ground-based data.
4. Validating the estimation of water balance from remote sensing observations using ground based data after calculating the daily AET during all cloud free days in the study period.
5. At this time, it is better to use SEBS model with EUMETSAT products to estimate daily or hourly AET than using MET in hydrological modelling and other related water resource management issues.

References

- Abdelghani, C.H., Hoedjes, J.C.B., Rodriquez, J.-C., Watts, C.J., Garatuza, J., Jacob, F. and Kerr, Y.H., 2008. Using remotely sensed data to estimate area-averaged daily surface fluxes over a semi-arid mixed agricultural land. *Agricultural and Forest Meteorology*, 148(3): 330-342.
- Adler, R.F., Negri, A.J., Keehn, P.R. and Hakkarinen, I.M., 1993. Estimation of Monthly Rainfall over Japan and Surrounding Waters from a Combination of Low-Orbit Microwave and Geosynchronous IR Data. , 32, 335-356. .
- Allen, R.G., Pereira, L.S., Raes, D. and Smith, M., 1998. Crop Evapotranspiration (guidelines for computing crop water requirements), FAO Irrigation and Drainage Paper No. 56:.
- Anderson, M.C., Norman, J.M., G.R.Diak, Kustas, W.P. and J.R.Mecikalski, 1997. A two-source time-integrated model for estimating surface fluxes using thermal infrared remote sensing, *Remote Sensing Environ.*, 60, 195-216.
- Arkin, P.A. and Meisner, B.N., 1987. The relationship between largescale convective rainfall and cold cloud over the Western Hemisphere during 1982–84. *Mon. Wea. Rev.*, 115, 51–74.
- Azevedo, P.V. and Verma, S.B., 1986. Aerodynamic characteristics of grain sorghum. *Agricultural and Forestry Meteorology*, 38, 193-204.
- Ba, M.B. and Gruber, A., 2001. GOES Multispectral Rainfall Algorithm (GMSRA). *Journal of Applied Meteorology*, 40(8): 1500-1514.
- Bastiaanssen, W.G.M., 1995. Regionalization of surface flux densities and moisture indicators in composite terrain. Ph.D Thesis, Wageningen Agriculture University, The Netherlands: 273 pp.
- Bastiaanssen, W.G.M., Menenti, M., Feddes, R.A. and Holtslag, A.A.M., 1998a. A remote sensing surface energy balance algorithm for land (SEBAL). part 1. Formulation. *Journal of Hydrology*, 212-213: 198-212.
- Bastiaanssen, W.G.M., Molden, D.J. and Makin, I.W., 2000. Remote sensing for irrigated agriculture: examples from research and possible applications. *Agricultural Water Management*, 46(2): 137-155.
- Bastiaanssen, W.G.M., Pelgrum, H., Wang, J., Ma, Y., Moreno, J.F., Roerink, G.J. and van der Wal, T., 1998b. A remote sensing surface energy balance algorithm for land (SEBAL): Part 2: Validation. *Journal of Hydrology*, 212-213: 213-229.
- Bicheron, P., Defourny, P., Brockmann, C., L.Schouten, C.Vancutsem, M.Huc, S.Bontemps, M.Leroy, F.Achard, M.Herold, F.Ranera and Arino, O., 2008. Globcover Products Description and Validation Report
- Böhm, A.U., Podzum, B.R. and Jacob, C.D., 1998. Surface water balance estimation for a semi-arid region using a regional climate model and comparison of water balance components with global circulation model output and analysis data. *Physics and Chemistry of The Earth*, 23(4): 405-411.
- Borak, J.S., Jasinski, M.F. and Crago, R.D., 2005. Time series vegetation aerodynamic roughness fields estimated from modis observations. *Agricultural and Forest Meteorology*, 135(1-4): 252-268.
- Bormann, H., Diekkrüger, B. and Richter, O., 1996. Effects of data availability on estimation of evapotranspiration. *Physics and Chemistry of The Earth*, 21(3): 171-175.
- Brisson, A., Le Borgne, P. and Marsouin, A., 1999. Development of Algorithms for Surface Solar Irradiance retrieval at O&SI SAF low and Mid Latitude, Météo-France/CMS, Lannion
- Brutsaert, W., 1982. *Evaporation into the atmosphere*. Reidel, Dordrecht: 299 pp.
- Calvet, J.-C., Noilhan, J., Roujean, J.-L., Bessemoulin, P., Cabelguenne, M., Olioso, A. and Wigneron, J.-P., 1998. An interactive vegetation SVAT model tested against data from six contrasting sites. *Agricultural and Forest Meteorology*, 92(2): 73-95.
- Carlos, A.C.d.S., Bernardo, B.d.S. and Christopher, M.U.N., 2009. Analyses of the evaporative fraction using eddy covariance and remote sensing techniques. *Anais XIV Simpósio Brasileiro de Sensoriamento Remoto*, Natal, Brasil, 25-30 abril 2009, INPE, p. 451-458.

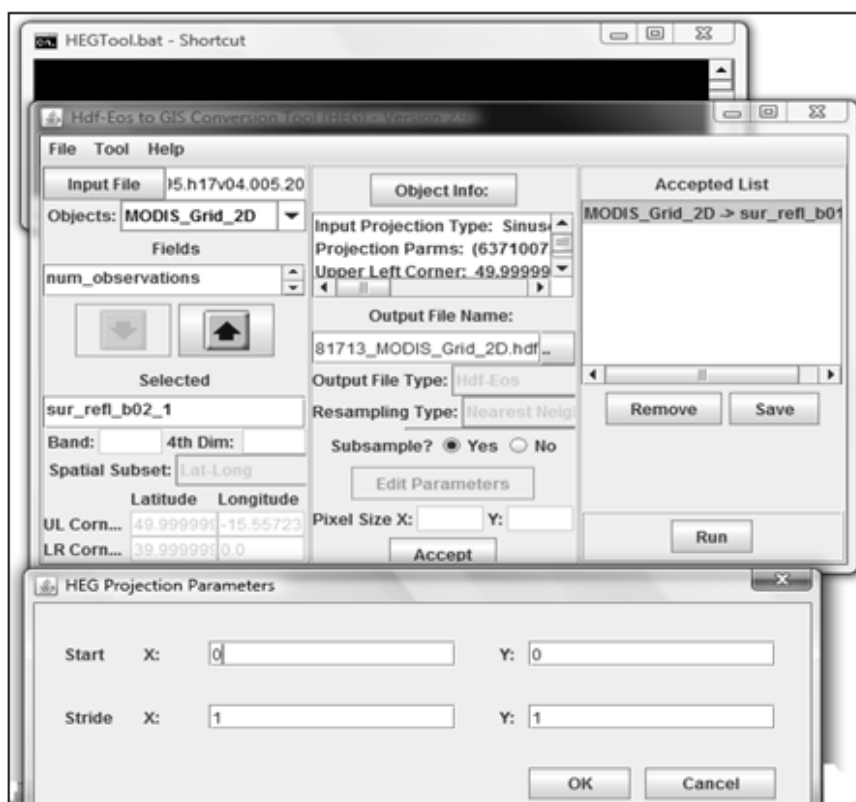
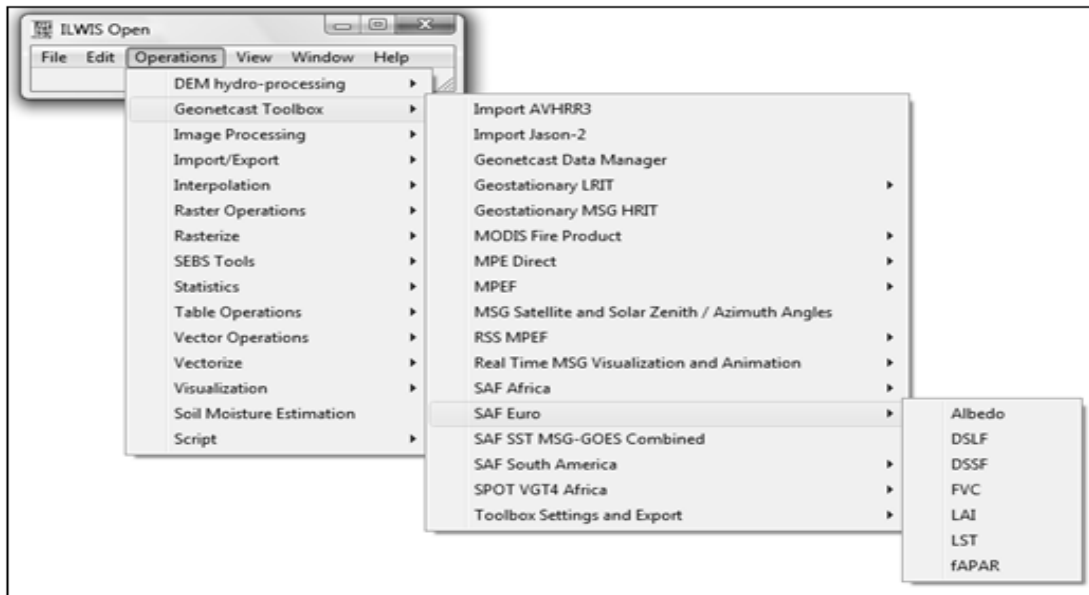
- Champeaux, J.L., Arcos, D., Bazile, E., Giard, D., Goutorbe, J.P., Habets, F., Noilhan, J. and Roujean, J.L., 2000. AVHRR-derived vegetation mapping over Western Europe for use in Numerical Weather Prediction models. *International Journal of Remote Sensing*, 21(6): 1183 - 1199.
- Choudhury, B.J. and Monteith, J.L., 1988. A four-layer model for the heat budget of homogeneous land surfaces. *Quarterly Journal of the Royal Meteorological Society*, 114(480): 373-398.
- Cleugh, H.A., Leuning, R., Mu, Q. and Running, S.W., 2007. Regional evaporation estimates from flux tower and MODIS satellite data. *Remote Sensing of Environment*, 106(3): PP.285-304.
- Colwell, J.E., 1974. Vegetation canopy reflectance, *Remote Sens. Environ.*, 3:175-183.
- Courault, D., Seguin, B. and Olioso, A., 2005. Review on estimation of evapotranspiration from remote sensing data: From empirical to numerical modeling approaches. *Irrigation and Drainage Systems*, 19(3): 223-249.
- Dai, Y. and Coauthors, 2003. The common land model (CLM). *Bull. Amer. Meteor. Soc.*, 84(8), 1013–1023.
- Dash, P., Göttsche, F.M., Olesen, F.S. and Fischer, H., 2002. Land surface temperature and emissivity estimation from passive sensor data: theory and practice—current trends”, *Int. J. Remote Sens.*, vol. 23, 2563–2594.
- Deering, D.W., 1978. Rangeland reflectance characteristics measured by aircraft and spacecraft sensors. Ph.D. Dissertation, Texas A & M University, College Station, TX, 338 pp.
- Dickinson, R.E., Henderson-sellers, A. and Kennedy, P.J., 1993. Biosphere-Atmosphere Transfer Scheme (BATS) Version 1e as coupled to the NCAR Community Climate Model. National Center for Atmospheric Research (NCAR) Tech. Note, NCAR/TN-387+STR, 72pp.
- Door, W.G. and Teresa, M. (Editors), 2002. *Geology of Spain* (Hardback). GSL, Spain, 632 pp.
- Dorman, J.L. and Sellers, P.J., 1989. A global climatology of albedo, roughness length, and stomatal resistance for atmospheric general circulation models as represented by the Simple Biosphere Model (SiB). *J. Appl. Meteor.*, 21, 833-855.
- Farah, H.O., Bastiaanssen, W.G.M. and Feddes, R.A., 2004. Evaluation of the temporal variability of the evaporative fraction in a tropical watershed. *International Journal of Applied Earth Observation and Geoinformation*, 5(2): 129-140.
- Ferguson, C., Wood, E., Sheffield, J., Gao, H. and Lettenmaier, D., 2009. Quantifying uncertainty in remote sensing based estimates of evapotranspiration due to data inputs over the continental United States. *Int. Journal of Remote Sensing*, TRES-SIP-2009-0124(Special Issue paper): pp.51.
- Garratt, J.R., 1992. *The atmospheric boundary layer*. Cambridge Atmospheric and Space Science Series, Cambridge University Press, Cambridge, UK, 316pp.
- Gash, J.H.C. and Shuttleworth, J., 2007. Evaporation. Benchmark papers in hydrology. International Association of Hydrological Sciences (IAHS), Wallingford, pp131.
- Gellens-Meulenberghs, F., Arboleda, A. and Ghilain, N., 2006. Status of development of the LSA-SAF evapotranspiration product. *Proc. 2nd LSA-SAF Training Workshop*, Lisbon, 8-10 March, 10 pp. .
- Gellens-Meulenberghs, F., Arboleda, A. and Ghilain, N., 2008. *Meteosat Second Generation Evapotranspiration (MET)*, Product User Manual. 27pp
- Gentine, P., Entekhabi, D., Chehbouni, A., Boulet, G. and Duchemin, B., 2007. Analysis of evaporative fraction diurnal behaviour. *Agricultural and Forest Meteorology*, 143(1-2): 13-29.
- Hanna, L.W. and Siam, N., 1981. The empirical relation between sunshine and radiation and its use in estimating evaporation in North East England. *International Journal of Climatology*, 1(1): 11-19.
- Hatfield, J.L., 1989. Aerodynamic properties of partial canopies. *Agricultural and Forestry Meteorology*, 46, 15-22.
- Hennemuth, B. and Lammert, A., 2006. Determination of the Atmospheric Boundary Layer Height from Radiosonde and Lidar Backscatter. *Boundary-Layer Meteorology*, 120(1): 181-200.

- Hoedjes, A. Chehbouni, F. Jacob, J. Ezzahar and G. Boulet, 2008. Deriving daily evapotranspiration from remotely sensed instantaneous evaporative fraction over olive orchard in semi-arid Morocco. *Journal of Hydrology* 254, 1-4 (2008) 53-64.
- Huete, A., Justice, C. and Leeuwen, W.V., 1999. MODIS Vegetation Index (MOD 13) Algorithm Theoretical Basis Documents, Version 3. University of Virginia Department of Environmental Sciences Clark Hall Charlottesville, VA 22903.
- Huete, A., Justice, C. and Liu, H., 1994. Development of vegetation and soil indices for MODIS-EOS, *Remote Sens. Environ.*, 49:224-234.
- Iguchi, T., Meneghini, R., Awaka, J., Kozu, T. and Okamoto, K., 2000. Rain profiling algorithm for TRMM Precipitation Radar data. *Advances in Space Research*, 25(5): 973-976.
- Iqbal, M., 1983. An introduction to Solar Radiation. Academic Press Canada, Ontario. 416pp
- Kidd, C., Kniveton, D.R., Todd, M.C. and Bellerby, T.J., 2003. Satellite Rainfall Estimation Using Combined Passive Microwave and Infrared Algorithms. *Journal of Hydrometeorology*, 4(6): 1088-1104.
- Kustas, W.P., Choudhury, B.J., K. E. Kunkel and Gay, L.W., 1989. Estimate of the aerodynamic roughness parameters over an incomplete canopy cover of cotton. *Agricultural and Forestry Meteorology*, 46, 91- 105.
- Lhomme, J.P. and Elguero, E., 1999. Examination of evaporative fraction diurnal behaviour using a soil-vegetation model coupled with a mixed-layer model. *Hydrol. Earth Syst. Sci.*, 3(2), 259-270.
- Lin, W., Z. Su, Rogier, v.d.V. and Shan, X., 2008. Satellite Based Daily Evapotranspiration in Hebei Plain, Northeastern China. *Proc. Dragon 1 Programme Final Results 2004–2007*, Beijing, P.R. China 21– 25 April 2008 (ESA SP-655, April 2008).
- Liu, S., HU, G., LU, L. and MAO, D., 2007. Estimation of regional evapotranspiration by TM/ETM+ data over heterogeneous surfaces, 73. *American Society for Photogrammetry and Remote Sensing*, Bethesda, MD, ETATS-UNIS, 10 pp.
- LSA SAF RMI Team, 2008. Algorithm Theoretical Basis Document ,Meteosat Second Generation Evapotranspiration (MET) Product, EUMETSAT. 32 pp.
- Lu, L., Liu, S., Xu, Z., Yang, K., Cai, X., Jia, L. and Wang, J., 2009. The characteristics and parameterization of aerodynamic roughness length over heterogeneous surfaces. *Advances in Atmospheric Sciences*, 26(1): 180-190.
- Lyra, G.B. and Pereira, A.R., 2007. Parâmetros de rugosidade aerodinâmica sobre vegetação esparsa em região semi-árida. *Revista Brasileira de Meteorologia*, 22: 262-272.
- Martín, N.S., 2009. Teledetección Óptica Aplicada A un Modelo Distribuido De Balance Hídrico (Hidromore) Para el Cálculo DE Evapotranspiración Y Humedad DE Suelo, University of Salamanca, Spain. PhD Thesis: 379pp.
- Mathias, A.D., Kustas, W.P., Gay, L.W., Cooper, D.I., Alves, L.M. and Pinter, P.J., 1990. Aerodynamic parameters for a sparsely roughened surface composed of small cotton plants and ridged soil. *Remote Sens. Environ.*, 32, 143-153.
- Mecikalski, J.R., Diak, G.R., Anderson, M.C. and Norman, J.M., 1999. Estimating fluxes on continental scales using remotely-sensed data in an atmospheric-land exchange model, *J. Appl. Meteorol.*, 35, 1352-1369.
- Menenti, M., 1993. Understanding land surface evapotranspiration with satellite multispectral measurements. *Advances in Space Research*, 13(5): 89-100.
- Minacapilli, M., Agnese, C., Blanda, F., Cammalleri, C., Ciralo, G., D'Urso, G., Iovino, M., Pumo, D., Provenzano, G. and Rallo, G., 2009. Estimation of actual evapotranspiration of Mediterranean perennial crops by means of remote-sensing based surface energy balance models. *Hydrol. Earth Syst. Sci.*, 13, pp.1061-1074.
- Mu, Q., Heinsch, F.A., Zhao, M. and Running, S.W., 2007. Development of a global evapotranspiration algorithm based on MODIS and global meteorology data. *Remote Sensing of Environment*, 111 (2007) 519–536.
- Mutiga, K., Su, Z. and Woldai, T., 2008. Using satellite remote sensing to assess evapotranspiration : case study of the Upper Ewaso Ng'iro north basin, Kenya. In: *ISPRS 2008 : Proceedings of*

- the XXI congress : Silk road for information from imagery : the International Society for Photogrammetry and Remote Sensing, 3-11 July, Beijing, China. Comm. VII, ThS 17 . Beijing : ISPRS, 2008. : pp.1457-1461.
- Norman, J.M., Anderson, M.C., Kustas, W.P., French, A.N., Mecikalski, J., Torn, R., Diak, G.R., Schmugge, T.J. and Tanner, B.C.W., 2003. Remote sensing of surface energy fluxes at 101-m pixel resolutions. *Water Resour. Res.*, 39.
- Norman, J.M., Kustas, W.P. and Humes, K.S., 1995. Source approach for estimating soil and vegetation energy fluxes in observation of directional radiometric surface temperature. . *Agricultural and Forest Meteorology*, 77: 263-293.
- Pan, M., Wood, E.F., Wójcik, R. and McCabe, M.F., 2008. Estimation of regional terrestrial water cycle using multi-sensor remote sensing observations and data assimilation. *Remote Sensing of Environment* 112 (2008) pp.1282–1294.
- Peel, M.C., Finlayson, B.L. and McMahon, T.A., 2007. Updated world map of the Köppen-Geiger climate classification. *Hydrology and Earth System Sciences.*, 11, 1633–1644.
- Prata, A.J., 1993. Land surface temperature derived from the advanced very high resolution radiometer and the along-track scanning radiometer: 1. Theory”, *J. Geophys. Res.*, vol. 98, 16,689–16,702.
- Prueger, J.H., Kustas, W.P., Hipps, L.E. and Hatfield, J.L., 2004. Aerodynamic parameters and sensible heat flux estimates for a semi-arid ecosystem. *Journal of Arid Environments*, 57(1): 87-100.
- Rwasoka, D.T., 2010. Evapotranspiration in water limited environments: up-scaling from crown canopy to the eddy flux footprint; MSc thesis, University of Twente, ITC faculty, The Netherlands: 79 pp.
- Savenije and G. Hubert, 1995. New definitions for moisture recycling and the relationship with land-use changes in the Sahel. *Journal of Hydrology*, 167(1-4): 57-78.
- Schmetz, J., Pili, P., Tjemkes, S., Just, D., Kerkman, J., Rota, S. and Ratier, A., 2002. An introduction to Meteosat Second Generation (MSG)”, *Bull. Amer. Meteor. Soc.*, vol. 83, 977-992, 2002a.
- Schmugge, T.J., Kustas, W.P., Ritchie, J.C., Jackson, T.J. and Rango, A., 2002. Remote sensing in hydrology. *Advances in Water Resources*, 25(8-12): 1367-1385.
- Shaw, R.H. and Pereira, A.R., 1982. Aerodynamic roughness of a plant canopy: A numerical experiment. *Agricultural Meteorology*, 26(1): 51-65.
- Sobrino, J.A., Kharraz, J. and Li, Z., 2003. Surface temperature and water vapour retrieval from MODIS data. *International Journal of Remote Sensing*, 24(24): 5161 - 5182.
- Sobrino, J.A., Raissouni, N. and Li, Z.-L., 2001. A Comparative Study of Land Surface Emissivity Retrieval from NOAA Data. *Remote Sensing of Environment*, 75(2): 256-266.
- Su, Z., 2002. The Surface Energy Balance System (SEBS) for estimation of turbulent heat fluxes. *Hydrology and Earth System Sciences*, 6(1): P.85-100.
- Su, Z. and Jacobs, Z.C., 2001. ENVISAT: actual evaporation. BCRS Report 2001: Beleidscommissie Remote Sensing (BCRS), Delft., USP-2 Report 2001 01-02.
- Su, Z., Schmugge, T., Kustas, W.P. and Massman, W.J., 2001. An Evaluation of Two Models for Estimation of the Roughness Height for Heat Transfer between the Land Surface and the Atmosphere. *Journal of Applied Meteorology*, 40(11): 1933-1951.
- Tang, Q., 2007. Estimation of evapotranspiration using remote sensing data. Land Surface Hydrology Research Group, Department of Civil and Environmental Engineering, University of Washington (<http://www.geog.umd.edu/eos/>), November, 2009.
- Trigo, I.F., Peres, L.F., DaCamara, C.C. and Freitas, S.C., 2008. Thermal Land Surface Emissivity retrieved from SEVIRI/Meteosat. *IEEE Trans. Geosci. Remote Sens.*, Doi: 10.1109/TGRS.2007.905197.
- Tsouni, A., Kontoes, C., Koutsoyiannis, D., Elias, P. and Mamassis, N., 2008. Estimation of Actual Evapotranspiration by Remote Sensing: Application in Thessaly Plain, Greece. *Sensors*, 8, 3586-3600; DOI: 10.3390/s8063586.

- Venturini, V., Islam, S. and Rodriguez, L., 2008. Estimation of evaporative fraction and evapotranspiration from MODIS products using a complementary based model. *Remote Sensing of Environment*, 112(1): 132-141.
- Vicente, G.A., Davenport, J.C. and Scofield, R.A., 2002. The role of orographic and parallax corrections on real time high resolution satellite rainfall rate distribution. *International Journal of Remote Sensing*, 23(2): 221 - 230.
- Wan, Z. and Dozier, J., 1996. A generalized split-window algorithm for retrieving land surface temperature from space", . *IEEE Trans. Geosci. Remote Sens.*, vol. 34,892-905.
- Waters, R., Allen, R., Bastiaanssen, W., Tasumi, M. and Trezza, R., 2002. Surface energy balance algorithms for land, Idaho implementation, advanced training and users manual. Version 1.0, The Idaho Department of Water Resources, 98pp.
- Wenjing, L., Velde, R.v.d. and Su, 2006. Satellite based regional-scale evapotranspiration in the hebei plain, northeastern china. *Proc. Dragon 1 Programme Final Results 2004–2007*, Beijing, P.R. China 21– 25 April 2008 (ESA SP-655, April 2008).
- Wieringa, J., 1993. Representative roughness parameters for homogeneous terrain. *Boundary-Layer Meteorology*, 63(4): 323-363.

Appendix B GEONETCast toolboxes integrated to ILWIS, and HDF-EOS to GeoTIFF (HEG) tool interfaces for remote sensing data importing and processing



Appendix C The missing pattern of land surface temperature record throughout the day for randomly selected pixels

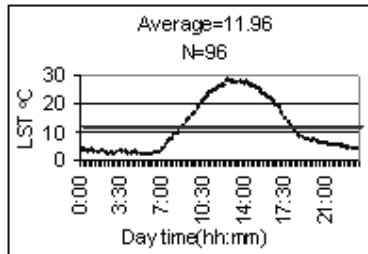


Fig. a

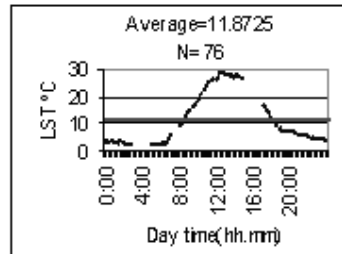


Fig. b

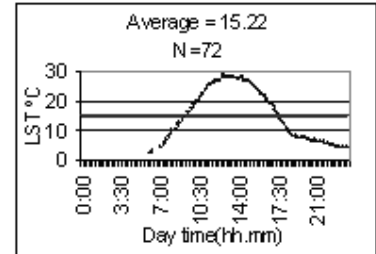


Fig. c

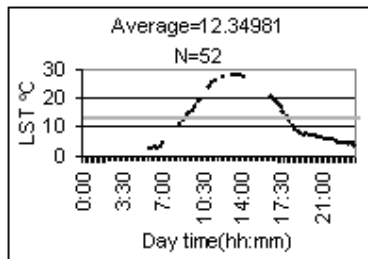


Fig. d

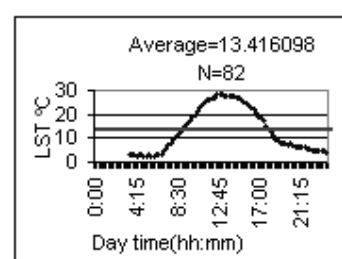


Fig. e

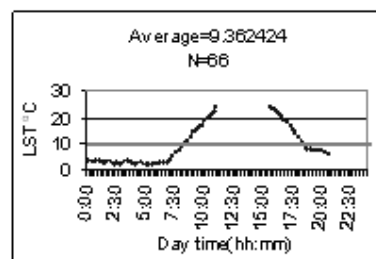


Fig. f

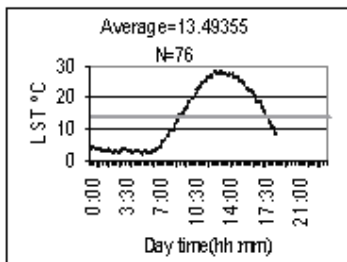


Fig. g

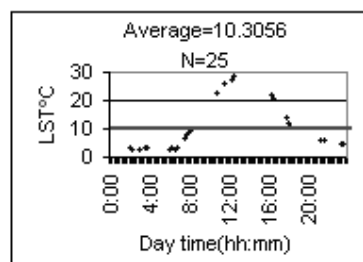


Fig. h

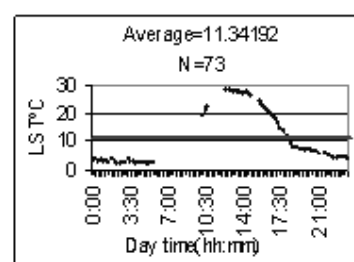


Fig. i

Appendix D Detailed land cover classification used for the assignment of vegetaion height

11 - Irrigated croplands	130 - Closed to open shrubland
12 - Irrigated shrub or tree crops	131 - Closed to open broadleaved or needleleaved evergreen shrubland
13 - Irrigated herbaceous crops	134 - Closed to open broadleaved deciduous shrubland
14 - Rainfed croplands	140 - Closed to open grassland
15 - Rainfed herbaceous crops	141 - Closed grassland
16 - Rainfed shrub or tree crops	143 - Open grassland
20 - Mosaic Croplands/Vegetation	145 - Lichens or mosses
21 - Mosaic Croplands/Grassland-Shrubland	150 - Sparse vegetation
22 - Mosaic Croplands/Forest	151 - Sparse grassland
30 - Mosaic Vegetation/Croplands	152 - Sparse shrubland
31 - Mosaic Grassland-Shrubland/Croplands	153 - Sparse trees
32 - Mosaic Forest/Croplands	160 - Closed to open broadleaved forest regularly flooded (fresh-brackish water)
40 - Closed to open broadleaved evergreen or semi-deciduous forest	161 - Closed to open broadleaved forest (semi-)permanently flooded (fresh-brackish water)
41 - Closed broadleaved evergreen or semi-deciduous forest	162 - Closed to open broadleaved forest temporarily flooded (fresh-brackish water)
42 - Open broadleaved evergreen or semi-deciduous forest	170 - Closed broadleaved forest permanently flooded (saline-brackish water)
50 - Closed broadleaved deciduous forest	180 - Closed to open vegetation regularly flooded
60 - Open broadleaved deciduous forest	181 - Closed to open woody vegetation regularly flooded
70 - Closed needleleaved evergreen forest	185 - Closed to open grassland regularly flooded
90 - Open needleleaved deciduous or evergreen forest	190 - Artificial areas
91 - Open needleleaved deciduous forest	200 - Bare areas
92 - Open needleleaved evergreen forest	201 - Consolidated bare areas
100 - Closed to open mixed broadleaved and needleleaved forest	202 - Non-consolidated bare areas
101 - Closed mixed broadleaved and needleleaved forest	203 - Salt hardpans
102 - Open mixed broadleaved and needleleaved forest	210 - Water bodies
110 - Mosaic Forest-Shrubland/Grassland	220 - Permanent snow and ice
120 - Mosaic Grassland/Forest-Shrubland	230 - No data

Appendix E ILWIS script for assignment of vegetation height and estimation of roughness height

```

canoHeight=IFF(land cover_Catilla=11,0.5,IFF(land cover_Catilla=12,1.0,IFF(land
cover_Catilla=13,2.4,IFF(land cover_Catilla=14,0.01,IFF(land cover_Catilla=16,1.6,IFF(land
cover_Catilla=20,3.5,IFF(land cover_Catilla=30,2.4,IFF(land cover_Catilla=40,5.5,IFF(land
cover_Catilla=50,7.5,IFF(land cover_Catilla=60,6.5,IFF(land cover_Catilla=70,8.5,IFF(land
cover_Catilla=90,7.0,IFF(land cover_Catilla=100,7,IFF(land cover_Catilla=110,5,IFF(land
cover_Catilla=120,5.5,IFF(land cover_Catilla=134,2,IFF(land cover_Catilla=130,3.5,IFF(land
cover_Catilla=140,0.15,IFF(land cover_Catilla=150,6,IFF(land cover_Catilla=151,0.10,IFF(land
cover_Catilla=160,7.5,IFF(land cover_Catilla=170,6.5,IFF(land cover_Catilla=180,5.2,IFF(land
cover_Catilla=190,6.7,IFF(land cover_Catilla=200,0,IFF(land
cover_Catilla=210,0.009,?))))))))))))))))))))))))))
CanopyHeight_Castilla=IFF(Boundary_Layout="Seg 1", canoHeight,?)
Roughness2=0.136*CanopyHeight_Castilla
Roughness3=0.005+0.5*(NDVI_Resam12/0.9)^2.5
DisplacementHeight1=2/3*(CanopyHeight_Castilla)
X=0.2*LAI_Resam
DisplacementHeight2=CanopyHeight_Castilla*(ln (1+X^(1/6)) +0.03*ln(1+X^(1/6)))
ZOM1=0.009+(0.28*CanopyHeight_Castilla*X^0.5)
ZOM2=0.3*CanopyHeight_Castilla*(1-(DisplacementHeight2/CanopyHeight_Castilla))
Roughness4= IFF(X<=0.2,ZOM1,ZOM2)

Roughness_5=IFF(land cover_Catilla=11,Roughness4,IFF(land
cover_Catilla=12,Roughness4,IFF(land cover_Catilla=13,Roughness4,IFF(land
cover_Catilla=14,Roughness3,IFF(land cover_Catilla=16,Roughness3,IFF(land
cover_Catilla=20,Roughness4,IFF(land cover_Catilla=30,Roughness4,IFF(land
cover_Catilla=40,Roughness2,IFF(land cover_Catilla=50,Roughness2,IFF(land
cover_Catilla=60,Roughness2,IFF(land cover_Catilla=70,Roughness2,IFF(land
cover_Catilla=90,Roughness2,IFF(land cover_Catilla=100,Roughness2,IFF(land
cover_Catilla=110,Roughness2,IFF(land cover_Catilla=120,Roughness4,IFF(land
cover_Catilla=134,Roughness2,IFF(land cover_Catilla=130,Roughness4,IFF(land
cover_Catilla=140,Roughness4,IFF(land cover_Catilla=150,Roughness4,IFF(land
cover_Catilla=151,Roughness4,IFF(land cover_Catilla=160,Roughness2,IFF(land
cover_Catilla=170,Roughness2,IFF(land cover_Catilla=180,Roughness2,IFF(land
cover_Catilla=190,Roughness2,IFF(land cover_Catilla=200,Roughness4,IFF(land
cover_Catilla=210,Roughness4,?))))))))))))))))))))))))))
Roughness_Castilla=IFF(Boundary_Layout="Seg 1",Roughness_5,?)
Displacement=iff(land cover_Catilla=13,DisplacementHeight1,iff(land
cover_Catilla=14,DisplacementHeight1,iff(land cover_Catilla=70,DisplacementHeight1,iff(land
cover_Catilla=50,DisplacementHeight1,DisplacementHeight2))))

```

Appendix F Statistical formulas used in this research

$$\text{Standard error} = \sqrt{\frac{1}{(n-2)} \left[\sum (y - \bar{y})^2 - \frac{\left[\sum (x - \bar{x})(y - \bar{y}) \right]^2}{\sum (x - \bar{x})^2} \right]}$$

$$\text{Absolute error (Abs.error)} = y - x$$

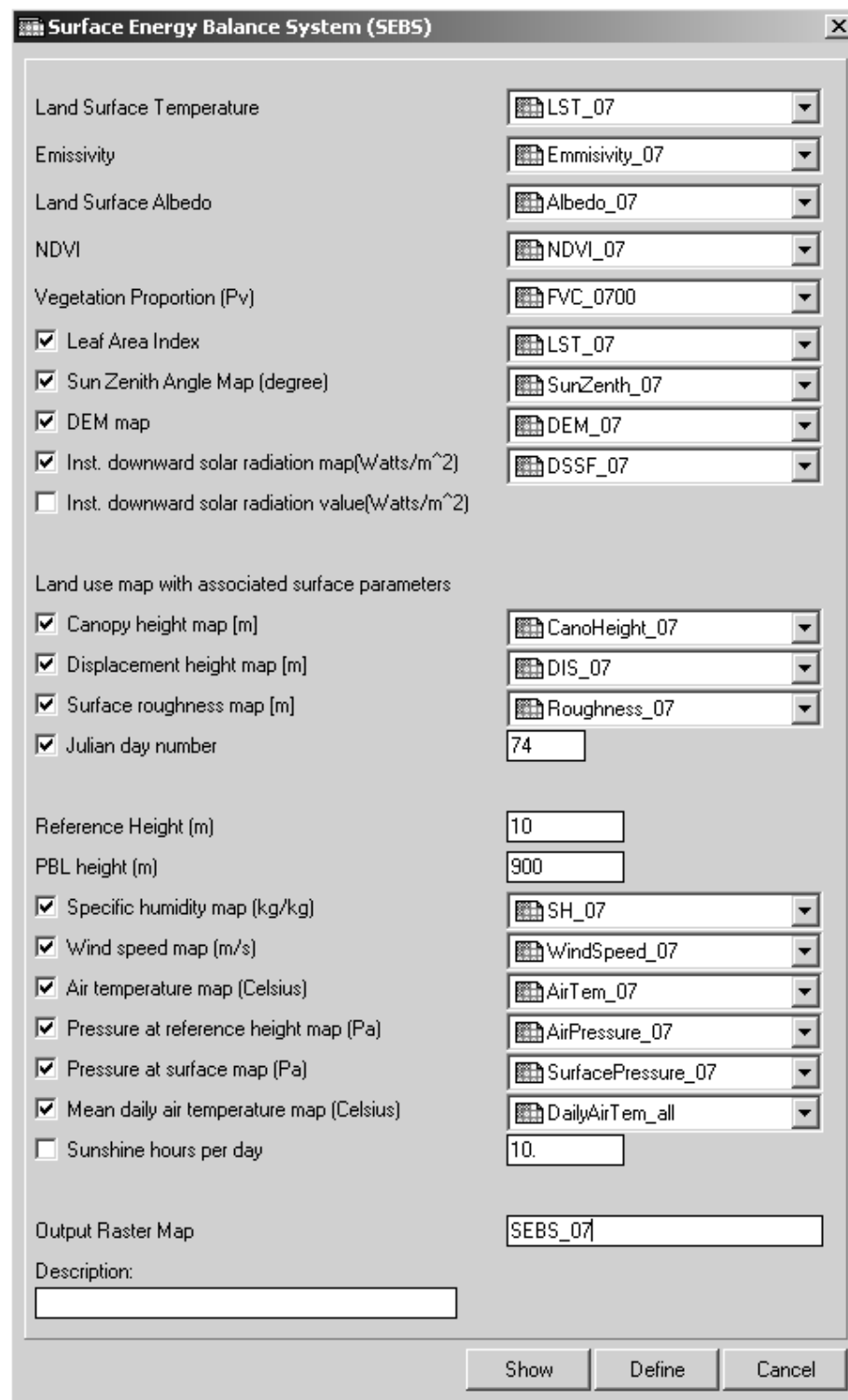
$$\text{Percentage error (\% error)} = \left(\frac{y - x}{x} \right) * 100$$

$$\text{Correlation coefficient (r)} = \frac{\sum (x - \bar{x})(y - \bar{y})}{\sqrt{\sum (x - \bar{x})^2 \sum (y - \bar{y})^2}}$$

$$\text{Coefficient of determination (R}^2\text{)} = \{ (1/n) * \sum [(x_i - \bar{x}) * (y_i - \bar{y})] / (\sigma_x * \sigma_y) \}^2$$

where n is the number of observations, \sum is the summation symbol, x and y are parameters to be fitted or compared. x_i is the x value for observation i , \bar{x} is the mean of x value, y_i is the y value for observation i , \bar{y} is the mean of y value, σ_x is the standard deviation of x , and σ_y is the standard deviation of y

Appendix G Surface Energy Balance System model SEBS interface



Surface Energy Balance System (SEBS)

Land Surface Temperature: LST_07

Emissivity: Emmissivity_07

Land Surface Albedo: Albedo_07

NDVI: NDVI_07

Vegetation Proportion (Pv): FVC_0700

☒ Leaf Area Index: LST_07

☒ Sun Zenith Angle Map (degree): SunZenth_07

☒ DEM map: DEM_07

☒ Inst. downward solar radiation map(Watts/m²): DSSF_07

☐ Inst. downward solar radiation value(Watts/m²)

Land use map with associated surface parameters

☒ Canopy height map [m]: CanoHeight_07

☒ Displacement height map [m]: DIS_07

☒ Surface roughness map [m]: Roughness_07

☒ Julian day number: 74

Reference Height (m): 10

PBL height (m): 900

☒ Specific humidity map (kg/kg): SH_07

☒ Wind speed map (m/s): WindSpeed_07

☒ Air temperature map (Celsius): AirTem_07

☒ Pressure at reference height map (Pa): AirPressure_07

☒ Pressure at surface map (Pa): SurfacePressure_07

☒ Mean daily air temperature map (Celsius): DailyAirTem_all

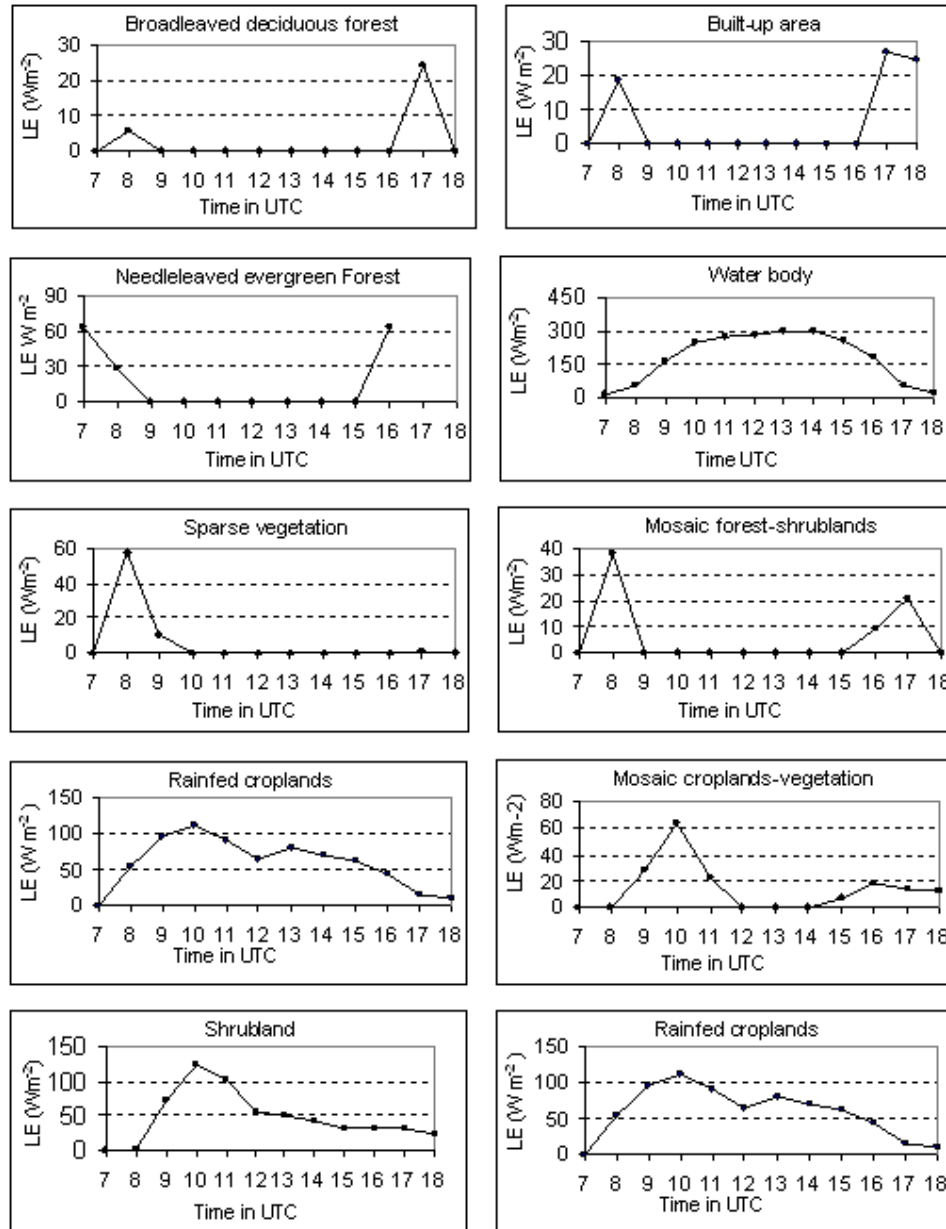
☐ Sunshine hours per day: 10.

Output Raster Map: SEBS_07

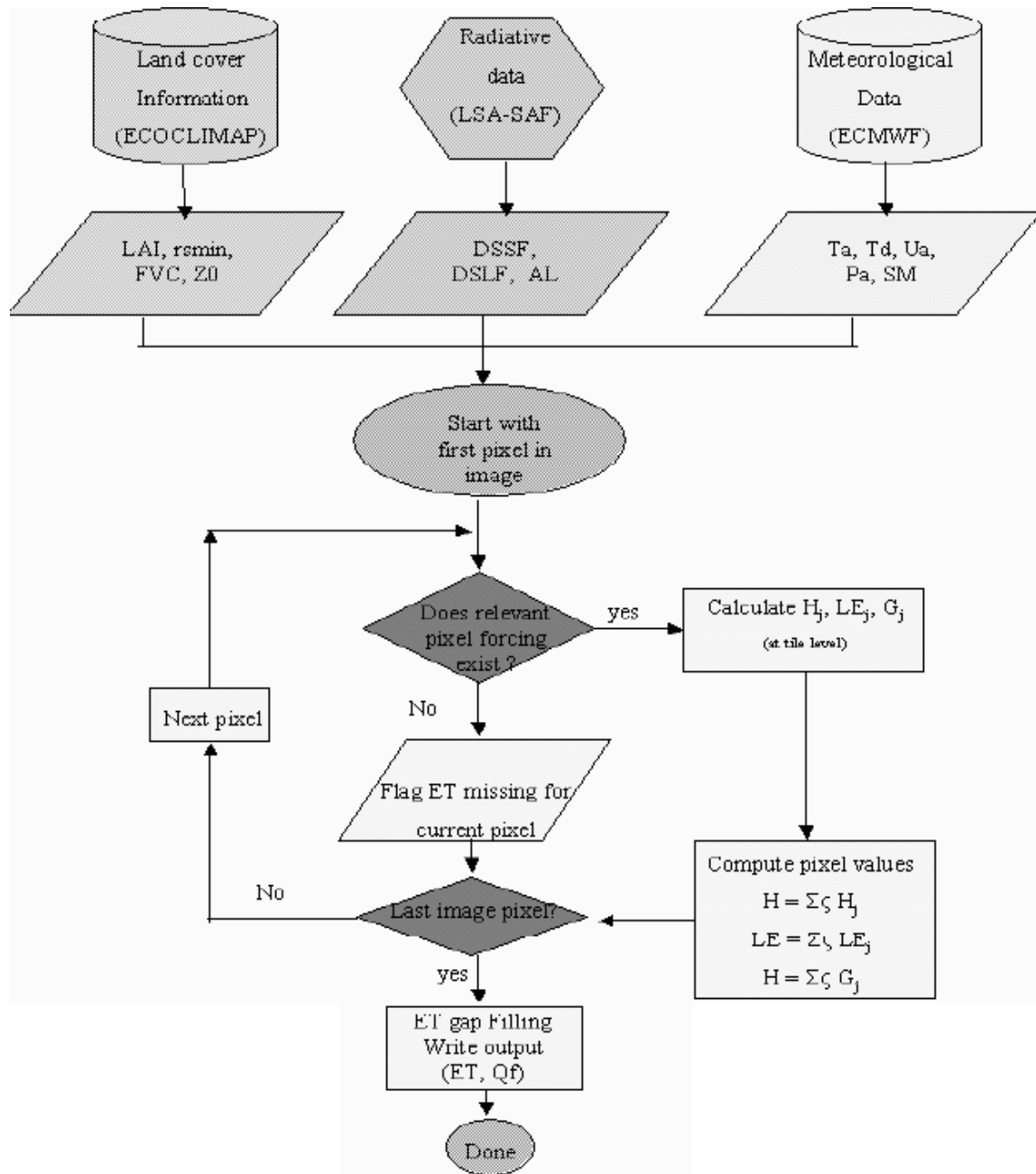
Description:

Show Define Cancel

Appendix H Diurnal variation of latent heat flux over different land cover classes on March, 15, 2009



Appendix I Flow chart of MET Algorithm



Source: SAF for Land Surface Analysis (LSA SAF), Product User Manual for Meteosat Second Generation Evapotranspiration (MET) - <http://landsaf.meteo.pt/algorithms.jsp?seltab=7&starttab=7>